Mixed Carbonate-Siliciclastic Sequence Development and Chemostratigraphy On A Distal Foreland During Miocene Glaciation, Eastern Saudi Arabia

Fawwaz Muhammad Alkhaldi

Dissertation submitted to the Faculty of the Virginia Polytechnic Institute and State University in partial fulfillment of the requirements for the degree of

Doctor of Philosophy

In

Geosciences

J. Fred Read, Chair
Kenneth A. Eriksson
Shuhai Xiao
Aus Al Tawil

May 1, 2012
Blacksburg VA

Keywords: Miocene, Saudi Arabia, Lidam area, Arabian foreland, Mixed carbonate-siliciclastic, Dam Formation, Hadrukh Formation, Hofuf Formation, Milankovitch cycles, Sequence development, Indian monsoons

Mixed Carbonate-Siliciclastic Sequence Development and Chemostratigraphy On A Distal Foreland During Miocene Glaciation, Eastern Saudi Arabia

Fawwaz M. Alkhaldi

ABSTRACT

The Miocene of the Lidam area, Eastern Province, Saudi Arabia, was studied to examine the interaction of glacio-eustasy during moderate Antarctic glaciation, within a small back bulge basin on the slowly subsiding distal Arabian foreland, distal from the active Zagros fold-thrust belt. Low subsidence rates of 1 to 4 cm/k.y generated the long-term accommodation, which were considerable slower than those in the proximal foredeep in Iran. Deposition of the siliciclastics was driven by lowered sea levels, and moderately humid to arid climate. Rising sea levels pushed the siliciclastics updip allowing mixed siliciclastics and carbonates to form downdip, under semi-arid climate and locally hypersaline conditions. Maximum transgression slightly predated the Middle Miocene climatic optimum when prograding siliciclastics migrated across the platform. Falling triggered siliciclastic deposition under semi-arid climate.

Sequences appear to relate to long-term obliquity (~1.2 m.y. cycles) and long-term eccentricity (400 k.y.) cycles. The succession contains numerous missing beats reflecting the updip position of the study area, and sea level changes of tens of meters that frequently exposed the platform. Siliciclastic units commonly are incised into muddy sediments beneath sequence boundaries. Multiple exposure surfaces occur within Hadrukh brecciated palustrine carbonates. Within Dam carbonates, parasequence boundaries commonly are capped by tidal flat laminites (some of which are incipiently brecciated).

High frequency negative excursions of $\partial^{13}C$ within the succession appear to relate to

near-surface diagenesis by soil gas depleted in $\partial^{13}C$ beneath sequence boundaries. Positive C isotope excursions in the Lidam Miocene section can be tied to similar excursions in Qatar and UAE, where Sr isotope dates constrain the ages of the units. The overall C isotope profile at Lidam shows depleted values early in the Miocene to heavy values in the Middle Miocene, becoming lighter again in the late Miocene. The profile appears to follow the long-term global $\partial^{13}C$ curve. Incursion of meteoric groundwaters into the study area was driven by the long-term global sea level changes. Oxygen isotopes are surprisingly light, extending down to -12.5 $‰_{VPDB}$. The very light $\partial^{18}O$ values of the meteoric waters may be explained by rainfall associated with enhanced Miocene Indian monsoons, and with far travelled air mass trajectories migrating across north Africa and from the polar region.

TABLE OF CONTENTS

LIST OF FIGURES

LIST OF TABLES

CHAPTER 1

INTRODUCTION

This dissertation is divided into two parts. The first part (Chapter 2) deals with the sequence development of a mixed carbonate siliciclastic succession in the Miocene of eastern Saudi Arabia. For the study, several outcrops were examined, along with four shallow cores 600 m drilled by Saudi Aramco. The study examines the sequence stratigraphic development within a small back-bulge basin on the distal Arabian Foreland during onset of Miocene glacio-eustasy, driven by Antarctic glaciation. The succession studied was deposited within a structurally influenced embayment similar in size to those occurring along the southern Arabian Gulf coastline today. The low subsidence rates generated very thin sequences and parasequences bounded by numerous non-depositional hiatuses.

The succession preserves a record of tectonic subsidence and warping, and global sea level changes that deposited the depositional sequences and parasequences. In the deep sea, the oxygen isotopes provide a record of these global sea level changes due to the light oxygen isotope being locked in the ice, thus making the ocean isotopically heavy and hence marking times of glaciation and sea level fall. The proxy sea level curves from the oxygen isotopes were used to generate a time framework of deposition in the area, in the absence of Sr isotope dates, and well define biostratigraphic zone fossils.

The study also provides an example of the complex interactions between siliciclastic sediments from the land, and marine carbonate sediments formed from the resident biota in the ancestral gulf. Besides posing a classification problem, the mixed carbonates and siliciclastics

generate a very complicated array of facies. The moderate magnitude sea level changes locally incised sequence boundaries, and caused formation of numerous exposure surfaces with paleosols and brecciation.

Milankovitch climate forcing of ice sheet growth and decay has been well documented in the deep ocean record using C and O isotopes and forams (Zachos et al., 2001). Thus the studied interval should contain at least a partial record of these climatically induced sea level changes. These are developed as small parasequences, stacked into parasequence sets, which are in turn stacked into sequences.

The succession differs markedly from greenhouse platforms, which are characterized by tidal flat capped cycles extending over much of the shallow platform. In contrast, tidal flat laminites are relatively rare in the Miocene succession, while paleosols and exposure surfaces of various types are common. These reflect the 20 to 40 m sea level changes during the Miocene, compared to much smaller greenhouse sea level changes, although in the updip part of the platform studied, marine flooding events probably only involved water depths of a few meters to 10 m to 20 m.

The second part (Chapter 3) describes the C and O chemostratigraphy of one of the updip cores sampled. The purpose was to use the Carbon isotope profile to enhance the correlation of the succession to biostratigraphically and Sr isotope dated sections elsewhere in the world. The study evaluates the reasons for the observed C and O isotope excursions on the profile. These include global C cycling and local effects of soil formation and diagenesis. For oxygen isotopes, they include waxing and waning of ice sheets at the poles, changes in atmospheric climate patterns, and local meteoric diagenesis associated with emergence surfaces with the stratigraphy.

The C isotope profile appears to grossly resemble the global deep-sea signal, but is

considerably amplified. It is explained by the intrusion of light C meteoric ground waters into the region during lowered sea levels coupled with local C isotope depletion beneath vegetated emergent surfaces. The surprisingly light oxygen isotopes within the profiles appear to be lighter than any in the region. Given the lack of burial resetting, they must reflect changes in oxygen isotope composition of the rainfall in the region in the Miocene. Consequently, they provide insight into Miocene climatic atmospheric circulation patterns.

CHAPTER 2

Mixed Carbonate-Siliciclastic Sequence Development On A Distal Foreland During Miocene Glaciation, Eastern Saudi Arabia

Abstract

The Miocene of the Lidam area, Eastern Province, Saudi Arabia, was studied to examine the interaction of glacio-eustasy during moderate Antarctic glaciation, within a small back bulge basin on the slowly subsiding distal Arabian foreland, distal from the active Zagros fold-thrust belt. The Aquitanian Hadrukh Formation (~60 m thick) is dominated by non-marine siliciclastics and minor palustrine carbonates and is a composite sequence with two subsequences and 8 high frequency sequences. The late Aquitanian to early Langhian Dam Formation (up to 80 m thick) is a mixed carbonate-siliciclastic composite sequence with updip sections dominated by siliciclastics, grading downdip into carbonates. It is composed of 8 small-scale 3rd order sequences, each typically composed of about 4 parasequence sets. The Langhian to Serravallian Hofuf Formation (90 m thick) is a 3rd order non-marine sequence with a lower siliciclastic unit; the middle carbonate- and upper siliciclastic unit of the Hofuf Formation were not studied.

Facies within the siliciclastic units include paleosols, cross-bedded sands (fluvial), red mudrock (mudflat), near shore siliciclastic green gray mudrock (lagoon), brecciated micritic quartz sands (ephemeral lake), gypseous calcareous quartz sands and wacke (saline coastal plain and evaporitic flats), and quartz sand sheets (intertidal shallow marine). Carbonate facies include brecciated carbonates (incipient paleosols), lime/clay clast quartz wackestone (transgressive basal sheet), microbial laminites and microbial mounds (tidal flat and shallow subtidal) , argillaceous variably quartzose marl (near-shore lagoon), fine peloid mudstone –

wackestone (shallow lagoon), oolitic grainstone (shoal or tidal bars), mollusk packstone (nearshore shelf) and foraminiferal-mollusk packstone-grainstone (seagrass meadows).

Subsidence rates of 1 to 4 cm/k.y were considerably slower than those in the proximal foredeep in Iran. This together with long-term sea level changes generated the accommodation. Differential warping during the Oligocene-Miocene generated a structurally controlled embayment within the study area, which influenced bathymetry of facies.

Deposition of Hadrukh siliciclastics was driven by lowered sea levels and moderately humid to arid climate, with siliciclastics brought into the area by ephemeral streams and eolian processes. Arid phases are marked by gypseous quartz sands. Rising sea levels pushed the siliciclastics updip allowing Dam mixed siliciclastics and carbonates to form downdip, under semi-arid climate and locally hypersaline conditions. Maximum transgression slightly predated the Middle Miocene climatic optimum when prograding siliciclastics migrated across the platform. Falling sea levels triggered Hofuf siliciclastic deposition under semi-arid climate.

The sequences, which represent the updip terminations of much thicker, more conformable downdip sediment wedges, were generated by glacio-eustatic sea level changes. Sequences appear to relate to long-term obliquity (~1.2 m.y. cycles) and long-term eccentricity (400 k.y.) cycles. The succession contains numerous missing beats, reflecting the updip position of the study area, and sea level changes of tens of meters that frequently exposed the platform. These resulted in numerous paleosols on redbeds near sequence boundaries in the Hadrukh and the Dam formations, and siliciclastic units commonly incised into muddy sediments beneath sequence boundaries, as well as multiple exposure surfaces within Hadrukh brecciated palustrine carbonates. Within Dam carbonates, some parasequences are capped by tidal flat laminites (some of which are incipiently brecciated) but most lack tidal flat caps.

INTRODUCTION

In order to provide a sequence stratigraphic example in both outcrop and core close to Aramco's Dhahran facility, eastern Saudi Arabia, the company drilled several continuous cores through the Early to Middle Miocene in the Lidam area (Figures 2.1, 2.2, and 2.3). The cores, along with the limited outcrops in the area, record the effects of glacio-eustasy on a mixed carbonate-siliciclastic ramp system in a distal foreland setting marginal to the tectonically active Zagros fold-thrust belt. In such foreland successions elsewhere, eustasy commonly has been an important control on sequence development while tectonics controlled thicknesses (Smith et al., 1995; Pope and Read 1997; Lomando, 1999; AlSharhan and Kendall, 2002).

The Miocene siliciclastic and carbonate succession has well developed, local to regional paleosols and exposure surfaces that bound 3rd order and 4th order high frequency sequences and component parasequences, reflecting glacio-eustasy acting on the distal foreland. Warping of the foreland likely controlled the shape of the coastline and position of embayments as in the coastal Arabian Gulf today. The Miocene facies and biotas have modern (and Plio-Pleistocene) analogs in the Arabian Gulf today, which facilitated environmental analysis.

Detailed oxygen isotope records from coeval Miocene deep sea deposits show well documented Milankovitch forcing of ice volumes on Antarctica (Zachos et al. 2001). Also, there are relatively robust global 3rd order sea level curves for the Miocene constrained by seismic sequence stratigraphy, microfossils, and paleomagnetism, that can be compared with the oxygen isotope record (Figure 2.3; Hardenbol et al., 1998; Zachos et al., 2001; Billups et al., 2002; Snedden and Liu, 2010). The Miocene also appears to be characterized by moderate sized sea level changes 20 to 40 m in magnitude, based on deep sea oxygen isotope records (Zachos et al., 2001) and facies analysis of Miocene shelf successions (Boreen and James, 1993). Thus the

present study should provide an example of transitional eustasy (Read, 1998) prior to the onset of full- blown Late Pleistocene icehouse conditions. If the published eustatic sea level curves are consistent, then this should make easier the task of recognizing any tectonic components of the relative sea level signal in the study area. Given the well documented Milankovitch forcing of climate, ice volumes and sea level in the Miocene, it should be possible to evaluate how the stacking of parasequences on the platform relates to the deep sea Milankovitch record, as well as the relative completeness of the platform record.

The Miocene of the study area is a mixed siliciclastic-carbonate systems that appears to have formed in a dominantly arid setting, thus posing problems of sediment classification, and processes of ephemeral terrigenous sediment transport and mixing with indigenous carbonate components in marginal marine settings. Facies development was complicated by major shifts in base level related to long-term glacio-eustasy. Additionally, the change from siliciclastic- to mixed siliciclastic-carbonate back to siliciclastic deposition during the Aquitanian to Langhian interval appears to be related to a paleo-monsoon system, documented in the Plio-Pleistocene of north Africa-Arabia (Trauth et al., 2009).

METHODS

Fourteen outcrop sections south of the Lidam escarpment (Figures 2.1 and 2.2) were logged and a facies photomosaic constructed to document vertical and lateral facies changes. In addition, 4 shallow cored wells (Figure 2.2), totaling over 600 m, were drilled and logged from the surface through the Miocene succession to the top of Eocene. These were drilled especially for the project by Saudi Aramco, and are housed in the Saudi Aramco core laboratory, Dhahran. The outcrops and cores were logged noting mineralogy, sedimentary structures, extended

Dunham classification (Dunham, 1962; Embry and Klovan, 1971) for the carbonates and the Williams, Turner, and Gilbert (1982) classification for the siliciclastics, along with color, grain size, shape, sorting, grain types and diagenetic overprint. Mixed siliciclastic-carbonate facies were classified with marls 35 to 65% carbonate with the remainder siliciclastic mud (and lesser sand), sandy limestones 25 to than 50 % quartz sand, and limy sands and sandstones 50% to 75% quartz sand (Pettijohn et al., 1987; Williams, Turner, and Gilbert, 1954). The slabbed cores were examined under a binocular microscope and the core data plotted at a scale of 5 feet per inch (1.5 m / 2.5 cm). Representative samples of each facies from the outcrops and the cores were thin sectioned, stained using ARS (Dickson, 1966) and examined under the petrographic microscope. Stratigraphic columns from core logs and outcrop sections were color-coded for facies-type and parasequences, parasequence sets and sequences tentatively picked.

Interpretive sequence stratigraphic cross sections were constructed from the core data integrated with a composite section from the outcrop data. The cross sections extend from south-west to north-east and were constructed separately for the Hadrukh, Dam and Hofuf formations, datuming each cross section on the formation top to facilitate facies and parasequence correlations. Identification of formation tops was helped by the type section descriptions of Powers and others (Steineke and Hoover, 1936; Steineke and Bramkamp, 1952; Steineke et al., 1958; Powers et al., 1966; Powers, 1968). The sequence stratigraphic cross sections show the vertical and lateral lithofacies distribution, parasequence and parasequence set picks, maximum flooding surfaces and sequence boundaries. Given the spacing of the wells (from 9 to 17 km), the extension of the lithofacies between wells is highly interpretive and was guided by Walther's law.

A regional cross section using data from the literature was created running through the

study area to the Zagros Mountains in Iran, to provide a regional context for the study, and evaluate the effects of synsedimentary tectonics on the development of the regional succession. A more local cross section was constructed for the study area and environs to evaluate syndepositional warping. Core SC-4 was sampled for carbon and oxygen isotope analysis using the fine carbonate mud fraction to evaluate any chemostratigraphic trends and diagenetic overprints associated with sequence boundary development.

TECTONIC AND STRATIGRAPHIC SETTING

For much of the Late Permian through the Mesozoic, the Arabian carbonate platform was a passive margin (Al-Husseini, 2000). This was terminated by Semail Ophiolite emplacement in the Late Cretaceous, which initiated compressional tectonics in the region. During the Cenozoic, the continued spreading of the Atlantic, Mediterranean and Indian Oceans resulted in northeast movement of the Arabian Plate, which was mainly accommodated by subduction along the northern margin of the rapidly closing Neo-Tethys Ocean, which separated the Arabian platform carbonates from the tectonic blocks of Iran (Sharland et al., 2001). Subsidence during the Paleogene was mainly due to thrust-related tectonic loading of the eastern Arabian-plate margin, with a secondary contribution from sediment loading (Sharland et al., 2001). The Arabian Plate today is separating from Africa along the Red Sea rift at 1.2 cm per year in a NNE direction, with crust being subducted beneath the Zagros thrust belt (Edgell, 1992).

From Early Paleogene to Latest Eocene (30 Ma), accommodation space varied from a few meters at most in the Red Sea area, to a few tens of meters in the plate center, to hundreds of meters within the inherited foreland basins to the northeast (Figure 2.4; Sharland et al., 2001). During the Eocene, tectonic activity was limited to periods of minor deformation, including

continued movement of the Infra-Cambrian salt in the Arabian Gulf (Koop and Stoneley, 1982; Chaube and Al-Samahiji, 1995). Periods of minor folding also may have affected the structures in eastern Saudi Arabia during the Cenozoic (Ibrahim et al., 1981). The Paleocene-Eocene succession is thickest in the proximal foredeep of Iran beneath the Zagros orogen, thinning over a high on the Mesozoic (marking a Paleogene bulge?), and then thickening again onto the Arabian foreland (Figure 2.4).

The Late Oligocene to Early Middle Miocene marked closure of the Neo-Tethys Ocean (Beydoun, 1993), where carbonate sedimentation was replaced by continental siliciclastic deposition in the proximal foreland basin. Continued subsidence caused progressive northeast tilting of the Arabian Plate, due to structural loading by Zagros thrust sheets (Sharland et al., 2001). A gentle foreland bulge may have developed parallel to a line west of the Euphrates River (Sharland et al., 2001). The Oligo-Miocene succession is thickest within the foredeep, thinning northeastward toward the Main Zagros Reverse Fault, and onto the Arabian foreland onto a possible forebulge (Figure 2.4). It undergoes slight thickening into Saudi Arabia, into possible small back-bulge basins, which contains the study area (Figure 2.4). The region is cut by normal faults (Figure 2.5 A).

In Saudi Arabia, Zagros compression resulted in the inversion of some of the basement structures (Wender et al., 1998). Diapiric salt structures in the Arabian Gulf grew rapidly during the Miocene (Edgell, 1996). The orthogonal compression in the Zagros ended with the opening of the Red Sea in the Late Miocene (Crossley et al., 1992) and initiation of sinistral strike-slip movement along the Dead Sea transform fault, which changed the Zagros region into an oblique dextral transpression zone (Beydoun, 1993).

The study area is bounded by the Abqaiq anticline to the southeast and the northern part

of Ghawar anticline to the southwest (Figure 2.6). The Dammam dome lies between the study area and the present day coastline. All of these structures appeared to have continued to grow slowly during the Cenozoic (Abu-Ali and Littke, 2005). There appears to have been considerable syndepositional warping and associated faulting during deposition of the Miocene in the study area. For example, the cross section of the Miocene succession in the Lidam region and environs, when hung from the top of the Dam Formation (Figure 2.5 A and B), shows thinning onto a high updip, and thickening downdip into a central depression, which contains a narrow medial up warp over which both the Hadrukh and Dam formations thin. From the central depression the succession then thins slightly again downdip onto a downdip high. Note that the medial up warp was not cored as it was discovered after the coring program was completed.

Oligocene and Miocene uplift of the Red Sea margin and Arabian Shield associated with thermal doming and rifting provided elevated highlands that acted as a source of the siliciclastic sediment, as well as uplift of the Zagros Mountains (Sharland et al., 2001). Siliciclastic input from the southwest highlands into the Eastern Province today is via ephemeral streams from a major wadi and alluvial fan system named Wadi Sahba, and eolian dunes driven by the Shamal winds from the north and northwest (Figure 2.1; Al-Sulaimi and Pitty, 1995). However, this fan system is far to the south of the study area suggesting that siliciclastic input into the study area in the Miocene likely was due to sheet flooding, ephemeral small braided streams and via eolian processes.

The gross topography of the region during the Miocene can be envisaged using the structure map on the top of the Eocene (Figure 2.6), with the understanding that the structure has continued to evolve during the later Cenozoic. This suggests that the study area was an embayment tens of kilometers across in the Miocene. It was open to the northeast toward the

Arabian Gulf, bounded to the east by the Abqaiq anticline and to the west by the En Nala anticline.

STRATIGRAPHIC FRAMEWORK

The Miocene and Pliocene succession in the study area (Figure 2.3) consists of, in ascending order, the Hadrukh, Dam and Hofuf formations. The formations were defined by Steineke et al. (1958) and were further studied by Powers et al. (1966); and Powers (1968).

Hadrukh Formation (Early Miocene, Aquitanian)

The Hadrukh Formation unconformably overlies the limestones of the Eocene Dammam Formation in the study area (Figure 2.3). The Hadrukh Formation is dominated by siliciclastics and is 52 to 66 m thick. In general the basal bed of the Hadrukh Formation is a few meters of cream, gypseous sand and mudrock. The top is the contact on calcareous sandstone that is overlain by limestone and marl of the basal Dam Formation (Powers et al., 1966; Powers, 1968). The Hadrukh Formation is non-marine marly sandstone, sandy marl, sandy clay and sandy limestone; the sediments have minor amounts of interstitial gypsum and chert. In the type section, there are a few thin marine layers near the top with poorly preserved marine mollusks (Powers et al., 1966; Powers, 1968).

The age of Hadrukh Formation is poorly constrained. Because of the apparent continuity with the Dam Formation, it has been considered to be early Miocene (Powers et al., 1966). However, Whybrow et al. (1987, 1999) suggest a late early Miocene age based on terrestrial fauna.

Dam Formation (Late Aquitanian to Early Langhian)

The Dam Formation is a dominantly limestone formation ranging from 47 to 79 m thick in the study area. The base of the Dam Formation is placed at the change from sandstone of the Hadrukh Formation into fossiliferous marl and limestone of the Dam Formation. The basal boundary of the Dam Formation is relatively conformable according to Sharland et al. (2001) whereas the basal boundary is considered to be unconformable according to Haq and Al Qahtani (2005). The Dam Formation consists of marl, red, green, and olive clay with minor interbeds of sandstone, chalky limestone, and coquina; the unit has been subdivided into a basal marl unit, a middle limestone and an upper siliciclastic dominated unit (Powers et al., 1966; Powers, 1968). Within the study area the Dam Formation is dominantly siliciclastic updip and carbonate-prone downdip. The top of the Dam Formation is the contact on marl and fossiliferous marine limestone, and the overlying clay, sandstone and gravel of the basal Hofuf (Powers et al., 1966; Powers, 1968).

Cox (1936) considered the Dam Formation as late Early Miocene based on the occurrence of *Ostrea latimarginata* in southern Iran and Bahrain. Powers et al. (1966; 1968) assigned a Middle Miocene age to the formation in Saudi Arabia, correlating it with the Lower Fars Formation of Iraq on the presence of *O. latimarginata, Echinocyamus* sp., *Archaias angulatus* (foraminifera) and other invertebrate fossils in Saudi Arabia. Thomas et al. (1982) identified remains of Early Miocene, Burdigalian fossils of rodents, larger mammals, reptiles and birds from the Dam Formation of the As-Sarrar region in Saudi Arabia. Otero and Gayet (2001) identified Burdigalian cyprinid fish from the Dam Formation of the As-Sarrar and Ad- Dabtiyah regions in Saudi Arabia. Adams et al. (1983) and Whybrow et al. (1987; 1999) supported the Burdigalian age for the Dam Formation in Saudi Arabia based on its marine and terrestrial

vertebrate fossil assemblage.

Bristow (1999) reported the bivalve *Diplodonta* species from the Dam formation near As Sila, UAE that suggests a Burdigalian age. Hewaidy (1991), Khalifa and Mahmoud (1993) studied foraminifera from the Dam Formation at Al-Kharrara and Jebel Al-Nakhash in Qatar and dated it as Burdigalian. The benthic foraminifera *Borelis melo* was used as a marker species for biostratigraphic zonation (*Borelis melo melo* Zone) of the Dam Formation succession. Al-Saad and Ibrahim (2002) recognized a *Borelis melo melo* local Range Zone of Burdigalian age within the Dam Formation in Qatar. Strontium isotope data suggests that the Dam Formation in Qatar, whose upper part is truncated, ranges from 21.6 Ma (Late Aquitanian) to 18.9 Ma (Early Burdigalian; Howarth and McArthur, 1997; Dill et al. 2005; 2007). This can be tied to the lower half of the Dam Formation of the study area using the carbon isotope profiles and the sequence stratigraphy (Chapter 3). Peebles (1999) obtained an Early-Middle Miocene (Burdigalian to Early Langhian) age from strontium isotope analysis from Dam outcrops near As Sila, and Gachsaran Formation in Abu Dhabi, UAE.

The Gachsaran Formation of southwestern Iran has been correlated to the Dam Formation of eastern Saudi Arabia and Qatar (Adams et al., 1983; Peebles, 1999) and assigned a Burdigalian-Langhian age based on the occurrence of the index taxa of *Austrotrillina bowchini-Peneroplis evolutus* and *Neoalveolina (Borelis) melo curica* zones (Wynd, 1965; Jones and Racey, 1994). *Borelis melo* could be as old as Early Miocene (Al-Saad and Ibrahim, 2002) and extend into the Middle Miocene in the Mediterranean region (Bellini, 1969; Bassiouni et al., 1975; Hammad et al., 1976; Abuserwil, 1996; Ouda, 1998; Sadek, 1999; and Abdulsamad and Barbieri, 1999). From the above review this suggests that the Dam Formation extends from Late-Aquitanian through Burdigalian to Early Langhian (Early Miocene- Early Middle Miocene).

Hofuf Formation (Langhian-Serravallian)

The Hofuf Formation is a dominantly siliciclastic unit, ranging from 7 to 23 m thick in the study area. The base of the Hofuf Formation generally is placed beneath quartz-pebble-bearing gravels that overlie calcareous rocks of the Dam Formation (Powers et al., 1966; Powers, 1968). The basal contact of the Hofuf Formation is considered to be an unconformity in the study area (and most updip areas on the foreland, although there does not appear to be much time missing. The Hofuf Formation consists of unfossiliferous non-marine conglomerate, sandstone, sandy limestone, sandy marl, and sandy shale. In the study area, the Hofuf Formation consists of a basal gravelly sand, a middle carbonate rich unit, a sandstone unit and a capping nodular sandy limestone, previously misidentified as limestone conglomerate (Saner et al., 2005). The basal gravels are dominantly well-rounded pebbles of white quartz and lesser limestone clasts (as large as 12.5 centimeters in diameter) in a poorly sorted, earthy, sandy matrix (Powers et al., 1966; Powers, 1968). Non-diagnostic fresh-water fossils occur in the type section (Powers et al. 1966) and it has been dated using terrestrial vertebrate species as Langhian-Serravallian (Thomas *et al.*, 1978, Sen and Thomas, 1979; Thomas *et al.*, 1982; Thomas, 1983, 1984, 1985).

MIOCENE FACIES OF THE LIDAM AREA

A schematic model of the Miocene depositional systems in the study area is shown in Figure 2.7. The Miocene facies of the study area are summarized in Tables 1 and 2 and core-slabbed photos and thin sections representing main facies are shown in Figures 2.8 and 2.9. The key characteristics and depositional settings of the facies are briefly described below, in order of continental to offshore marine. Details of selected logged cores in Hadrukh and Dam Formations are shown in Appendix A, and C. The stratigraphic occurrence and the regional distribution of

the various facies for Hadrukh, Dam, and Hofuf Formations are shown on the cross sections and stratigraphic columns (Figures 2.10, 2.12, and 2.15) respectively. Facies distribution of Dam Formation from outcrop data is shown in Figure 2.13. Facies within parasequences of the Hadrukh and Dam Formations are shown in Figures 2.10 and 2.13.

Siliciclastic Facies

Paleosols

These rocks (Table 1; Figure 2.8 a) are red to green mottled units from 20 cm – 3 m thick. Typically they are silty mudrocks having blocky fabrics with crumb textures, root traces, caliche- and ferruginous nodules (Table 1). These facies are interpreted as paleosols based on the presence of crumb textures, root traces, caliche nodules and locally ferruginous nodules (Retallack, 1993; Kraus, 1999). They developed on terrigenous siliciclastic mud and sands. Red color, caliche and gypsum in associated facies suggest arid climate, as does the absence of organic layers or peats.

Cross bedded/planar bedded quartz sands and clay-clast conglomerate (Fluvial)

Cross- and planar-bedded quartz sands and conglomerates (Table 1; Figure 2.8 b and h) are reddish tan, 60 cm to 1.5 m thick units. They are composed of medium to coarse quartz sandstone with lags of granule- and cobble-size clasts of red clay mudrock.

These are fluvial deposits (Steineke et al., 1958; Powers et al., 1966) based on their updip location, tan colors, basal clay-clast conglomerates (locally with quartz pebbles in Hofuf Formation), cross- and planar bedding, association with red mudrocks and paleosols, presence of root traces, general lack of burrowing and lack of marine fossils (Walker and Cant, 1984). Given the arid setting they likely formed from ephemeral flash floods, which would have favored

preservation of clay clasts and rip-ups in channel lags.

Red mudrocks (Coastal plain and supratidal mudflats)

The red mudrocks (Table 1; Figure 2.8 c) are 20 cm to 1.5 m thick units that are commonly structureless, but may be locally laminated at the base. They are composed of silt-size quartz grains and clay matrix.

The red mudrocks are interpreted to have formed on the interfluve areas of exposed coastal plain mud-flats (Walker, and Cant, 1984) and on supratidal siliciclastic mudflats. Red oxidized color, root traces and close association with paleosols indicate exposure. Locally tops are gleyed where they were overlain by a transgressive facies.

Green gray mudrock (near-shore siliciclastic lagoon)

Gray green mudrock units (Table 1; Figure 2.8 d) are 20 cm to 1.5 m thick, and are massive to faintly laminated. They typically are sandy mudrocks composed of clay, silt- and lesser very fine to medium sand size quartz grains.

These are interpreted to have formed in restricted inshore lagoons that were settling ponds for land-derived mud similar to Pleistocene facies in the present Arabian Gulf (Darwish and Conley, 1989). The green mudrocks formed in moderately oxygenated conditions, whereas dark gray mudrocks likely formed in stratified poorly oxygenated lagoons in which organic material (both washed in from land or produced in the lagoon) depleted the oxygen. Water-filled flood basins are unlikely as a depositional setting given the arid climate and dominant tan and red colors of the coastal plain facies.

Brecciated micritic quartz sand and sandy lime mudstone to packstone (Palustrine or ephemeral lake)

These limy quartz sands and sandy carbonates (Table 1; Figure 2.8 e and i) are light tan to gray, and up to 8 m thick, and commonly show fitted-breccia fabrics infiltrated by more quartzose sediments. The carbonate-rich intervals are pisolitic and peloidal with local microbial clots, and are unfossiliferous.

These facies probably were formed in ephemeral coastal lacustrine or palustrine settings (Dunagan, 1998 and 2000a) given their position within and updip of siliciclastic facies, the lack of marine macrofossils, presence of abundant lime mud and admixtures with bimodal quartz (eolian rounded quartz and sheet-flood/eolian finer angular quartz). Breccia fabrics formed during emergence as cracks opened along joints and bedding planes that became infiltrated with quartzose sediment.

Gypsiferous, calcareous quartz sands and quartz wacke (saline coastal plain, evaporitic flats, intertidal shallow marine sand sheets, and nearshore lagoon)

These gypsiferous and/or limy quartz sands and quartz wacke (Table 1; Figure 2.8 f and j) form a spectrum of muddy sands to sandy muds. They are pale tan to light gray units of 30 cm to 1 m thick. They are structureless, except for the presence of hair-size rootlets some of which are filled with gypsum. The grain-supported quartz sands and mud-supported quartz wacke consist of variable amounts of terrigenous mud and angular to round, fine- to medium sand-size quartz, locally admixed with fine gypsum.

Quartz sands may have been deposited as eolian sand-sheets and interdune sheets on a semi-arid coastal plain with sparse, low vegetation (Fryberger et al., 1983), some being

subsequently modified by interstitial precipitation of gypsum or calcite from groundwaters. Quartz wacke probably formed in low energy near-shore lagoons dominated by siliciclastic influx, the quartz sand and silt perhaps having been carried in during winds storms (Shinn, 1973). The muddy quartz sands likely formed on intertidal and shallow subtidal coastal sand flats analogous to those that fringe the modern southern Arabian Gulf (Alsharhan and Kendall, 2002; Warren, 2006). The quartz sand was carried into the coastal zone by winds as parts of migrating dune systems, by ephemeral streams and by long shore drift. The sands were intermittently reworked and poorly winnowed by waves and currents, and the sands were admixed with small amounts of terrigenous and carbonate mud and burrow homogenized. Interstitial gypsum probably formed as a capillary-fringe evaporite just above the water table within coastal sand flats or sandy sabkhas (Warren, 2006).

Quartz sand sheets (coastal, intertidal and shallow marine)

Quartz sand sheets (Table 1; Figure 2.8 g and k) are reddish tan to light gray units 1 to 10 m thick. They generally are structureless, but locally have rootlets and rhizoconcretions along with root traces filled with quartz sand, and caliche nodules locally are present in the Hadroukh Formation.

These clean sand sheets possibly formed as eolian sand sheets and interdune sheets on a semi-arid coastal plain with sparse, low vegetation (Fryberger et al., 1983). This is supported by updip exposures of the Hofuf siliciclastic units on the Lidam Escarpment, in which large-scale cross-bedded eolian dune sands are interbedded with fanglomerates and cross-bedded fluvial sands (Powers et al., 1966). Others could have formed in coastal terrace settings, with the quartz introduced via wind, ephemeral sheet flooding, and long shore transport (Alsharhan and Kendall, 2002; Warren, 2006). The nearshore setting is indicated by downdip transition of the sands into

shallow marine carbonates in the Dam Formation (Figure 2.12). If these sands were reworked in marginal marine intertidal and shallow subtidal sandflat settings, they might be expected to contain fossils. The absence of shells argues against a marine origin, although any aragonitic mollusks likely were dissolved by meteoric ground waters and lack of cement prevented preservation as molds. Uniform grain size of sands may have masked sedimentary structures (Tucker, 2003) but homogeneous, massive fabrics also may be the result of bioturbation, which obliterated depositional structures (Moore and Scruton 1957; Tucker, 2003). With progradation, the ground waters remained below the gypsum precipitation field and on exposure, some of the sands were root-disrupted and rare caliche nodules were formed.

Carbonate Facies

Brecciated carbonate sheets (incipient paleosols) and karstified units

Brecciated carbonate *paleosols* (Table 2; Figure 2.9 a and i) are green to pale gray units 20 cm to 1.5 m thick. They are argillaceous carbonates with fitted-breccia fabrics, sheet-cracks and burrow/root traces. They consist of variably argillaceous sandy lime mudstone-packstone host containing infiltrated fine-to-medium sand-size quartz and lesser terrigenous mud. *Karst-modified facies* (Table 2) are up to 10 m thick in the upper Hadrukh Formation, commonly associated with palustrine mixed-carbonate siliciclastic units. They consist of fitted-brecciated carbonate host with several phases of sandy and argillaceous fill between clasts. Host typically consists of quartzose lime mudstone-sandy wackestone and the infills consist of fragmental carbonate and quartz in argillaceous or carbonate mud matrix. Boundaries of host carbonate are typically sharp and smooth rather than angular.

Similar paleosol facies in the Pleistocene were formed by exposure and desiccation of muddy argillaceous carbonate muds due to sea level fall (Darwish and Conley, 1989). The fitted

breccia fabrics probably reflect the presence of terrigenous clays mixed with the carbonates, which caused them to shrink markedly on drying during exposure. The thick, brecciated karstified units likely reflect very frequent, intermittent exposure of carbonate units typically at tops of palustrine units and on tops of some sequences. The complex fabrics of host and infills could reflect mixing aided by plant root bioturbation, as well as dissolution and infiltration of sediment from above down into the profile (Esteban and Klappa, 1983).

Lime/clay clast quartz wacke

Lime-clast/clay-clast quartz wackes (Table 2; Figure 2.9 b and j) are cream to greenish tan 0.5 – 1.5 m thick units that are structureless, poorly sorted and typically contain a mixture of granule to pebble-size clasts including white clay mudrock, abraded lime mudstone, skeletal grainstone, quartzose dolomudstone and green mudrock that float in a limy quartz wacke matrix of terrigenous clay and silt/very fine quartz sand. They are locally infiltrated with green clay.

These quartzose clast-bearing facies differ from transgressive lithoclastic units at the base of the Holocene in Shark Bay, which are dominantly carbonates (Hagan and Logan, 1974). They likely are transgressive ravinement lags that ripped up thin lagoonal shale or redbeds veneering the disconformity and in some cases admixed them with various types of carbonate clasts and incorporated them within a quartz wacke matrix. The energy could have been supplied either by storms or tsunamis impacting the low-lying exposed coastal areas (Shanmugam, 2011). Rapid deposition rather than long term wave reworking in beaches is suggested by locally abundant rounded clay clasts. Either these sediments were deposited as massive, structureless units or any sedimentary structures were obliterated by bioturbation following transgression. The lags graded up into silty mudrocks as water depths increased.

Carbonate laminite and stromatolites (Carbonate tidal flat and shallow subtidal)

Carbonate laminite (Table 2; Figure 2.9 c and k) is relatively rare, occurring in beds 20 cm to 0.5 m thick. It overlies oolitic grainstone and sandy peloid facies and some units underlie red and green mudrock paleosols. The laminites have local bioturbation, teepee structures, and local stromatolitic domes. Some have superimposed fitted-breccia fabrics and fractures filled with fibrous gypsum. Laminae consist of alternating millimeter layers of variably quartzose peloid packstone (of fine-medium sand-size peloids, variable amounts of quartz grains, and intraclasts), capped with lime mud.

Stromatolites and massive, thombolite-like mounds were observed in outcrops in the Lidam area, but were not recognized in the cores (Alkhaldi, 2009). The stromatolites include crinkly laminated, laterally linked hemispheroid and discrete vertically stacked hemispheroids. Small hemispheroids coalesced to form digitate heads of close spaced laminated fingers (2 to 6 cm wide) and laminated domes of 10 cm to 2 m wide. The thombolite mounds are associated with the stromatolitic units. There are biostromal with coalescent-mounded tops up to 1 m relief. Internal fabrics are quartz silty pellet packstone, which appear to lack fenestrae or other evidence of microbial binding.

The carbonate laminites formed in arid, low energy tidal flats covered by microbial mats analogous to those of present day Arabian Gulf and Shark Bay (Kendall and Skipwith 1969; Logan, Hoffman and Gebelein, 1974; Kirkham, 1998). The setting was less restricted than present, or the climate was less arid, because evaporite beds are not present in the Miocene of the study area, although they are present in nearby Qatar (Al-Saad and Ibrahim, 2002). The stromatolitic heads and mounds are strikingly similar to those in Shark Bay (Hagan and Logan, 1974; Jahnert and Collins, 2011). The digitate stromatolite heads formed under the influence of

colloform mats in shallow subtidal hypersaline areas subjected to multidirectional waves. Domal laminated stromatolites formed in the lower intertidal zone, analogous to the smooth mat heads in Shark Bay tidal flats (Logan, Hoffman and Gebelein, 1974; Hagan and Logan, 1974). The thrombolite-like mounds, although they grow on digitate stromatolitic units, appear to lack distinctive internal fabrics typical of thrombolites (such as microbial clots and fenestrae; Riding et al., 1991), although their coalescent-mounded morphologies are highly suggestive of thrombolitic mounds.

Argillaceous, variably quartzose marl (near shore lagoon)

The marl occurs in tan colored units 1 – 3 m thick commonly capping parasequences. It is structureless, argillaceous sandy marl composed of clay- and very fine-to-fine sand-size grains of quartz and some clay clasts (Figure 2.9 d and l). Upper parts of units may contain rare anhydrite nodules and clay infiltrated into desiccation cracks. Locally the top of the marls are brecciated and bleached.

This facies resembles near shore marls in the present Arabian Gulf (Sarnthein and Wagner, 1973) and lagoonal nearshore marls beneath exposure surfaces in the Pleistocene succession near Saudi Arabia-Bahrain causeway (Darwish and Conely, 1989). They likely formed in restricted low energy near-shore lagoons subject to *in situ* accumulation of carbonate that was admixed with terrigenous mud washed in from the land. The arid to semi-arid climate promoted hypersalinity, which together with the turbidity and very shallow water depths resulted in sparse faunas (Weaver and Beck, 1977; Darwish and Conely, 1989).

Fine peloid mudstone – wackestone (Pond/ shallow restricted lagoon)

These peloid mudstone-wackestones (Figure 2.9 e and m) are light tan to creamy mottled

units 0.5 – 2 m thick. They are mudstone and wackestone composed of silt-to-medium sand-size peloids with variable amounts of quartz grains and clay. Some contain granule-size clasts of quartzose lime mudstone and fine green claystone. The sediments are structureless to burrowed, with burrows filled with packstone, sandy mudstone, quartz sand or green clay. Some are disrupted by root- and rootlet-traces. Foraminiferal species include: *Reophax* spp., *Elphidum* spp., *Quinqueloculina* spp., and *Sorites* sp. Other fossils include scattered bivalve and rarely bryozoan fragments. Locally this facies is calcite-cemented, iron-stained or contains rare gypsum crystals. Mollusk shells commonly are leached and filled with calcite cement and clay.

The occurrence of peloid mudstone-wackestone above oolitic grainstone and beneath tidal flat facies suggest shallow near-shore restricted lagoonal settings, as in Shark Bay and the Arabian Gulf and in the Pleistocene of the Gulf (Wagner and Togt 1973; Hagan and Logan, 1974; Darwish and Conley, 1989). The foraminiferal assemblage indicates water depths less than 6 m (Al-Enezi, 2006) and *Sorites* could indicate some seagrass cover. More mud-prone facies formed in lower energy parts of lagoons, with high mud production or accumulation, whereas the more grainy facies developed in more shallow, slightly higher energy settings, perhaps near margins of lagoons (Hughes and Keij, 1973). Fine-grained quartz likely was blown into the lagoons (Shinn, 1973; Warren, 2006) and the abundant fine peloids formed by microbial micritization and recrystallization of fine skeletal debris or ooids.

Oolitic grainstone, variably quartzose (agitated hypersaline shoal or tidal bars)

This facies is tan and 20 cm – 1 m thick, and commonly caps sandy peloid packstone and grades up into peloid packstone- mudstone (Figure 2.9 f and n). Beds commonly are upward-fining, and some have bidirectional cross-bedding and horizontal layering. They are composed of fine-to-coarse sand-size ooids, sand- and less common gravel-sized mollusk, variable amounts of

quartz (from 0 to 10 per cent) and rare gravel-sized ooid-grainstone intraclasts.

The oolitic carbonates formed on beaches, oolitic sand-flats and tidal bars analogous to those forming today in Shark Bay and the Arabian Gulf (Loreau and Purser 1973; Hagan and Logan, 1974; Darwish and Conley, 1989; Alsharhan and Kendall, 2002). The thinness of most of the oolitic units suggests that they did not form oolitic barriers, but rather were thin oolitic caps on sublittoral peloidal sand sheets or were oolitic beaches (Loreau and Purser, 1973).

Mollusk packstone – rudstone (Border of hypersaline shallow- moderately deep embayments)

Mollusk packstone-rudstone forms tan to dark tan, 20 cm – 1.5 m units that are generally structureless (Figure 2.9 g and o), or have burrow mottles of coarse quartz sand and may be capped by hardgrounds. They are dominantly composed of abundant medium sand- to gravel-sized whole and lesser-fragmented monospecific bivalve and gastropod (as molds), rare crab, some peloids, rare oolitic clasts and minor lime mud. Foraminifera include *Elphidium* and *Triloculina*.

These moldic shelly packstone-rudstones formed within fair weather wave base, as shallow sublittoral shell beds analogous to those bordering hypersaline embayments in Shark Bay, occupied by monospecific dwarf mollusk accumulations of *Fragum hamelini* (Logan and Cebulski 1970; Hagan and Logan, 1974). Presence of *Triloculina* species is compatible with shallow to moderately deep hypersaline settings (Al-Enezi, 2006).

Foraminiferal-mollusk packstone-grainstone (Seagrass meadows)

These foram mollusk packstone-grainstones (Figure 2.9 h and l) are tan, 0.5 – 2 m thick, massive units composed of poorly sorted fine- to coarse-sand-size whole- and fragmented mollusks, foraminifera and peloids, along with interstitial lime mud (in packstones); some are

patchily cemented with calcite (lining moldic mollusks or as rim cements on echinoderm grains). Benthic foraminifera include: *Elphidium* spp., *Reophax* spp., *Archaias, Sorites sp., Peneroplis, Nonion, Quinqueloculina* spp., *Triloculina* spp., *Spiroloculina* spp*., Miliolid,* Borelis *melo melo*, rare *Ammodiscus* sp., *Ammonia* spp., rare *Alveolinella* sp., rare *Textularia* spp., rotalids, and rare *Cibicides* spp. Other fossils included gastropods, bivalve, echinoid fragments, brachiopods, and ostracods.

This facies and biota is analogous to shallow open marine facies on the Pearl bank barrier of the modern Arabian Gulf (Wagner and Togt, 1973), beneath seagrass meadows in shallow lagoons in the Arabian Gulf (Al-Enezi, 2006), and on sea grass banks in Shark Bay (Davies, 1970; Hagan and Logan, 1974), although red and green algae are notably lacking. Slight restriction is inferred from the presence of *Spiroloculina* and *Triloculina* specis (Al-Enezi, 2006), which is compatible with metahaline salinities, using the Shark Bay analog where seagrasses are well developed in salinities of 40 to 50 p.s.u. (low metahaline) dying off as waters become hypersaline (Logan and Cebulski 1970; Hagan and Logan 1974).

Skeletal peloid mudstone, wackestone, packstone, variably quartzose (Shallow to moderately deep lagoon to low energy shelf)

Variably quartzose, skeletal peloid mudstone-packstones are gray to pale tan units 30 cm to 1 m thick that are structureless to locally burrow-mottled, and some are laminated at the top. They are composed of silt-to-medium sand-size peloids, medium – very coarse skeletal grains and variable amounts of silt- and fine-sand size quartz. They also may contain rare gravel-size clasts of green or black-rimmed claystone, bored phosphatic carbonate hardground and locally granule-size lime mudstone. Foraminiferal species include: *Elphidium* spp*., Quinqueloculina*

spp., *Miliolid,* and *Nonion.* Other fossils include whole and fragmented gastropod, bivalve, brachiopod, dasyclad alge and bryozoa.

Skeletal peloid mudstone, wackestone and packstone probably formed in low to moderate energy open marine lagoons between fair weather and storm wave base on the ramp. In the modern Arabian Gulf, analogous facies occur just seaward of mollusk grainstone in coastal lagoons, intermediate lows and on the deeper ramp in areas where winnowing is less efficient (Wagner and Togt, 1973; Hughes and Keij, 1973; Gischler and Lomando, 2005). The fossil assemblage indicates shallow to moderate water depths up to 18 m (Al-Enezi, 2006).

SEQUENCE STRATIGRAPHY

The Miocene succession in the study area was divided into *depositional sequences,* that is, genetically related successions of strata bounded by unconformities (sequence boundaries) or their correlative conformities. They are composed of parasequence sets and parasequences arranged in systems tracts in which the maximum flooding surface separates the transgressive and highstand systems tracts (Mitchum and Van Wagoner, 1991). Given the updip position of the Lidam study area on the Arabian platform, low stand systems tracts are unlikely to be present.

Most sequence boundaries in the succession are characterized by evidence of local to regional exposure. Where evidence of exposure was lacking the sequence boundaries were placed at tops of shallowing-upward successions, beneath deepening upward units. Maximum flooding surfaces were placed within or at the base of the deepest water facies in a sequence. The depositional sequences were broken into major sequences, which in turn are composed of high frequency sequences. The various scales of sequences are composed of individual parasequences which are genetically related beds bounded by marine flooding surfaces; they are

bundled into parasequence sets (Mitchum and Van Wagoner, 1991).

Hadrukh Formation Sequence Stratigraphy

Sequences and parasequences are difficult to map regionally in the Hadrukh Formation (Figures 2.10; Appendix A), because of relatively monotonous facies, lateral facies changes, and lack of regional marker beds.

Hadrukh Formation parasequences

The basic types of parasequences in the Early Miocene (Aquitanian) Hadrukh Formation are illustrated in Figure 2.11. They range from 1 to 8 m thick and are dominated by unconsolidated very fine- and fine sand with lesser medium sand, but each has a distinctive type of capping facies either related to lithologic change (fining) or diagenetic overprinting on the parent siliciclastic unit. The Hadrukh parasequences are laterally highly variable and difficult to trace between cored wells.

Incipient paleosol-capped parasequences: These consist of medium sand locally at the base, with very fine- and fine sand locally with rip-ups of calcareous sandstone, making up the bulk of the cycle (Figure 2.11 A). The cap is incipiently brecciated sandstone with rootlet traces. These caps result from incipient pedogenic brecciation on exposure.

Mudrock-capped parasequences: These consist of very fine-to-fine sand that is locally calcareous at the base and capped by gray-green and red mudrock, which is locally pedogenically altered with rootlet traces (Figure 2.11 B). These mudrock caps were formed in supratidal to coastal plain settings, in which waterlogged areas were sites of gray-green mudrock deposition while well-drained emergent areas were sites of deposition of red mudrock that

became pedogenically altered during emergence.

Gypseous sand-capped parasequences: These very fine-to-fine sand parasequences have interstitial fine-grained gypsum that commonly increases upwards or is confined to upper parts of parasequences (Figure 2.11 C). Lower parts may contain interstitial carbonate. Rarely the sands are burrowed and rooted. Locally fibrous gypsum fills sheet cracks. Rarely, quartzose lime-mudstone (lacustrine?) clasts occur in lower parts of cycles. These parasequences formed in marginal sandy palustrine settings, in which interstitial pore waters gradually became more saline, causing fine-grained gypsum to be deposited interstitially in sands in upper parts of cycles.

Carbonate-capped parasequences: Carbonate-capped parasequences consist of very fine to fine sand, rarely with clay rip-ups at the base, capped by a thin (less than 1 m) sandy lime mudstone, sandy dolomudstone or limy sandstone (Figure 2.11 D). Some caps may be laminated, or incipiently brecciated, overprinted with incipient caliche fabrics and infiltrated by clay. Rare caps are underlain by rooted silicified mudrock. These limy sand-capped parasequences probably formed in marginal ephemeral lakes in which wind-blown sand was initially deposited. With shallowing, sand was admixed with carbonate mud precipitated on the lake floor, or fine carbonate was precipitated within the sands. On emergence, caps were brecciated and overprinted with caliche fabrics.

Brecciated sand/sandy lime wacke parasequences: These consist of very fine to coarse sandy wacke and limy sand with abundant lime matrix (>30% locally with clasts of brown claystone) (Figure 2.11 E). The caps are incipiently to highly brecciated sandy lime wacke locally with lime-mudstone clasts, rare zones of leached thin mollusk shells, along with sheet cracks, rootlet

traces and rhizoconcretions. Rarely they consist of thick (up to 10 m) zones of brecciated sandy carbonate with coated grains and pisolite, containing clay-filled rootlets. The brecciated intervals commonly extend through several parasequences. These formed in marginal ephemeral lakes in updip (palustrine) settings, in which lime mud was admixed with an eolian sand component. These ephemeral lake deposits were repeatedly brecciated and locally overprinted with caliche fabrics during successive emergence events.

Hadrukh Formation depositional sequences (Aquitanian)

The Early Miocene (Aquitanian) Hadrukh Formation forms an unconformity bounded 3rd order sequence (Figure 2.3). It is dominated by siliciclastics, with a major unconformity at the base on the Eocene Dammam Formation carbonates, and a smaller unconformity at the top on the Hadrukh Formation beneath Dam Formation carbonates (Figures 2.3 and 2.10). In the study area, the Hadrukh Sequence is relatively thin *updip* (56 m thick in SC-4), then thickens slightly to 67 m into a *central depression* (beneath SC-2) and then thins to 52 m over a *downdip high* in the northeast (SC-1).

Subdivision of the Hadrukh Formation into sequences is difficult. However eight high frequency sequences (HFS) were tentatively recognized, labeled Mhk 1 to 8 (Figure 2.10), which are summarized in Table 3. The HFSs were recognized on the basis of paleosols at the base, and the presence of gypseous, calcareous or dolomitic sands and/or red beds in the late HST. Maximum flooding surfaces were hard to define in these siliciclastic successions, and so systems tracts were not picked. The HFSs thus are discussed in terms of sequence boundaries and component parasequences.

The high frequency sequences appear to be bundled into two larger scale sequences Hd 1

and 2. These are separated by regional gypseous sand, overlain by thick clay-clast conglomeratic sands downdip (Figure 2.10).

High frequency sequence boundaries, Hadrukh Formation

The boundaries of the HFSs in the Hadrukh Formation are characterized by local to regional exposure surfaces evidenced by incipient paleosols, red mudrock, brecciated clastic-prone and carbonate-prone facies, and dissolution features filled with infiltrated siliciclastic sediment. Four main types of HFS boundaries have been recognized in the Hadrukh Formation (Figure 2.10): They include the following types. Sharp irregular contacts on sandy dolomitic mudstone or dolomudstone as at the base of Mhk 3 in SC-2. Sharp erosional or irregular contacts on top of fitted fabric brecciated calcareous sandstone, or calichified sandstone (paleosol) as at the base of Mhk3, 4, and 6 in SC-1. Sharp erosional contacts on top of gypseous quartz sandstone or gypseous wacke such as occur at the base of Mhk8 in SC-2, the base of Mhk5 in SC-1 and 8,base of Mhk1 in SC-1, base of Mhk4 in SC-1 and 8. Sharp contacts on terrigenous red mudrock beneath quartz sandstone such as occur at the base of Mhk 7 and 8 in SC-1.

Transgressive and Highstand System Tracts of Hadrukh High Frequency Sequences

High frequency sequence Mhk1 contains two paleosol-capped sandy parasequences updip. In the central depression the parasequences are gypseous sands capped by mudrock. Downdip there are numerous clay-clast conglomeratic sandstones within two gypseous sand-capped parasequences in which gypsum abundance increases upward.

High frequency sequence Mhk2 has numerous incipient paleosol-capped parasequences updip. These pass downdip into several dolomudstone-capped parasequences in the central

depression. Further downdip over the high, there are four parasequences that have well developed caliche caps with abundant calcareous nodules and incipient brecciation.

High frequency sequence Mhk3 updip has a set of poorly defined sandy parasequences of mottled friable sand grading up into limy sand and then a thin red mudrock with calcite nodules and spar-filled sheet cracks. It is difficult to trace the upper HFS boundary into the central depression (poor core recovery of sands), but the unit splits into a set of three thinning-up gypseous sand-capped parasequences in SC 8 and then over the downdip high (SC-1) it has a thinning-up set with a lower thick sandy parasequence capped by mudstone and a thin upper carbonate mudstone-capped parasequence.

High frequency sequence Mhk4 updip has a set of several sandy and sandy lime wacke parasequences, which pass into the central depression into a poorly cored set of limy sands capped by sandy gypseous wacke. These pass downdip into a set of two to three sandy parasequences that are capped by sandy gypseous wacke.

High frequency sequence Mhk5 updip consists of several very limy sand parasequences capped by sandy lime wacke with numerous exposure features; in places the parasequence set is heavily brecciated, which has made it difficult to define the upper boundary of Mhk-5. In SC2 only a portion of a single sandy parasequence can be recognized comprising Mhk5. Downdip (in SC 8), Mhk5 has a set of 3 thin sandy parasequences that have limy lower parts and gypseous upper parts, the upper parasequence being capped with red-gray mudrock. Further downdip, there is a single parasequence with a thick, basal clay-clast conglomeratic gypseous sandstone passing up into gypseous sand- and mudrock, the gypsum decreasing upward.

High frequency sequence Mhk6 updip is dominated by limy sands, which are highly brecciated throughout. This made picking parasequences and defining the top of the sequence

updip difficult. In the central depression, it is slightly limy, gypseous sand. Downdip in SC-8 and 1, it consists of a parasequence of limy sand/sandy lime wacke capped with thin sand, overlain by a thick sandy parasequence capped by gypseous sand in SC-8 and redbeds in SC-1.

High frequency sequence Mhk7 updip is within the brecciated limy sand interval. In the central depression Mhk7 is a sandy parasequence, limy at the base and gypseous upward. Downdip in SC-8 there is a basal sand parasequence capped with mudrock, and two mudrock parasequences capped by red mudrock paleosols.

High frequency sequence Mhk8 updip lies within the brecciated limy sand zone, which pass downdip into parasequences of sands capped with faint erosional surfaces. These parasequences become limy downdip in SC-8, and pass into two paleosol-capped sand-parasequences, overlain by a mudrock parasequence with a capping paleosol.

Dam Formation Sequence Stratigraphy (Late Aquitanian to Early Langhian)

The facies and sequence stratigraphy of the Dam Formation is shown on the cross section (Figure 2.12) and the selected column (Appendix C). The sequence stratigraphy of the outcrops is shown in Figure 2.13. The unconformity separating the Dam Formation from the underlying Hadrukh Formation is probably relatively small (less than 1 m.y. duration; Figure 2.3). There are eight disconformity-bounded sequences in the Late Aquitanian to Early Langhian Dam Formation that are regionally mappable through the study area (Figure 2.12), and are summarized in Table 4. The Dam sequences appear to be bundled into a composite sequence. The lower sequences are siliciclastic-dominated and the siliciclastics progressively backstep in the lower Dam Formation and then step basinward in the upper Dam Formation (Figure 2.12). The depositional sequences in the Dam Formation were labeled Md1 to Md8, and the parasequence sets were labeled PS-1 to 26. The basic types of Dam parasequences are shown on

Figure 2.14.

Parasequences within the Dam Formation

Five basic types of parasequence occur in the Dam Formation (Figure 2.14), and are defined on the facies in the lower part of the parasequence, as these marks the intensity of the flooding event. Typical parasequences are outlined below with the caveat that one or more of the facies may be missing. The parasequences average about 3 to 3.5 m thick, and are bounded by marine flooding surfaces, which in some parasequences is superimposed on a disconformable or erosional surface, especially updip.

Open marine parasequences: These (Figure 2.14 A) consist of (1) locally developed transgressive, thin lime-clast rudstone lag or sandy marl, (2) peloid skeletal wackestone-packstone, locally with clay intraclasts (sub-fairweather wave base) passing up into skeletal grainstone (open marine, above fairweather wave base shoal), (3) laterally discontinuous ooid grainstone (oolitic shoal/channel fill), (4) fine grained carbonate laminite (tidal flat) or gray to red mudrock (paleosol), capped by (5) disconformity and/or marine flooding surface.

Offshore-lagoon parasequences: These (Figure 2.14 B) consist of (1) basal, lenticular limy sand, or sandy clay-intraclast rudstone, (2) sandy marl, with sand decreasing upward, (3) peloid skeletal fragment wackestone/packstone (lagoon), grading up into peloid-skeletal packstone or cross-bedded grainstone (lime sandflat), (4) locally developed sheet-like to channelized ooid grainstone, (5) microbial carbonate laminite and or red mudrock capped by (6) disconformity or marine flooding surface.

Nearshore-lagoon parasequences: These (Figure 2.14 C) consist of (1) common basal sand, (2)

fining upward sandy marl with quartz sand decreasing or less commonly increasing upward, (3) carbonate laminite or less commonly, red mudrock capped by (4) disconformity or marine flooding surface.

Marginal marine parasequences: These (Figure 2.14 D) are dominated by siliciclastics and include sandy parasequences and mudrock parasequences. *Sandy parasequences* commonly consist of (1) sand (1.5 to 5 m), typically massive, less commonly laminated to cross bedded, locally gypseous, fining up into, (2) cream or gray marl commonly overprinted by pedogenesis, and (3) disconformity or marine flooding surface.

Mudrock parasequences: (Figure 2.14 E) these typically consist of (1) thin basal sand, sharply overlain by, (2) gray mudrock capped by, (3) thin unit of either laminated thin sandstone (locally with clay clasts), skeletal wackestone or carbonate laminite (any of which may be overprinted by pedogenesis, and (4) disconformity or marine flooding surface.

Most parasequences in the Dam Formation are easily defined downdip but are not easily traced updip into the siliciclastic-dominated sections. In the Dam succession, there are roughly equal numbers of transgressive-regressive parasequences (deepening upward followed by shallowing upward) versus simple shallowing upward parasequences. The Dam sequences have 3 to 4 parasequences downdip except for sequence Md 3 which has only 2 parasequences downdip. The sequences have fewer (1 to 2) parasequences updip. The parasequences average 3.5 m thick updip, where most are capped by disconformities. Downdip, the parasequences are only slightly thinner (average about 3 m) and their tops are relatively conformable. In sequences Md 1 to 5, parasequences in the TSTs are thicker than the parasequences in the HSTs. In contrast, in sequences Md 6, 7 and 8, the parasequences in the TSTs are thinner than those in the

HSTs.

Sequence boundaries, Dam Formation

Sequence boundaries in the Dam Formation are characterized by local to regional exposure evidenced by red mudrock paleosols, fitted-fabric carbonate breccia, small-scale karst features and sand-filled channels which in outcrop are incised into underlying facies (Figures 2.12 and 2.13). Where evidence of exposure is lacking, sequence boundaries were placed at tops of shallowing-upward successions beneath deepening upward units. The Dam sequence boundaries are traceable throughout much of the study area. Sequence boundaries on carbonate units commonly are characterized by a sharp contact on carbonate laminite (tidal flat facies) of the underlying sequence. They are typically overlain by marl or locally by sandstone, for example at the bases of sequences Md 1, 2, and 3 (Figures 2.12 and 2.13). Sequence boundaries on red mudrock (commonly a paleosol) are sharp erosional contacts generally beneath sand, for example at the base of sequences Md 4, 5 and 8 (Figures 2.12 and 2.13). Local relief on the erosional sequence boundaries and incision-surfaces beneath sands in outcrop is up to 2 m (Figure 2.13), but was not able to be determined for the sequence boundaries in core. However, significant erosion of mudrocks beneath sequence boundaries is suggested by abundant mudrock clasts eroded from subjacent units and incorporated into many of the basal sands of the Dam sequences.

Lowstand System Tracts, Dam Formation

Lowstand system tracts were not recognized in the study area. These likely developed far downdip of the study area, in more rapidly subsiding parts of the basin beneath the present-day Arabian Gulf and on the Miocene paleo-shelf bordering the Arabian Sea.

Transgressive System Tracts, Dam Formation

Transgressive system tracts (TSTs) in the lower parts of sequences include a portion of a parasequence to four parasequences (Figures 2.12). Updip units within TSTs of Md 1 to 3 have increased terrigenous mud and sand in the carbonates compared to downdip. The TSTs of Sequences Md 1 to 3 are characterized by carbonate-prone parasequences that become progressively more open-marine upward. They commonly have a locally developed basal marl and grade upward into peloid wackestone (lagoon) and then into more open marine skeletal packstone-grainstone, along with upward decrease in the siliciclastic component and dolomite.

The TST of sequence Md 4 is siliciclastic-prone updip, with thick estuarine- or fluvial sandstone grading up into peloid packstone (lagoon) (Figures 2.12). Downdip the TST is carbonate-prone and composed of a siliciclastic estuarine-fill grading upward into lenses of oolitic grainstone, laminated peloid mudstone (tidal flat) to peloid packstone (lagoon). In outcrop, microbial bioherms (mounds) up to 5 meters thick, with domal tops and clotted to structureless fabrics occur in the TST of sequence Md 4 (Figure 2.13; Alkhaldi, 2009).

The TSTs of sequences Md 5 and 6 contain widespread basal quartz sands that thin downdip. Local thin red beds and paleosols cap some of the basal sands (Figures 2.12). Basal quartz sands are absent from Md 7, but are developed updip in Md8. The remainder of the TSTs in sequences Md 5 to 8 deepen up into lagoonal marl and muddy carbonates. Downdip, they contain more open marine skeletal fragment-wackestone and packstone. The TSTs of sequences Md 7 and 8 appear to pinch out downdip onto the sequence boundary.

Maximum flooding surfaces, Dam Formation

Maximum flooding surfaces were placed beneath the deepest water facies in the

sequences (Figures 2.12). In sequences Md 1, 2, 4, 5, and 7 the maximum flooding surfaces occur near the base of open marine skeletal fragment grainstone. The most regionally developed and most distal open marine carbonate facies in the Dam Formation occur in sequence Md 5 within parasequence 14 (PS14; Figures 2.12). This would appear to coincide with the maximum flooding surface of the Dam-Hofuf composite sequence. Maximum flooding surfaces in sequences Md 3, 4, 7, and 8 occur within or at the base of skeletal peloid wackestone-packstone (lagoonal or offshore facies). The MFS in sequence Md 6 was placed at the base of an extensive but thin updip sandy marl that grades downdip into marl.

Highstand System Tracts, Dam Formation

The HSTs in the Dam sequences are composed of from 1 to 11 parasequences, the number typically decreasing updip. Within the HST, the parasequences are bundled into from 1 to 3 parasequence sets (Figures 2.12). The updip portions of the HST of sequences Md 1, 2, 3, and 5 are mixed carbonate-clastic systems. In contrast, updip the HST of sequences Md 4, 6, 7 and 8 are siliciclastic-prone albeit with carbonates in some of the early HST. Downdip, the HST are carbonate-prone in sequences Md 1 to 4 whereas the younger sequences Md 5 to 8 are siliciclastic-prone, and successively pass from thick, dark gray shale-dominated units (sequence Md 5) to mixed gray and red mudrock (Md 6 and 7) and finally to red mudrock- and paleosol-dominated units (Md 8; Figures 2.12).

Within the downdip carbonate-prone HSTs of sequences Md 1 to 3, open marine skeletal carbonates are common, passing updip into more restricted muddy carbonates. Skeletal carbonates are rare in the carbonate-prone HST of Md 4, which has more common lagoonal mudstones, peloidal and oolitic grainstones. Within the siliciclastic-prone highstands of (sequences Md 3 to 8), open-marine carbonates are confined to downdip areas in the early HST

of sequences Md-5 and 8, and locally in sequence Md-7.

Carbonate laminites (tidal flat facies) cap the HSTs in sequences Md 1 and 2. Red mudrock which overlies carbonate laminites, cap sequences Md 3 and 4. Red mudrock (paleosol) overlying quartz sand caps sequences Md 5, Md 6, Md 7, and Md8.

Hofuf Formation Sequence Stratigraphy (Langhian)

The Middle Miocene (Langhian) Hofuf Formation (Figures 2.3 and 2.15) is up to 95 m thick, but has limited core coverage, with 22 m of the basal part from SC-4 updip and only the basal 4 m from SC-2 and SC-1 downdip, thus only the basal one-fifth of the formation was cored. The overlying sandy limestone, sandstone and thin capping sandy nodular limestone units described from outcrop by Steineke et al. (1935) are shown in Figure 2.15. According to Sharland et al. (2004) the Hofuf Formation is bounded at the base by a major unconformity on the Miocene (Burdigalian) Dam Formation (as on the structurally high Qatar area (Dill et al., 2005). Howerver, Haq and Al Qahtani (2005) show the Hofuf Formation as being conformable on the Dam Formation. In the study area, it seems likely that the Hofuf Formation disconformably overlies the Dam Formation with a relatively short time break (Figure 2.3). Within the cored interval of the Hofuf Formation, two high frequency sequences (Mhf 1 and 2) and part of a third sequence were recognized provisionally (Figure 2.15).

The basal boundary of *Mhf 1* is a regional sharp irregular erosional contact on top of regional red mudrocks of the Dam Formation, beneath Hofuf conglomeratic quartz sandstone. Mhf1 is about 8 m thick, with clay- and sand-clast conglomeratic sand forming the lower parts of the basal three parasequences. The lower two parasequences are capped by thin redbeds, while the upper parasequence is capped by rooted clayey sandstone.

The basal boundary of *Mhf-2* is a sharp contact on white rooted clayey quartz sandstone. *Mhf2* is about 10 m thick and contains up to 6 sandy parasequences, the lowermost one having a basal lag of mud- and sand-clasts at the base of 60 cm thick sandy argillaceous lime mudstone. Most of the parasequences have basal sands containing clay- and sandstone rip-ups. Thin limy sands cap some parasequences; while the uppermost parasequence is capped by a heavily rooted clayey gypseous sand that. Only the basal 3 m of *Mhf 3* was penetrated in core, and consists of massive slightly calcareous sand.

DISCUSSION

Accommodation

Estimates of ages and durations of the formations (Figure 2.3) were based on the latest geologic time scale (Gradstein et al., 2004), oxygen isotope curves (Billups et al, 2002; Pekar et al., 2002; Pekar and DeConto, 2006), timing of global 3rd order sequences (Hardenbol et al., 1998), glacial events (Miller et al., 1991; Abreu and Anderson, 1998), maximum flooding events (Sharland et al., 2004), and referenced to the calculated eccentricity and obliquity curves (Laskar et al., 2004). The accommodation rates (in cm/k.y.) calculated by dividing the thickness of the formation (in centimeters) by duration (in kiloyears), are dominantly the product of long-term subsidence rates modified by long term changes in sea level, The Hadrukh Formation is estimated to be 1.6 m.y duration, and given its thickness of 65.5 meters, this suggests accumulation rates of ~ 4 cm/k.y. The Dam Formation is estimated to be 7 m.y duration, and given its thickness of 79 meters this suggests accumulation rates of ~1 cm/k.y. The Hofuf Formation is estimated to be 3.6 m.y duration and assuming a total thickness of ~100 m in the region, subsidence rates were under 3 cm/k.y.

Thus subsidence rates in the study area were relatively low (1 to 4 cm /k.y.) during Miocene deposition, which is supported by the relatively flat slopes on the geohistory plots of eastern Arabia (Abu-Ali and Littke, 2005). These low subsidence rates reflect the updip position of the study area on the distal foreland. Subsidence rates increased markedly into the foreland basin toward the Zagros fold-thrust belt, where the Miocene to recent succession is almost five times as thick as in the study area (Figure 2.4; Bahroudi and Talbot, 2003). This foreland basin subsidence probably was largely due to thrust-sheet loading of the Arabian foreland, coupled with water- and sediment- loading. The low accommodation in the study area is reflected in the numerous unconformities in the post-Eocene to Miocene succession and the dominant shallow water facies.

Structural Controls on Lidam Embayment

Major anticline structures in the area were controlled and affected by basement uplifts of complex horst blocks with step-faults trending NE (Henson, 1951; Edgell, 1992). However, some of the growth of the structures could be associated with slow growth of basement-induced salt-wall diapirs (Sugden, 1962). The Ghawar, Abqaiq and other anticline structures in the region have a long history as subtle positive features (Abu-Ali and Littke, 2005). These uplifts were intermittently reactivated until at least Mid-Tertiary time (Edgell, 1992).

Thinning of the Early Miocene Hadrukh Formation toward En Nala (Ghawar) anticline (well SC-4) compared to Hadrukh sections off-structure (wells SC-2 and SC-1) indicates Early Miocene growth of the Ghawar anticline. Given that the span of Hadrukh formation is about 1.6 m.y duration and the difference in Hadrukh thickness between crestal and flank wells is about 10 meters, implies a slow growth rate of ~0.7 cm/ k.y. in the Early Miocene, which maintained this feature as a subtle positive high relative to the downdip areas.

The study area appears to have developed within an elongate embayment that developed on the Eocene surface as a result of gentle post-Eocene warping, coupled with basement faulting and or salt tectonics (Figure 2.5 A and B). It is likely that Cenozoic growth of the En Nala and Abqaiq anticlines during the later Cenozoic formed structurally positive areas bounding the embayment to the west and southeast. This resulted in the embayment being open to the north via a narrow strait connecting it to the ancestral Arabian Gulf. Warping continued into the Miocene, which is indicated by significant thickening and thinning of the Miocene Hadrukh and Dam formations within the study area and environs (Figure 2.5 A and B). The thinning evident over the medial high within the central depression of the embayment probably is associated with folding and faulting that caused the up warp to resist subsidence compared to the surroundings. This up warp and one immediately to the north parallel the Zagros trend, and the northern up warp probably partially barred the embayment.

Given the limited outcrop and core control, the regional facies cannot be mapped throughout the study area, but based on modern analogs along the Gulf coastline today, it is likely that the depositional strike tended to parallel the contours of the embayment (outlined by the top-Eocene structure; Figure 2.6). This would have resulted in paleostrike wrapping around the margins of the embayment, and becoming more open marine into the central depression and to the north, toward the narrow strait connecting the study area to the ancestral gulf.

The regional paleoslope was to the northeast, which would have governed the southwest to northeast transport direction of siliciclastics into the study area. Local topography on the Eocene and subsequent younger surfaces would have been controlled by structure, and by erosional incision by streams. Assuming some inheritance of structure, this suggests that during siliciclastic phases, during lowered sea levels a regional ephemeral stream system may have

entered the embayment from the southeast and exited via the northern strait

Ages and Duration of Sequences and Cycles

Estimates of likely ages and durations of component sequences within the formations, which are below resolution of the biostratigraphy, were estimated using published sea level curves based on oxygen isotopes that are relatively well constrained in terms of time (Figure 2.3; Abreu and Anderson, 1998; Billups et al., 2002; Pekar and DeConto, 2006), with the time scale adjusted to that of Gradstein et al. (2004). This assumes that the relatively rapidly changing glacio-eustatic signal was the dominant signal recorded in the stratigraphy, and overpowered any slow subsidence/uplift on the distal foreland. Such a strong eustatic component overwhelming the tectonic signal at the high frequency sequence scale has been documented in Paleozoic foreland basin successions in North America (Pope and Read 1997; Al-Tawil et al., 2003).

To estimate the duration and ages of the Hadrukh and Dam sequences within the study area in the absence of Sr isotope dating or refined biostratigraphy, three oxygen isotope curves were used as a proxy for base-level changes driven by sea level, the generalized oxygen isotope curve of Abreu and Anderson (1998) and the oxygen isotope curves of Billups et al. (2002) and Pekar and DeConto (2006; Figure 2.3). The sea level scale from Miller et al. (2011), used a $d^{18}O$ value of $1‰_{PDB}$ equal to ~40 m of sea-level change. Unfortunately there is considerable variation between the oxygen isotope curves, perhaps related to local bottom water conditions at the time and problems in dating, all of which increase the uncertainty in using the curves for dating the sequences. For the Dam sequences, deposition was assumed to start just below the highstand position. Paths of subsidence (using 1 cm/k.y.) for the Dam Formation were drawn (inclined lines sloping down to top right on Figure 2.3, and the measured thickness of each 3rd order sequence was added to shallow up to intersect the sea level curve. Non-deposition was assumed

to occur when sea level was below the platform surface, and marine deposition was assumed to have occurred when sea level was above the platform surface. For each sea level curve, this then defined the possible timing of deposition versus non-deposition in the succession within the study area. Using data from all the curves helped bracket the possible ages of the units (Figure 2.3).

These age estimates are supported by the carbon isotope profiles from the Miocene succession in the study area (Chapter 3). Distinctive C-isotope excursions can be correlated with the successions in the lower Dam Formation in nearby Qatar (Dill et al., 2005, 2007) and the middle Dam formation in UAE (Peeble et al., 1999). The Qatar and UAE sections have Sr isotope dates, which tie them to the absolute time scale. Confirmation of the correlations in the study area need to be confirmed by $^{87/86}$Sr dates. This is possibly complicated by the terrigenous clays and fine terrigenous clastics admixed within the carbonate sediments, which because of decay of ^{87}Rb to ^{87}Sr, could raise the $^{87/86}$Sr value giving an age that is too young (Banner, 1995).

Given 9 Ma for the duration of the Aquitanian to Serravallian interval (Gradstein et al. 2004), the 8 sea level cycles of Abreu and Anderson (1998) within the interval suggest average durations of 1.1 Ma / cycle. Taking another route, there are a total of 2 sequences in the Hadrukh and 8 sequences in the Dam formations combined, spanning a total time of 9 Ma, suggesting a periodicity of about 0.9 Ma. Thus this suggests that the Hadrukh-Dam sequences span between 0.9 and 1.1 Ma. This is suggestive of the long-term obliquity cycle of 1.2 Ma (Boulila et al., 2011), which typified the Cenozoic prior to major Pleistocene bi-polar glaciation. These cycles are related to cooling associated with the pronounced 1.2 Ma obliquity nodes, which result in buildup of ice sheets and sea level lowering.

Miocene Cooling and Warming Events and Glacio-Eustasy

The oxygen isotope record from deep ocean sediments indicates a gradual cooling in global climate during the Late Eocene-Early Oligocene (~36 Ma) following the initiation of major Antarctic continental ice-sheets (Prentice & Mathews, 1988; Kennett and Barker, 1990; Barron et al., 1991; Ehrmann, 1991; Denton et al., 1991; Miller et al., 1991; Hambrey et al., 1991; Abreu & Anderson, 1998; Zachos et al., 2001). The increasingly positive, Miocene to Recent $d^{18}O$ record from deep ocean sediments marks the significant expansion of the Antarctic ice-sheets during the Miocene culminating in biopolar glaciation in the Pleistocene. The oxygen isotopes record a number of Miocene cooling events within the study interval (Figure 2.3), which are defined by positive excursions of $\delta^{18}O$; these events include Mi-1 (23.2 Ma), Mi-1a (21.2 Ma), Mi-1aa (20.4 Ma), Mi-1ab (18.4), Mi-1b (17.8), Mi-2 (15.8 Ma), Mi-3a (14.3 Ma), and Mi-3b (13.8 Ma) (Miller et al., 1991; Pekar et al. 2002; Pekar and DeConto, 2006). The last two events in the early middle Miocene mark pronounced expansion of the Antarctic ice-cap leading to its permanent existence, significant cooling of bottom waters and establishment of the modern thermohaline pattern of bottom water circulation (Miller et al., 1991; Wright et al., 1992; Flower and Kennett, 1995). The overall cooler climate in the Middle Miocene was interrupted from 17 to 15 Ma by a significant warm phase, the Middle Miocene climatic optimum that peaked at 15 Ma (Figure 2.3; Vincent and Berger, 1985; Flower and Kennett, 1995; Pekar at al., 2002).

Using the Sr dating and the biostratigraphically constrained formation ages and estimated ages of the component sequences, it is perhaps possible to tie the sequence framework to the major Miocene events which are shown in Figure 2.3. In the following discussion, sequence boundary refers to the *basal* boundary of a sequence.

The Hadrukh sequence boundary correlates with Aq1 on the global curve and the cooling

event Mi-1, when the ice sheet was up to 25% larger than the present day (Pekar and DeConto, 2006). The global MFS event appears to lie within the upper sequence (Hd 2).

The sequence boundary (Md 1) of the Dam Formation likely developed during sea level fall coeval with sequence boundary Aq2 on the global chart, and the Mi-1a cooling event (21.2 Ma; Miller et al., 1991; Hardenbol et al., 1998; Pekar et al., 2002). This probably resulted from northward movement of Australia by 20 Ma, widening of the Australian-Antarctic seaway and development of the Antarctic circumpolar current that allowed polar cooling (Lawver and Gahagan, 2003). During Mi-1a, $\partial^{18}O$ values are consistent with an ice sheet up to 25% larger than the present day East Antarctic ice sheet (Pekar and DeConto, 2006). The MFS of Md1 probably formed during the Aq2 maximum flooding on the global chart.

Dam sequence boundary Md 2 may correlate with the sequence boundary and sea level fall of Bur1 of the global chart, which is synchronous with the Mi-1aa cooling event (20.4 Ma) (Miller et al., 1999) related to a heavily glaciated East Antarctica (Pekar and DeConto, 2006). The MFS of Md2 probably ties with the Ng10 (Sharland et al., 2004) flood, and coeval Bur 1 MFS on the global curve. The Dam Md 3 sequence boundary may correlate with the sequence boundary and sea level fall Bur 2. However the Md3 flood does not appear to correlate to any global event.

The Dam Md 4 sequence boundary likely developed during seal level fall associated with Mi-1ab glacial event (at 18.4 Ma; Miller et al., 1991; Pekar and DeConto, 2006) and likely correlates with Bur 3 sequence boundary. The Ng 20 (Sharland et al., 2004) MFS probably is the maximum flood within Md 4. The maximum flood Md4 may tie to low oxygen isotopic values at 18.4 Ma, which is consistent with a significant reduction of the east Antarctic ice sheet to less than 50% of present values (Pekar and DeConto, 2006). The Dam Md 5 sequence boundary

likely correlates with Bur 4 sequence boundary on the global curve, synchronous with the Mi-1b cooling event (17.8 Ma; Pekar and DeConto, 2006). During Mi-1ab and Mi-1b events (Md 4 and 5 sequence boundaries respectively), the total area of grounded ice on East and West Antarctica was 15-25% greater than today (Denton and Hughes, 2002; Huybrechts, 2002; Pekar and DeConto, 2006). The Md 5 flood appears to tie to the Bur3 flood.

The Dam Md 6 sequence boundary likely correlates with Bur 5 sequence boundary. The Dam Md 7 sequence boundary likely correlates with Bur 5 sequence boundary, and the Md7 flood with the Ng 30 (Sharland et al., 2004) flood. The Miocene warm phase would appear to span Dam sequences Md 6 and 7.

The Dam Md 8 sequence boundary likely developed during sea level fall associated with Mi-2 cooling event at 15.8 Ma (Miller et al., 1991; Pekar et al. 2002). This cooling was probably related to the collision of the Australia-New Guinea block with Southeast Asia around 15 Ma which blocked substantial equatorial transport of water from the Pacific into the Indian Ocean (Lee and Lawver, 1995). This resulted in a shift in current flow southward along eastern Australia and northward along the East Asia margin. This enhanced flow of the Antarctic Circum-polar current and allowed expansion of the East Antarctic ice-sheet (Lawver and Gahagan, 2003). The Md 8 MFS probably ties to Bur5/Lan1 flood (Hardenbol et al., 1998) and the Ng40 flood (Sharland et al., 2004) coeval with the Mid-Miocene Climatic optimum.

The hiatus between the Dam and the overlying Hofuf Formation may encompass glacial events Mi-3a (14.3 Ma) and Mi-3b (13.8Ma), the latter marking the end of the Langhian. The top of the Dam Formation probably correlates with the Mi-3a cooling event in the latest Langhian. The Hofuf formation probably formed in the earliest Serravallian during successive base level rises triggered by sea level rise. A hiatus of about 0.5 – 1 m.y between Dam and Hofuf

deposition is suggested by the data on Figure 2.3. Late Middle Miocene cooling in the Langhian through Serravallian is evidenced by the increasing $\delta^{18}O$ values, which would have been accompanied by lowered sea levels and non-marine deposition of Hofuf siliciclastics.

Milankovitch Orbital Forcing of Miocene Sea Levels

Milankovitch orbital forcing of earth's climate (Imbrie, 1979; Berger et al., 1992; Matthews and Frohlich 2002) is generated by periodic and quasi-periodic oscillations in Earth's orbital parameters that affect the distribution and amount of incident solar energy received by a region on Earth (Hays et al., 1976). *Eccentricity* is related to the elliptical orbit of the earth around the sun, which in conjunction with the inclination of the earth's axis causes variation in the intensity of the seasonal changes on Earth. Eccentricity has quasi-periods centered around ~100 k.y Berger et al (1992) and there is a long term periodicity at ~412 k.y as well as at 2.4 m.y. (probably the driver of many third order sequences (Matthews and Frohlich, 2002). *Obliquity* is related to the variation in the tilt of the earth's axis, which changes the latitudinal distribution of insolation, taking approximately 41 k.y to shift between a tilt of 22.1° and 24.5°. There are obliquity nodes at about 1.2 m.y, which correspond to minima of insolation resulting in ice buildup and sea level falls. These may have generated the ~1 m.y. third order sequences throughout much of the Cenozoic (Boulila et al., 2011). *Precession* is related to wobble of the earth's rotational axis coupled with gradual shift in the semi-major axis of the elliptical orbit, which results in modern precessional quasi-periods of 19 to 23 k.y. Periods of precession and obliquity become shorter back in time, but this decrease would be negligible by the Miocene, and eccentricity is fairly stable (Berger et al., 1992).

Spectral analysis of early Miocene deep-sea sediments shows that power in the 400 k.y. band is exceptionally pronounced (Zachos et al., 2001) with large amplitude (0.5 to 1‰) oxygen

isotope excursions suggestive of ~20 to 40 m sea level changes, even though Antarctica was minimally or only partially glaciated for much of the time (Zachos et al., 2001). The ~100 k.y and ~400 k.y cycles also are well recorded in the middle Miocene (Flower and Kennett, 1993). In addition, there is a strong obliquity signal in the Oligo-Miocene records (~ 41 k.y.), and a weak precessional signal (Zachos et al., 2001).

Sea level cycles and 3rd order sequences on the global chart for the Miocene (Hardenbol et la., 1998) appear to show a predominance of ~1 m.y. cycles, suggestive of the 1.2 m.y. obliquity cycles (Boulila et al., 2011). This suggests that major sequences in the Miocene of the study area were the result of 1.2 m.y. obliquity forcing of glacio-eustasy, controlled by waxing and waning of Antarctic ice sheets. This contrasts with the common 2.4 m.y. eccentricity forcing that strongly influences sequence development in greenhouse worlds (Boulila et al., 2011).

Miocene Climate

Antarctic glaciation occurred throughout the Cenozoic while northern hemisphere glaciation developed in the latest Neogene (Miller et al., 1987). This sequential cooling occurred as a series of abrupt shifts representing threshold events (Kennett, 1995), with increase in aridity accompanying this cooling trend in low latitudes (Shackleton and Kennett, 1975a).

The paleolatitude position of the Arabian Gulf during the Miocene was between 20 and 30 degrees north latitude (Scotese, 2001; Figure 2.15). Generalized paleoclimate reconstructions suggest that the Arabian Plate lay within an arid belt evidenced by evaporites and caliche (Scotese, 2001). This arid desert belt is suggested to have completely covered the Arabian Plate, and extended northeastward into Eurasia. It was bounded to the south by an African tropical ever-wet climate belt and to the northwest in Europe by a warm temperate belt. Scotese (2002) suggests that overall, Miocene climate in the region was broadly similar to today's climate, but

warmer. Early and Middle Miocene warm global climate is indicated by low $\partial^{18}O$ values of planktonic and benthic marine foraminifera (Haq, 1980) which are the lowest in the Neogene, reflecting the peak of Neogene warmth (Grobe et al., 1990; Kennett and Braker, 1990).

Fossil data (including vertebrate and plant fossils) and paleoclimate reconstructions suggest that the Early Miocene spanning the Hadrukh and lower Dam deposition may have been more humid than today (Andrews and van Couvering, 1975) with open woodland or bushland ecosystems containing fossil palms (Thomas et al., 1978; Thomas et al., 1982b; Whybrow et al., 1987; Kingston and Hill, 1999), with tropical to subtropical near-shore tidal flats and estuarine systems (Gentry, 1987b). Limited closed habitats occurred along river or lake margins (Kingston and Hill, 1999). The climate may have become drier open savannah in the late Early Miocene (Whybrow et al., 1982) with intermittent arid conditions being marked by gypseous sands in the Hadrukh Formation (this study) and thin evaporites at the top of the Early Miocene Dam Formation in Qatar (Whybrow, 1984; Kingston and Hill, 1999; Dill et al., 2005).

In the Middle Miocene, the climate appears to have become more humid, with open woodland, bushland and more forested landscapes inhabited by browsers (Thomas et al., 1982b), with palms and tropical mangroves fringing the shores (Hamilton et al., 1978; Whybrow and McClure, 1981). Intermittent arid to hyperarid conditions existed locally if not extensively at times, marked by eolianites interbedded with sabkha facies in the UAE (Pye and Tsoar, 1990; Bristow, 1999). The climate became markedly arid and open during later Middle Miocene Hofuf deposition (Thomas et al., 1978; Sen and Thomas, 1979). However, the aridity may not have been widespread and persistent (Kortlandt, 1972; Sen and Thomas, 1979; Thomas, 1979; Whybrow and McClure, 1981; Thomas, 1982; Whitney et al., 1983; Whybrow, 1984).

The African-Arabian lake record shows that the monsoon under the influence of Milankovitch forcing affects climate in the region (McClure, 1978; Kutzbach et al., 1993; Roberts and Wright, 1993; Kingston and Hill, 1999; Trauth et al., 2009). Using the Plio-Pleistocene climate as a guide (Trauth et al., 2009), during eccentricity maxima, monsoons are strengthened and lake levels oscillate at the highest amplitudes, associated with alternating wetter and drier phases at precessional and half precessional time scales (Trauth et al., 2009). In contrast, during 100 and 400 k.y eccentricity minima, insolation peaks have the lowest amplitudes and weakened monsoon dynamics at precessional time scales result in desertification and dried-out lakes. In addition, during lowered sea-level phases, the floor of the Arabian Gulf was exposed and sand is driven southeastwards under the influence of the summer Shamal winds (Glennie and Singhvi, 2002).

SEQUENCE DEVELOPMENT

The Miocene sequences within the study area developed on the slowly subsiding foreland (1 to 4 cm/k.y. rates) landward of the peripheral bulge, while further east in the proximal foreland basin, there was rapid subsidence, accompanying uplift of the Zagros fold thrust belt (Figure 2.4; Sharland et al., 2001). Given the low rates of subsidence within the study area, the rapid changes in accommodation were largely dependent on the rates of sea level rise and fall driven by waxing and waning of the Antarctic ice sheets (Miller et al., 1991). The low subsidence rate coupled with rapid eustatic changes resulted in unconformity development even during initial sea level fall, compared to more rapidly subsiding, more proximal foreland basin settings where substantial sea level fall would be required to cause emergence. Thermal doming and uplift in the western Arabian plate associated with the early stages of the opening of the Red

Sea, may have supplied clastics to the foreland (Bordenave and Burwood, 1990; Mitchell et al., 1992; Goff et al., 1995).

Miocene (Early Aquitanian) Hadrukh Sequence Development

The dominantly siliciclastic composition of the Early Aquitanian Hadrukh Formation may reflect the relatively low position of long term sea level and base level (Figure 2.3), uplift of western Arabia associated with rifting (Bordenave and Burwood, 1990; Mitchell et al., 1992; Goff et al., 1995), and ephemeral streams traversing open woodland/savannah landscape (Gentry, 1987b). The dominance of sands and scarcity of terrigenous muds suggest a dominance of physical weathering over chemical weathering in the source area in a relatively dry environment and sand transport into the study area by ephemeral braided streams and intermittent eolian processes. Intermittent semi-arid phases are suggested by redbeds at the base and top of the Hadrukh Formation and by gypsum matrix of some sands. Updip palustrine carbonate-rich deposits that are brecciated, suggest ephemeral, seasonal lakes on low gradient coastal plains perhaps during slightly wetter phases (Wright and Marriott; 1993).

Sequence boundary development, Hadrukh Formation

The major unconformity at the base of the Hadrukh Formation developed during onset of major Antarctic glaciation, and lowered sea levels evidenced by oxygen isotopes in deep-sea cores (Abreu and Anderson, 1998; Billups et al., 2002). This in conjunction with relatively low subsidence rates of 4 cm/k.y on the distal foreland, and local warping resulted in long term exposure of the Eocene Dammam carbonates throughout the Oligocene in study area. The basal boundary of the Hadrukh Formation probably ties with the Mi1 (23 Ma) of Miller et al. (1991) glacial event and the beginning of the Aq1 global sequence.

The unconformity separating the two large scale Hadrukh sequences (Hd 1 and Hd 2) may correlate with lowered sea levels at 22.5 Ma on the Pekar and DeConto (2006) isotope curve (Figure 2.3). The sequence boundaries separating the 8 HFSs in the Hadrukh Formation are most regionally traceable, lack the necessary biostratigraphic control, and cannot be resolved on the global curves. However, the possible ~100 k.y average duration of these HFSs suggests that short term eccentricity driven sea level changes could have influencd base level, coupled with tectonic warping. This would suggest that the intra-Hadrukh break (Hd 1 to 2 boundary) separates two 400 k.y. cycles.

Fluvial, clay-clast conglomeratic sands were deposited on erosional sequence boundaries cut into underlying mudrocks, although some clasts could be reworked thin mud layers from within the fluvial sands. Other Hadrukh sequence boundaries developed on local sequence-capping dolomites and gypseous sands deposited during drier phases and limited clastic input. Multiple breccia horizons that extend down below sequence boundaries on palustrine carbonates were developed during repeated exposure of ephemeral lake carbonates updip. Sequence boundaries in the upper Hadrukh downdip (to the northeast) such as at the base of Mhk7 and the base and top of Mhk8 developed on coastal plain redbeds and paleosols.

Hadrukh Sequence Development

Given that maximum flooding surfaces were difficult to define in most of the Hadrukh sequences, only the controls on the broad scale facies within the Hadrukh sequences is discussed. The scarcity of sedimentary structures in the Hadrukh facies makes interpretation of depositional settings difficult. Fluvial channel or tidal channel deposits probably include the clay-clast conglomeratic sands at bases of many of the sequences (Mhk 1, 4, and 5), especially downdip. However, because most of the Hadrukh sands are very fine-to-fine, massive and structureless,

they provide little information as to original depositional processes that brought the sand into the study area. Given the evidence of open woodland/savannah settings, coupled perhaps with intermittent desert settings (Kingston and Hill, 1999), some of the very fine-to-fine sands could have been transported by eolian processes (Fryberger et al., 1983) while others could have been transported by ephemeral sheet flood and braided streams to be deposited in a coastal plain setting. Although diagnostic eolian features (such as eolian cross bedding) are lacking, local horizontal lamination is compatible with interdune flats and sabkhas (Glennie, 1970).

Gypseous sands in the Hadrukh sequences at bases and tops of some sequences were due to establishment of continental- to marginal marine sabkha and ephemeral saline lakes, in which continental, marine, or mixed groundwaters precipitated fine gypsum interstitially within the sands during semi-arid phases (Wood and Sanford, 1990). The multiple, brecciated carbonate-prone horizons in the late HSTs updip in sequences Mhk 4 to 7 mark the establishment of ephemeral lake- or palustrine settings within the late highstand, low gradient Hadrukh coastal plains (Wright and Marriott, 1993). Repeated exposure events resulted in cementation and brecciation extending down through multiple sequences (Wright, 1990).

Dam Sequence Development (Late Aquitanian-Burdigalian-Langhian)

The eight sequences comprising the Dam Formation composite sequence appear to be a mix of 3rd and 4th order sequences ranging from 0.4 to 1.5 Ma. These could include long-term orbital sea level cycles 1.2 Ma obliquity and 400 k.y. long-term orbital eccentricity (Boulila et al., 2011).

Sequence boundary development, Dam Formation

Because the ages of the sequence boundaries within the Dam Formation were estimated

from the oxygen isotope curves (Figure 2.3), which are a proxy for global sea level, we cannot use these to evaluate whether the boundaries are related to eustasy or not. However, if the age estimates are valid, the timing of most of the Dam sequence boundaries correlates with sequence boundaries on the global sea level chart of Hardenbol et al. (1998), supporting a eustatic origin related to Miocene glacial cooling events (Miller et al., 1991; Pekar and DeConto, 2006). Given the low rates of subsidence (~1 cm/ k.y) within the study area during Dam deposition and estimated 20 to 40 m magnitudes of sea level change (Abreu and Anderson, 1998), would suggest that the sequences would become exposed very early during the cycle of sea level fall.

The basal boundary of the Dam Formation developed during the major sea level lowering coeval with Aq2 on the global chart and the Mi1a cooling event, which caused base level lowering, exposure and erosion of the Hadrukh Formation. Of the sequence boundaries within the Dam Formation, one type of sequence boundary developed following deposition of late HST carbonate laminites (tidal flat facies), which on initiation of eustatic sea level fall became subaerially exposed. The other type of sequence boundary developed following subaerial deposition of redbeds in the late HST. These were partly to completely eroded following sea-level fall and base level lowering, locally to become incised.

Development of Transgressive System Tracts And Maximum Flooding Surfaces, Dam Formation

The shallow water parasequences of the TSTs resulted from slow subsidence (1 cm/k.y.), coupled with one or more 4th order flooding events. Differential subsidence was active in the area, resulting in downdip thickening of units into the central depression and thinning onto highs. During transgressions, any siliciclastics from the emergent phase were reworked to a thin local to regional basal sand or sandy carbonate. As the pulsed transgressions continued, siliciclastic

deposition shifted updip, and one or more carbonate-dominated parasequences or sets were deposited. Rare thin TSTs that only consist of a part of a parasequence set (e.g. MFSs of Md 5, 7 and 8) resulted from rapid initial flooding.

Given the likely open woodland or savannah setting for the early Middle Miocene (Whybrow et al., 1982; Gentry, 1987b), vegetation cover would not have provided much inhibition to erosion by water. Also, the dominance of sand in the TSTs of updip areas suggests that sediments stored in the coastal plain were easily eroded. If a monsoonal influence on aridity is accepted (McClure, 1978; Kutzbach et al., 1993; Roberts and Wright, 1993; Kingston and Hill, 1999) then the TSTs in the Dam Formation may have developed as aridity lessened and the climate became more humid with warming and base level rose. Thus the main control on siliciclastic input into the TSTs would appear to be landward shift in siliciclastic storage within the coastal plain system with rising base level.

The maximum floods terminating the TSTs occurred at the accommodation peak, associated with relatively high rates of glacio-eustatic flooding, perhaps associated with 100 k.y sea level rise and sediment- and water loading. Assuming 15 k.y for the sea level rise and 20 m to 40 m magnitude (Abreu and Anderson 1998; Pekar and DeConto, 2006) would give rise rates of over 1 to 2 m/k.y. These are minima, because an additional 40% of space would be due to water loading; long-term subsidence could almost be disregarded, as it would provide less than 1 m of space in 15 k.y. The eustatic rise rates would easily outpace the rate of carbonate sedimentation, given the lack of reefs or high productive ooid shoals (Enos, 1991), enabling periodic flooding over the platform during the TST.

The possible relation between maximum flooding events in the Dam Formation and the global eustatic chart (Hardebol et al., 1998) has been discussed previously, and indicates some

correlation between global flooding events and Dam maximum floods, with the exception of sequences Md3 and 7, although the latter ties to Ng30 flood (Figure 2.3). Assuming the age estimates for the Dam sequences are reasonable, then potential flooding events that affected the Dam Formation can be gleaned from the detailed deep-sea $\partial^{18}O$ record given in Pekar and DeConto (2006) (Figure 2.3). Md1 flooding event ties to an obvious sea level high at 20.9 Ma of about 45 m which ties to maximum flood of 3rd order sequence Aq2. Md2 likely ties to the second large flood at 20.2 (35m rise in sea level), which is close to Ng10 and maximum flooding of 3rd sequence Bur1, although there are other two sea level highs at 20.4 and 19.7 (40 and 35 m respectively). Md3 flood probably ties to a high sea level at 19.2 Ma, of about ~40 m rise, although there is another flooding event at 19.2 Ma of similar magnitude. Md4 ties to a high sea level (35 m) at 18.8 Ma. Md 5 probably ties to one of two sea level highs between 17.7 and 17.6 Ma of (30 -35 m), which is ties to maximum flooding of 3rd sequence Bur3. Md6 likely ties to a high sea level at 17.3 Ma of 34m, that ties to maximum flooding of 3rd sequence Bur4. Md7 probably ties to one of three high sea levels around 16.5 Ma of 45m, which close to Ng30.

Development of 3rd Order Highstand system tracts, Dam Formation

With such low long-term accommodation rates (1 cm/ k.y.) for the Dam sequences, the accommodation change from TST to HST was largely related to slowing of sea level rise followed by sea level fall, allowing sedimentation to exceed accommodation. From the $d^{18}O$ records (Figure 2.3) the 3rd order falls likely consisted of a series of staggered falls typical of Milankovitch glacioeustasy resulting in 2 or more parasequences or sets in the HSTs. The 4th order sea level changes, which were larger than any longer term accommodation change, thus governed the timing of the maximum flooding events. This is in contrast to greenhouse times, where the 4th and 5th order sea level signal is small compared to the 3rd or 2nd order sea level

change, which thus control the timing of maximum flooding.

Within the Dam Formation, the early HSTs contain siliciclastic-poor, carbonate-prone units because sea level rise had forced the shoreline siliciclastics updip, and allowed open marine clastic-free conditions to penetrate into the study area. The transition from carbonates into siliciclastic-prone units of the HSTs resulted from progradation of siliciclastics as accommodation decreased. The siliciclastic influence became even more pronounced in the upper Dam sequences Md 3 to 8, with deposition of prograding redbeds capping sequences. Increased siliciclastic input into the area may have accompanied warming into the Miocene climatic optimum, which appears to span Md 6 to 8, and likely was accompanied by increased rainfall. Warming even may have started in Md5 whose high stand has updip sands and redbeds and thick downdip gray and dark gray nearshore lagoonal mudstones that filled tectonically induced accommodation in the central depression. The increased abundance of fine siliciclastics in the upper Dam Formation compared to the lower part could reflect increased chemical weathering, accompanying increased rainfall and higher temperatures of the Mid-Miocene climatic optimum. It also could relate to more abundant fine sediment traps in the form of ephemeral flood basins and near-shore low energy lagoons, that were able to permanently store the deposited siliciclastic muds compared to more updip settings that typified the more sand-prone Hadrukh and Hofuf formations.

Development of Parasequence Sets and Parasequences, Dam Formation

In light of the well documented evidence for Milankovitch forcing in the Miocene, the parasequences and parasequence sets of the Dam Formation most likely resulted largely from flooding triggered by orbitally induced glacial melting, followed by progradation as sea level fell during ice buildup. The parasequence sets appear to have been associated with eccentricity-

induced platform flooding events. However, the individual parasequences could have been triggered by obliquity or precessional forcing, of which only a few would have been able to affect the study area given its updip position. Preliminary modeling of the succession supports this idea, with 400 k.y. and 100 k.y floods able to penetrate back onto the platform, while most of the obliquity and precessional beats were generally unable to flood the study area, only leaving a record downdip.

Sea level rise coupled with water- and later sediment loading created accommodation, supplemented by a small amount of tectonic subsidence. However, even though 20 to 40 m sea level changes may have been involved, only the final phase of sea level rise caused flooding in the study area, given its updip position. High energy, transgressive ravinement surfaces at the bases of parasequences above disconformable boundaries are overlain by gravel lags of lime-clast silty quartz wackes and rudstones. Many of these transgressive lags are from landward migration of the high-energy wave abrasion zone, or are amalgamated storm beds or they may have been deposited by tsunamis (Seilacher and Aigner, 1991; Shanmugam, 2010). The wide variety of clast types (from transgressive lagoonal green mudrock to open marine carbonates), indicate large-scale transport of coherent to lithified material into the lags. As each sea level rise slowed and then fell, a regressive upward shallowing parasequence formed. Downdip where accommodation was greatest, open marine carbonate parasequences formed, in contrast to the lower accommodation updip part of the study area, where siliciclastic-dominated parasequences developed.

Development of Hofuf Sequences

The base of the Hofuf Formation formed during either Ser1 or Ser 2 low stand on the global curve. The duration of the break appears to be about 1 Ma or less according to estimated

ages for the study area (Figure 2.3), and is no larger than some of the internal unconformities within the underlying Dam Formation. This supports the idea that the Hofuf siliciclastics form the late highstand of the Dam-Hofuf composite sequence.

Deposition of Hofuf siliciclastics was triggered by base level fall associated with global sea level fall during the later Middle Miocene (Figure 2.3). This moved the shoreline seaward of the study area, allowing the siliciclastics brought into the area by winds and ephemeral streams, to be deposited in coastal plain systems. This global sea level fall took place as a series of staggered falls, depositing the basal Hofuf parasequences cored.

Within the region, Middle Miocene arid to hyperarid climates existed in open environments with eolianites, sabkha facies, and vertebrates (Thomas et al., 1978; Sen and Thomas, 1979; Bristow, 1999) and may have been extensive at times (Pye and Tsoar, 1990). However, some workers suggest that Middle Miocene aridity in the region was not widespread or persistent (Kortlandt, 1972; Sen and Thomas, 1979; Thomas, 1979; Whybrow and McClure, 1981; Thomas, 1983; Whitney et al., 1983; Whybrow, 1984). These conflicting views may be reconciled if the monsoonal influence of climate was involved, as invoked earlier. During Milankovitch driven sea level highstands and insolation maxima, monsoonal circulation would increase, leading to higher rainfall and perhaps increase in siliciclastic influx into the area. As sea level fell with global cooling, the monsoon circulation likely was depressed, increasing aridity and perhaps increasing the role of eolian transport of sediment into the area. Given the open settings, erosion and transport of siliciclastics by flash flooding of ephemeral streams and associated sheet-floods would have been favored, as vegetation would not have formed a dense cover to inhibit erosion.

The sequence stratigraphic significance of the sandy chalky carbonate unit in the middle

Hofuf and the top of the Hofuf Formation is unclear, as these were not cored as part of the study. These are likely to be sandy carbonate lake deposits given the fresh water biota of the Hofuf Formation. Wright and Marriott (1993) suggest that such lake deposits in coastal plain siliciclastic systems form during the highstand due to low gradients of the coastal plain. If so, then it is possible that there are two sequences within the Hofuf Formation, each capped by lake deposits.

CONCLUSIONS

The Miocene of the Lidam area, Eastern Province, Saudi Arabia, is an example of the interaction of glacio-esustasy during moderate Antarctic glaciation, on the slowly subsiding distal Arabian foreland, within a small back bulge basin distal from the active Zagros fold-thrus belt.

Climate and sea level controlled siliciclastic input relative to marine carbonate deposition, while tectonics controlled the shape of the embayment within the study area, and the thickness of the units. The succession consists of the Early to Middle Miocene Hadrukh siliciclastics (52 to 66 m thick), Dam mixed siliciclastics and carbonates (47 to 79 m thick), and the Hofuf siliciclastics (90 m thick),

The Hadrukh Formation is dominated by non-marine siliciclastics and minor palustrine carbonates and is a composite sequence with two subsequences and 8 component, poorly defined high frequency sequences. The Dam Formation is a mixed carbonate-siliciclastic composite sequence composed of 8 small-scale 3rd order sequences, each typically composed of about 4 parasequence sets. The Hofuf Formation is a 3rd order non-marine sequence with a lower siliciclastic unit, a middle carbonate unit and upper siliciclastic unit of which only the lower unit

was studied.

Facies within the siliciclastic units include paleosols, cross-bedded sands (fluvial), red mudrock (mudflat and interfluve), near shore siliciclastic green gray mudrock (lagoon), brecciated micritic quartz sands (ephemeral lake), gypseous calcareous quartz sands and wacke (saline coastal plain and evaporitic flats), and quartz sand sheets (intertidal to shallow marine). Carbonate facies include brecciated carbonates (incipient paleosols), lime/clay clast quartz wackestone (transgressive basal sheet), microbial laminites and microbial mounds (tidal flat and shallow subtidal) , argillaceous variably quartzose marl (near-shore lagoon), fine peloid mudstone – wackestone (shallow lagoon), oolitic grainstone (shoal or tidal bars), mollusk packstone (nearshore shelf) and foraminiferal-mollusk packstone-grainstone (seagrass meadows).

The initial low position of sea level promoted deposition of Hadrukh siliciclastics, which pass up into Dam mixed siliciclastics and carbonates as global sea levels rose, peaking with the Middle Miocene climatic optimum, only to be succeeded by Hofuf siliciclastics as global sea level fell. Arid climate stages are evident in the Hadrukh by gypsum-bearing sands, and in the Dam Formation by the carbonate facies (oolite and stromatolites) that are compatible with semi-arid conditions and elevated salinity. During Hofuf deposition, climate probably remained semi-arid but the fomation lacks evaporites, suggesting seasonal conditions.

Low subsidence rates of 1 to 4 cm/k.y generated the long-term accommodation, which were considerable slower than those in the proximal foredeep in Iran. Differential warping during the Oligocene and the Miocene generated a structurally controlled embayment within the study area, which controlled bathymetry of facies. Eustatic sea level changes (indicated by oxygen isotope proxies in coeval deep sea sediments) appear to have controlled the timing of the

deposition of sequences. These sequences represent the updip terminations of much thicker, more conformable downdip sediment wedges.

Many of sequences appear to be about 1 m.y. duration, suggestive of long term obliquity forcing of sea level, associated with long term obliquity nodes. A few appear to be higher order 400 k.y sequences, perhaps associated with long-term eccentricity. Although sea level changes were 20 to 40 m, only a small amount of the sea level rise affected the study area because of its updip position. The moderate magnitude sea level changes locally incised sequence boundaries, and caused formation of numerous exposure surfaces with paleosols and incipient breccia. Individual parasequence sets and parasequences may be orbital eccentricity-precessional and obliquity cycles. The succession contains numerous missing beats reflecting updip position and tens of meters sea level changes that frequently exposed the platform. This resulted in paleosols on siliciclastic redbeds mainly near sequence boundaries in the Hadrukh and the Dam formations, as well as brecciation of Hadrukh palustrine carbonates. Within the Dam carbonates, some parasequence and parasequence sets are capped by tidal flat laminites (some of which are incipiently brecciated) but many are capped by paleosols or emergence surfaces, unlike greenhouse platforms where tidal flat capped cycles are dominant.

FIGURES AND FIGURE CAPTIONS

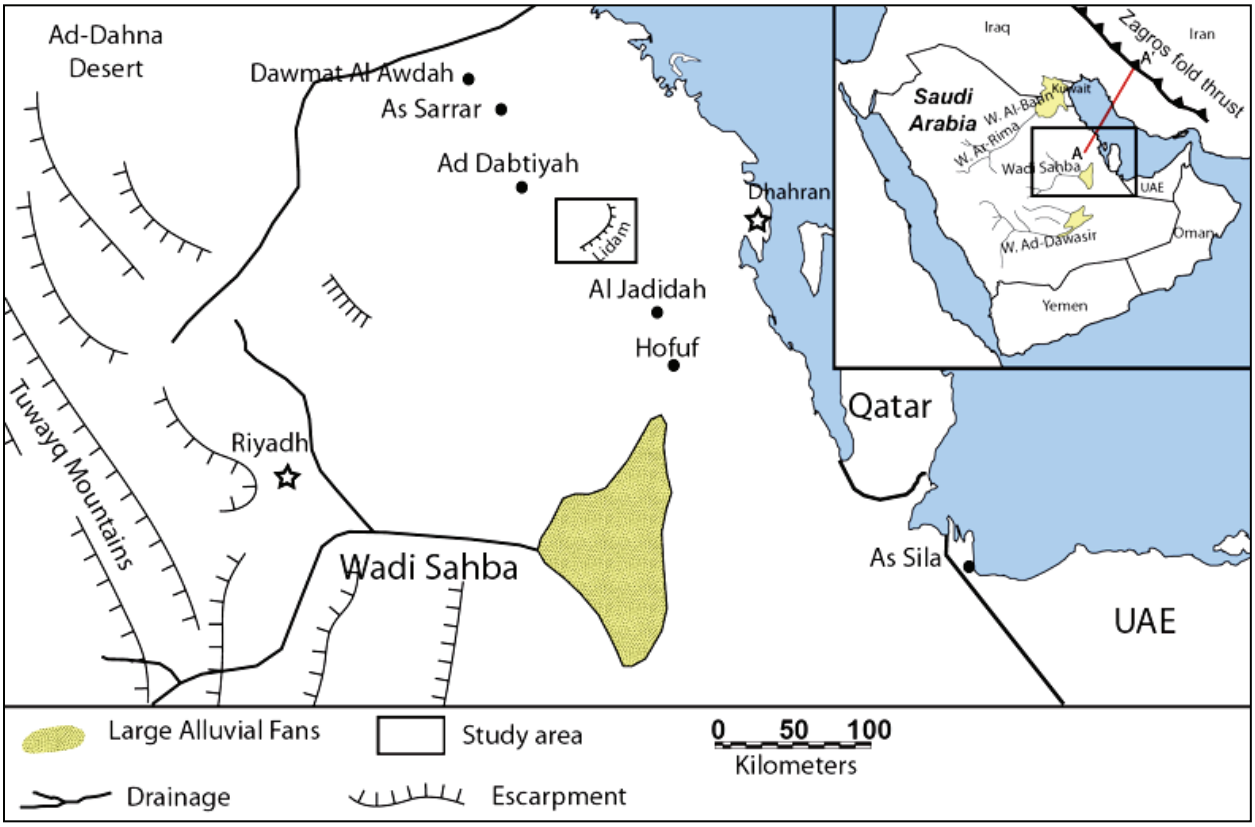

Figure 2.1 Regional map showing location of study area in the Eastern Province, Saudi Arabia. Lidam escarpment is oriented northeast and formed by the Hofuf Formation and overlying gravel plain. The large wadi and alluvial fan system of Wadi Sahba occurs south of the study area. Inset map shows location of Eastern Province within Saudi Arabia and the Middle East, along with the location of the regional cross section A-A' shown in Figure 2.4.

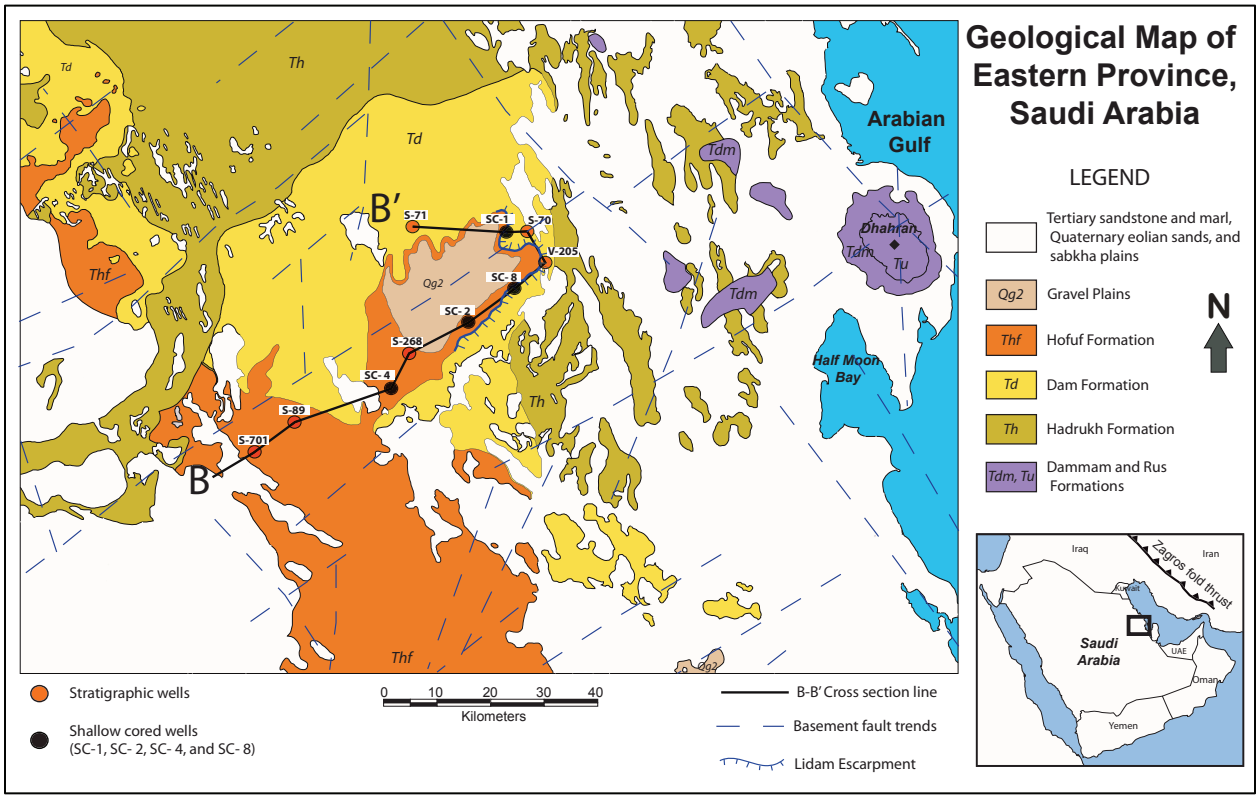

Figure 2.2 Geological map of study area within the Eastern Province, Saudi Arabia. Basement structural elements and trends are shown by dashed lines. Study area lies within the saddle between the Ghawar structure and the Abqaiq structure, which are major oil fields. Location of borehole cross section B-B' (Figure 2.5) is shown as well as location of cored wells (labeled SC 1, 2, 4, and 8) studied in detail. A SW-NE fault runs through the middle of the study area between SC-1 and 8.

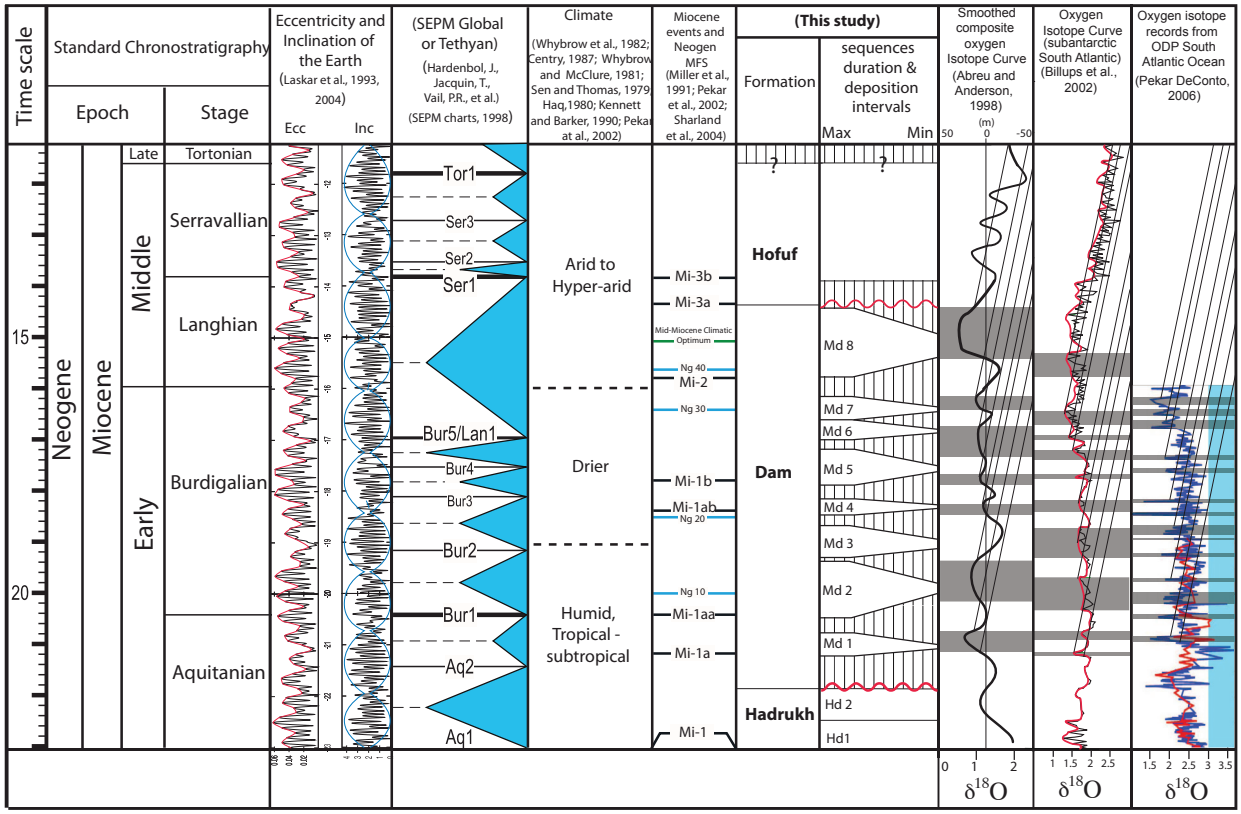

Figure 2.3 Chronostratigraphic chart of Early and Middle Miocene Hadrukh, Dam and Hofuf formations studied. Diagram also shows major eccentricity (Ecc.) and obliquity (Inc.) nodes that mark times of cooling. The SEPM global cycle chart is shown alongside major climatic phases, Miocene glacial-events (black lines) and Neogene flooding events (blue lines labeled Ng). The three right hand columns are proxy sea level curves based on oxygen isotopes from deep sea cores, which were used to estimate likely times of deposition within the study area; Inclined lines sloping to top right are paths of subsidence; deposition occurred when sea level lay above subsidence line. From various sources including Hardenbol et al., 1998; Miller et al., 1991; Abreu and Anderson, 1998; Billups et al, 2002; Pekar et al., 2002; Sharland et al., 2004; Laskar et al., 2004; Pekar and DeConto, 2005).

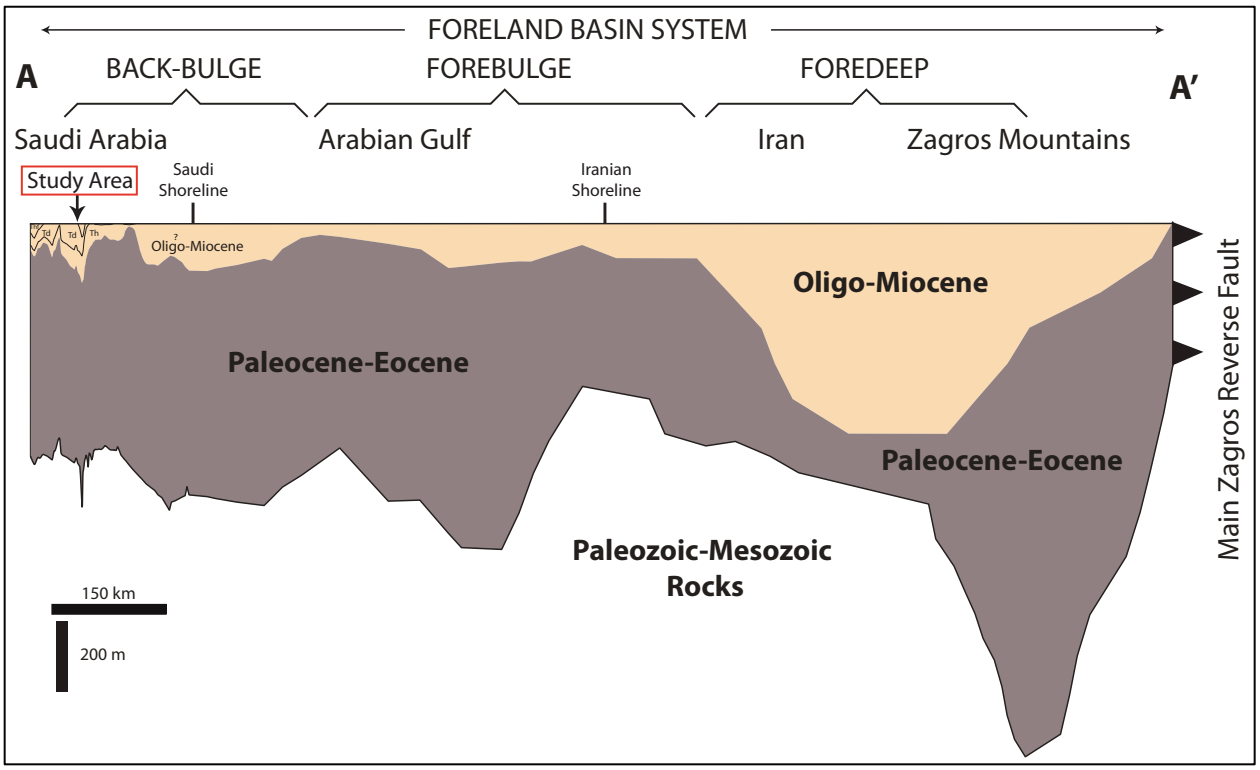

Figure 2.4 Regional cross section (A-A') showing regional setting of study area within the foreland basin. Cross section was constructed from isopach maps from Saudi Arabia, the offshore Arabian Gulf and the Zagros Mountains (Saudi Aramco data; Bahroudi, 2003). The cross section indicates the thickness variation of the Oligo-Miocene succession from the foredeep, and onto the forebulge and back-bulge depozones. Complex topography in Saudi Arabia probably related to reactivation of basements faults during the Cenozoic. The studied Miocene section of the Lidam area is in a small back-bulge basin.

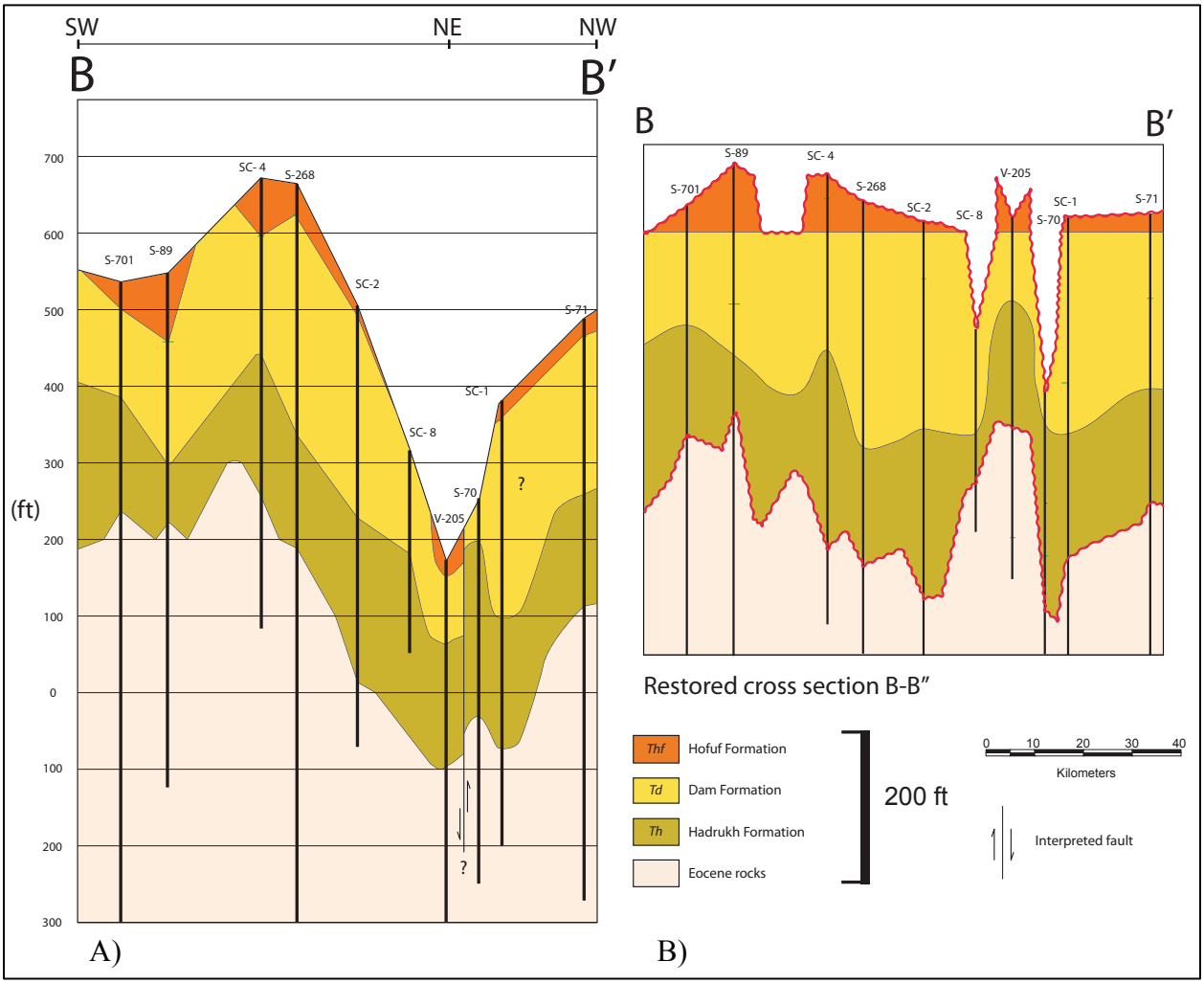

Figure 2.5 A) Local cross section B-B' constructed from data from stratigraphic wells and the shallow cored wells within the study area. Faults interpreted from lithologic correlation and location of the NE-SW fault trend in the study area; depth is in feet. B) Restored cross section B-B' datumed on base Hofuf Formation showing rapid thickness variation in the Hadrukh and especially the Dam Formation, probably associated with syndepositional deformation. Hofuf Formation is erosionally truncated in study area.

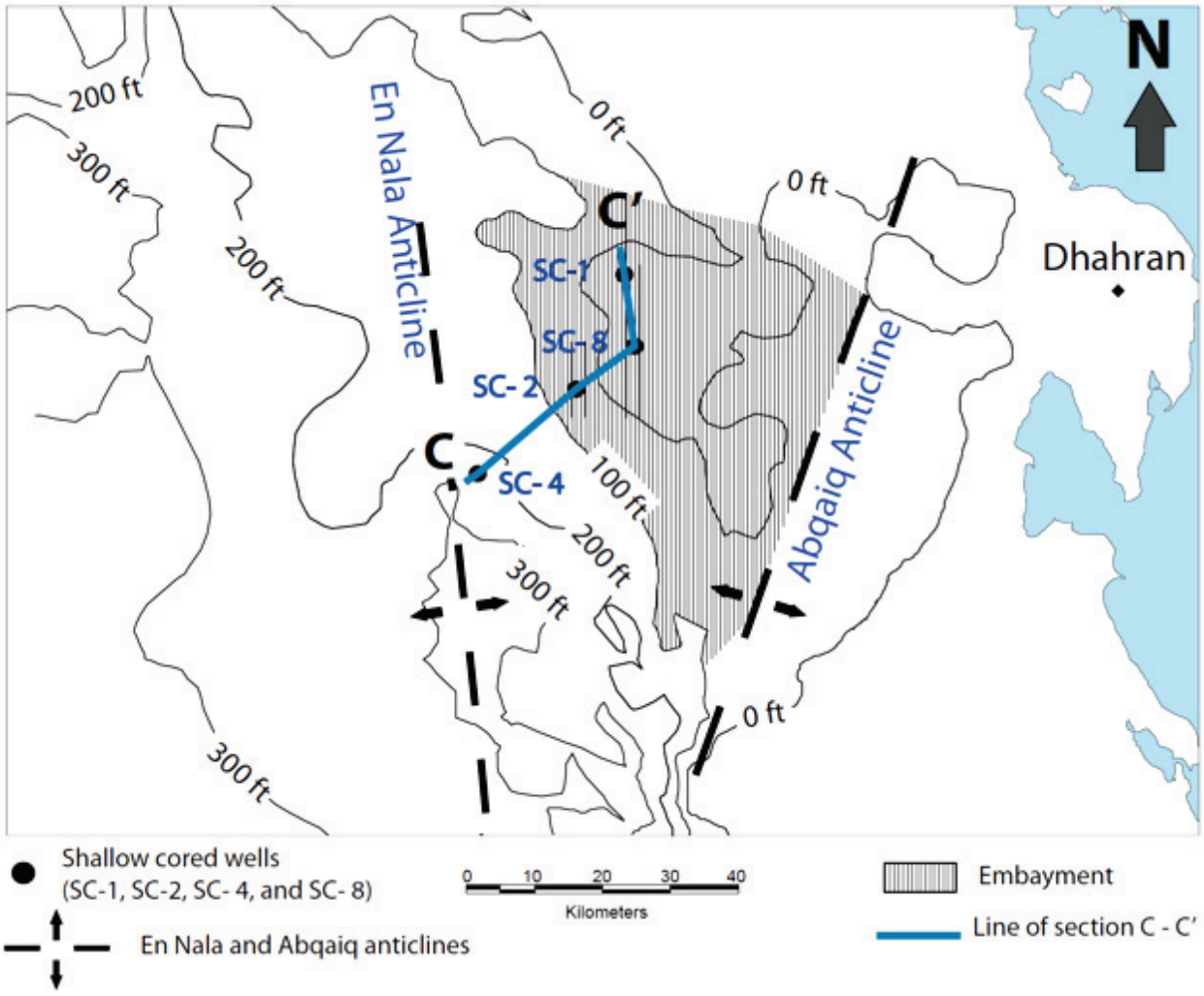

Figure 2.6 Simplified structure map of the study area showing the location of the studied cored wells (SC- 4, 2, 8 and 1) and their relation to the two major anticlines (En Nala and Abqaiq), which bounded a Miocene paleo-embayment to the west, south and east. The reentrant in the zero contour line suggests that the paleo-embayment opened into the ancestral Arabian Gulf via a narrow strait in the north, keeping the embayment from being fully isolated. The general trends of the contours suggest that regional paleoslope was to the northeast, which is confirmed by the facies changes documented in this study.

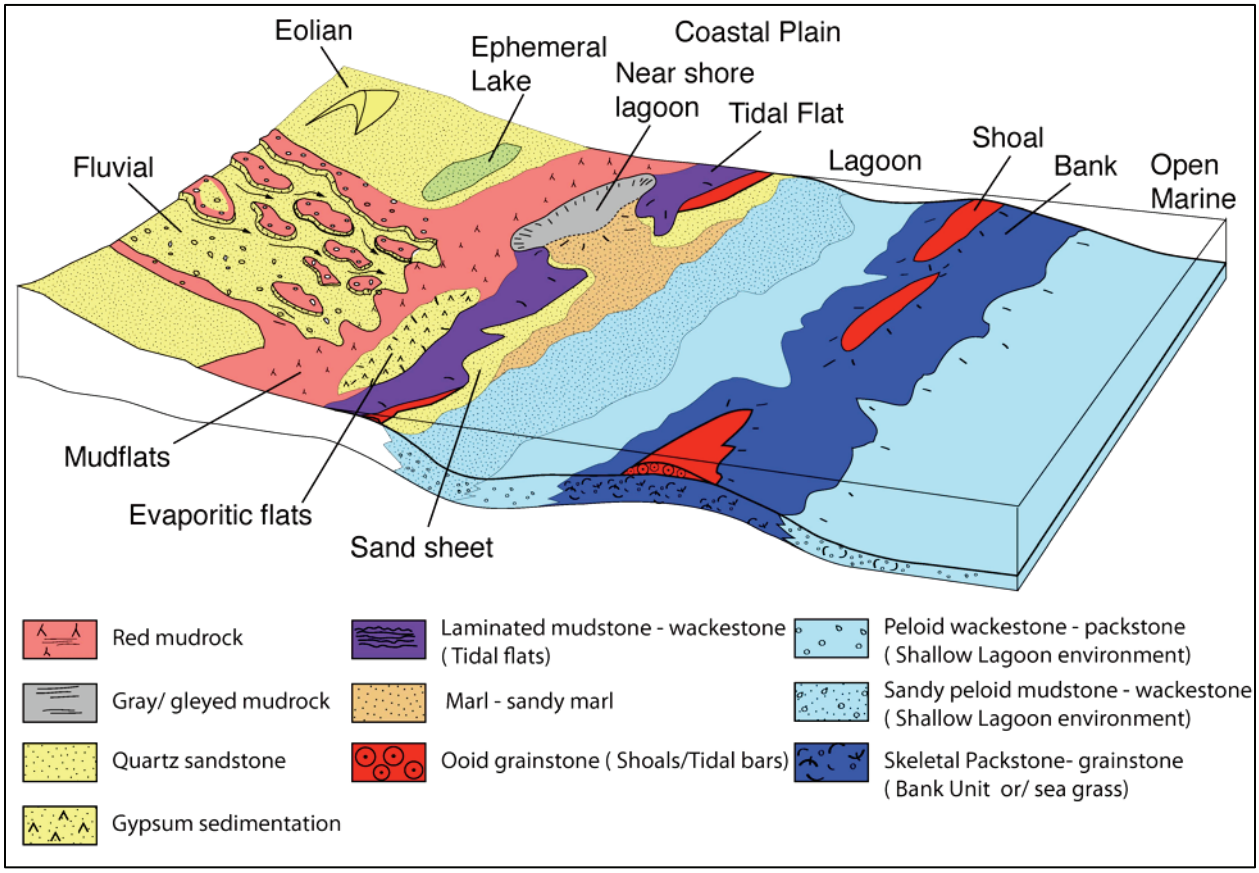

Figure 2.7 Schematic depositional model showing the facies distribution from fluvial to marginal marine siliciclastics out into shallow marine carbonates. Hadrukh and Hofuf formations formed in fluvial to marginal marine settings, while the Dam Formation developed in marginal marine siliciclastic to shallow marine carbonate settings.

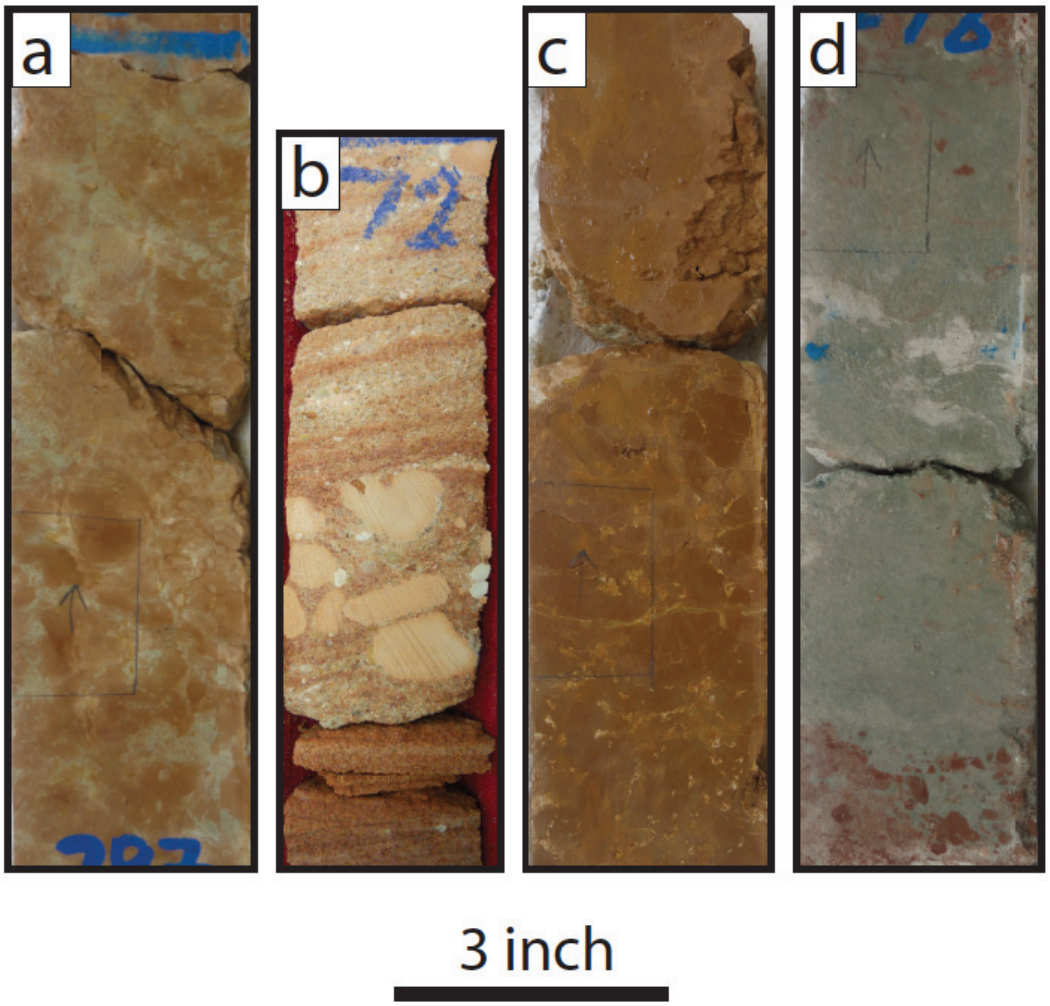

Figure 2.8 Slabbed core photos of siliciclastic facies: a) Red, green mottled (paleosols). b) Reddish tan cross bedded/planar bedded quartz sands and clay-clast conglomerates (fluvial). c) Red mudrock (coastal plain and supratidal mudflats). d) Green gray mudrock (near shore siliciclastic lagoon).

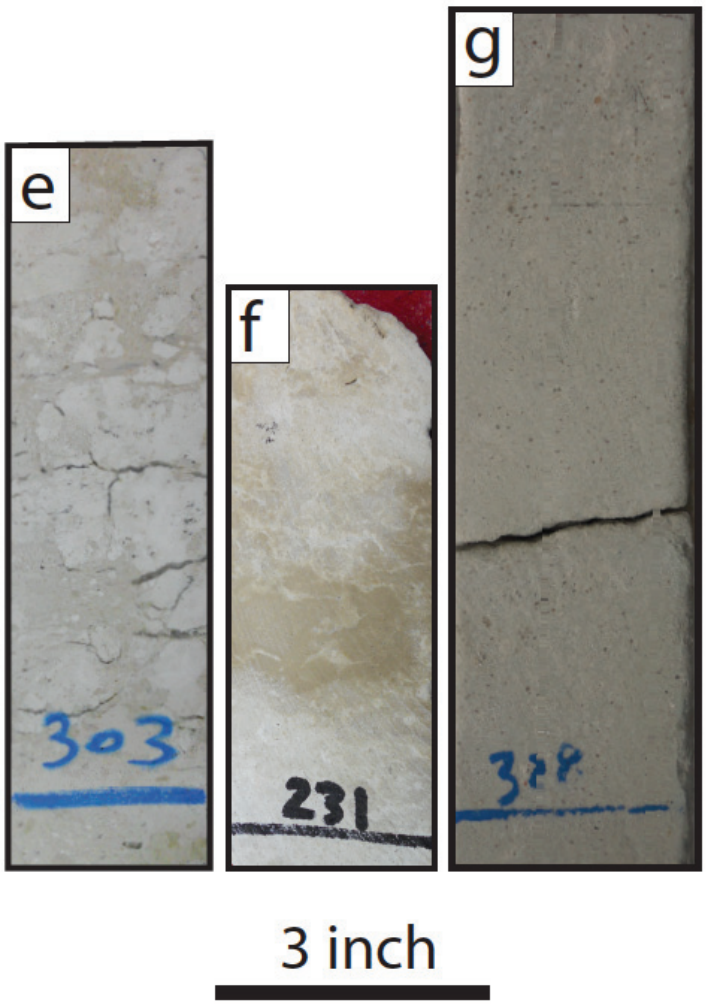

Figure 2.8 ***continued***. e) Brecciated micritic quartz sands and sandy lime mudstones to packstones (palustrine or ephemeral lake). f) Gypsiferous, calcareous quartz sands and quartz wacke (Saline coastal plain, evaporitic flats, intertidal shallow marine sand sheets, and nearshore lagoons). g) Quartz sands sheet (coastal, intertidal and shallow marine).

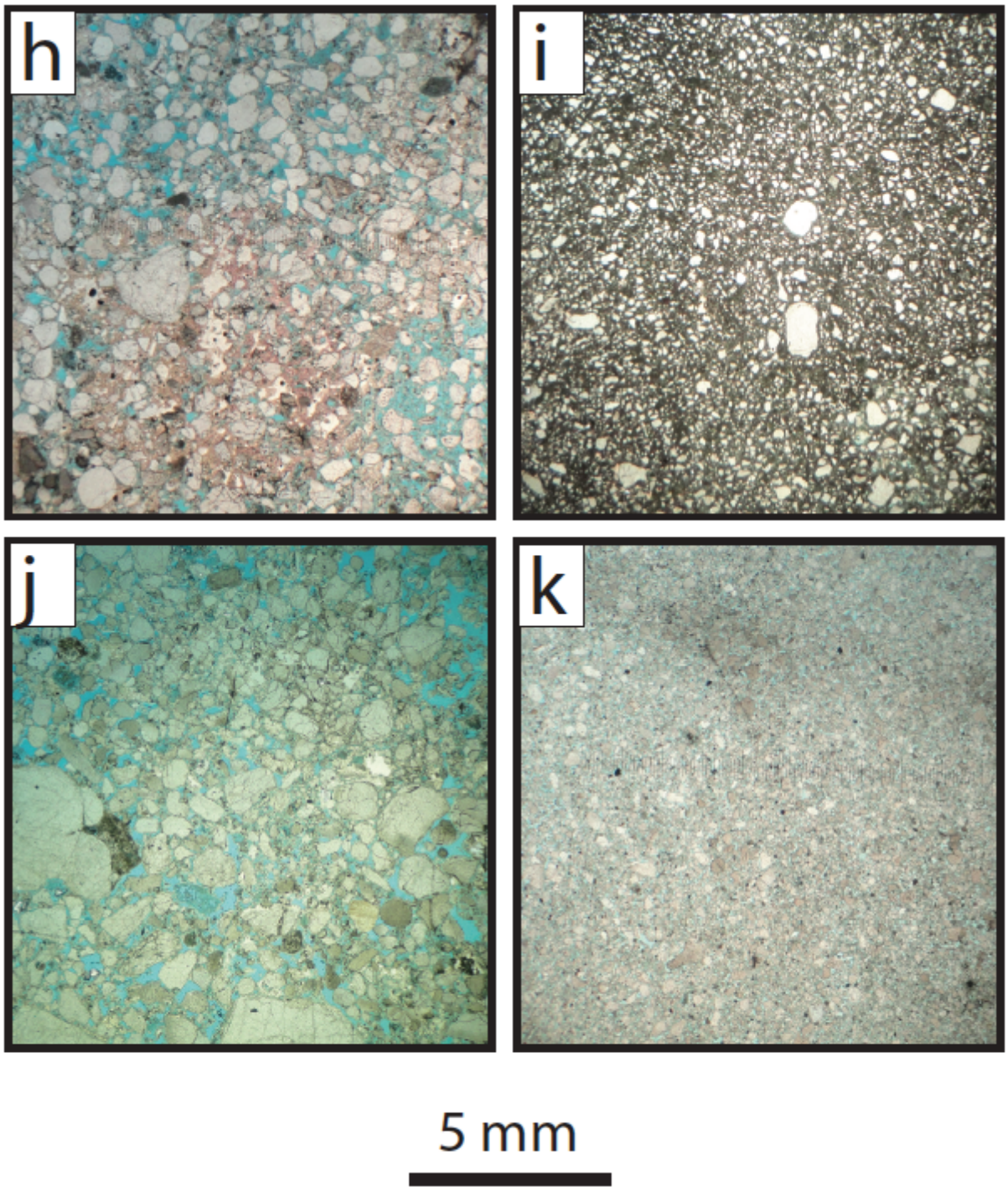

Figure 2.8 ***continued***. Thin sections of Siliciclastic facies: h) Medium to very fine sand size quartz with some medium size clast of clay mudrock (fluvial). i) Very fine-to-fine angular quartz sand in micritic matrix with some medium rounded quartz sands (palustrine or ephemeral lake). j) Gypseous and calcareous medium to coarse sand size quartz (Saline coastal plain, evaporitic flats, intertidal shallow marine sand sheets, and nearshore lagoons). k) Fine to medium size quartz sand (coastal, intertidal and shallow marine).

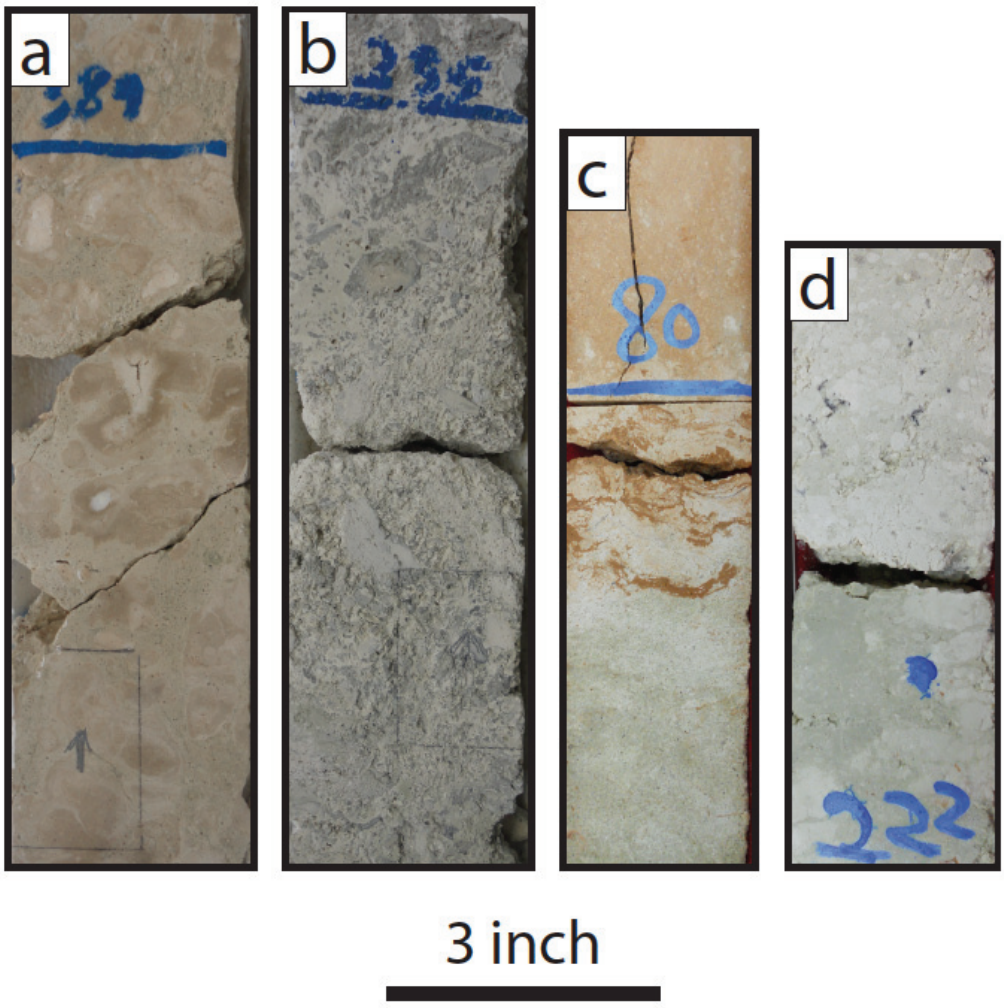

Figure 2.9 Slabbed core photos of carbonate facies: a) Caliche (Incipient paleosols). b) Lime/clay clast quartz wackestone-rudstone. c) Carbonate laminite mud cracks (Carbonate tidal flat and shallow subtidal). d) Argillaceous, variably quartzose marl (near shore lagoon).

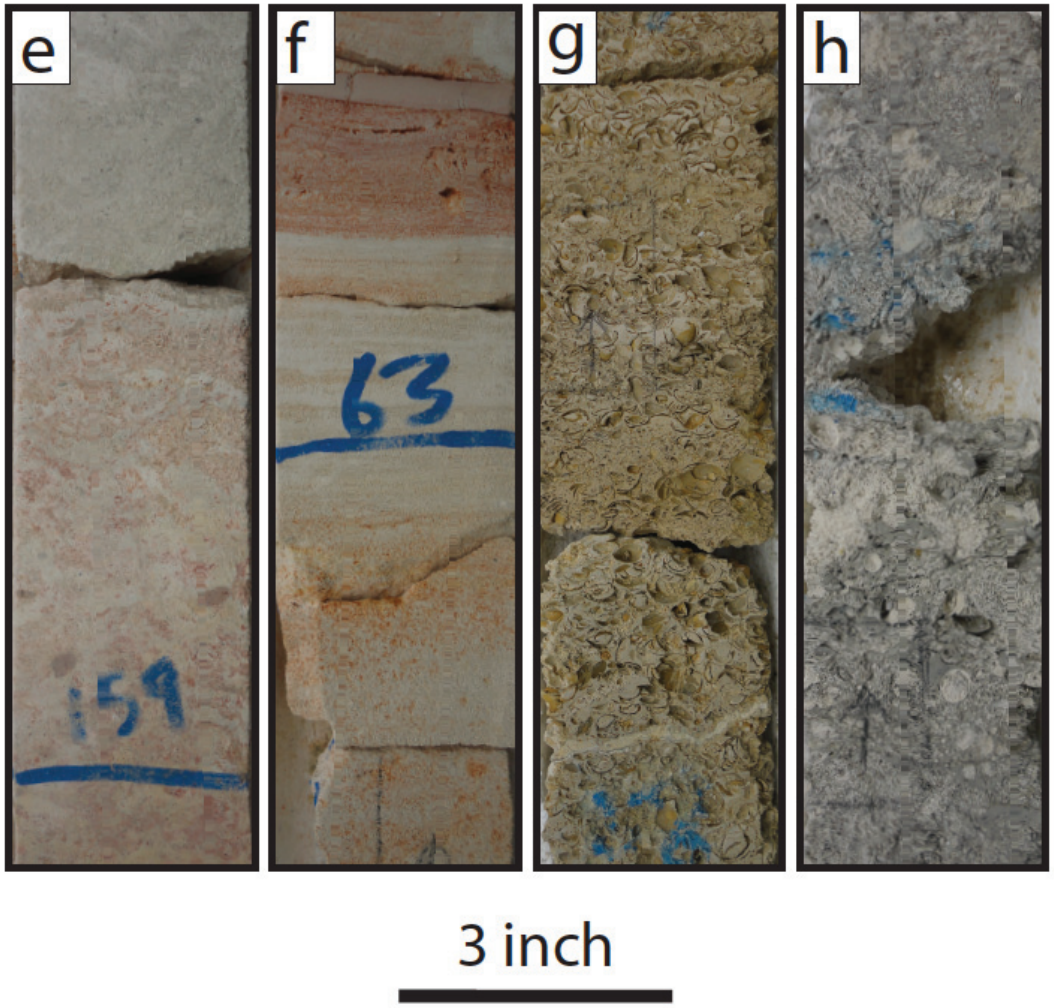

Figure 2.9 ***continued.*** e) Fine peloid mudstone-wackestone (pond/shallow restricted lagoon). f) Oolitic grainstone variably quartzose (Agitated hypersaline shoal or tidal bars). g) Mollusks packstone-rudstone (border of hypersaline shallow-moderately deep embayments). h) Foraminiferal-mollusk packstone-grainstone (Seagrass meadows).

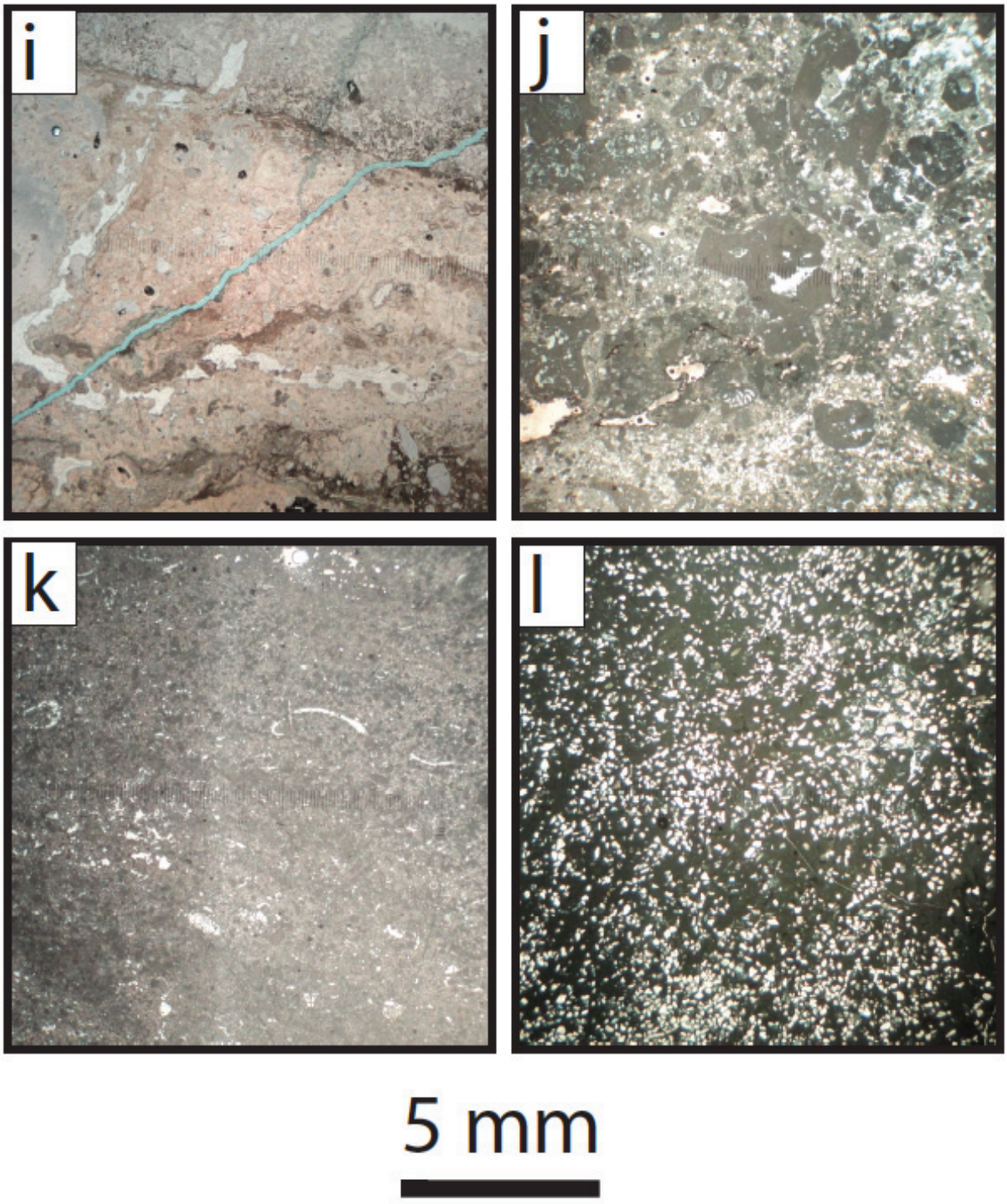

Figure 2.9 ***continued.*** Thin sections of carbonate facies: i) Calcite cemented fine to coarse sand size quartz, sandy lime mudstone to wackestone clasts in matrix, calcite spar locally in cracks (Incipient paleosols). j) Wackestone to packstone composed of fine to medium size clasts of clay mudrock in quartz wacky matrix (Transgressive basal facies). k) Weakly laminated wackestone to packstone composed of clay, silt, very fine to fine sand size peloids and quartz, laminated, leached shells filled with calcite (Carbonate tidal flat and shallow subtidal). l) Marl composed of fine sand size quartz in clay and silt matrix, argillaceous (Near shore lagoon).

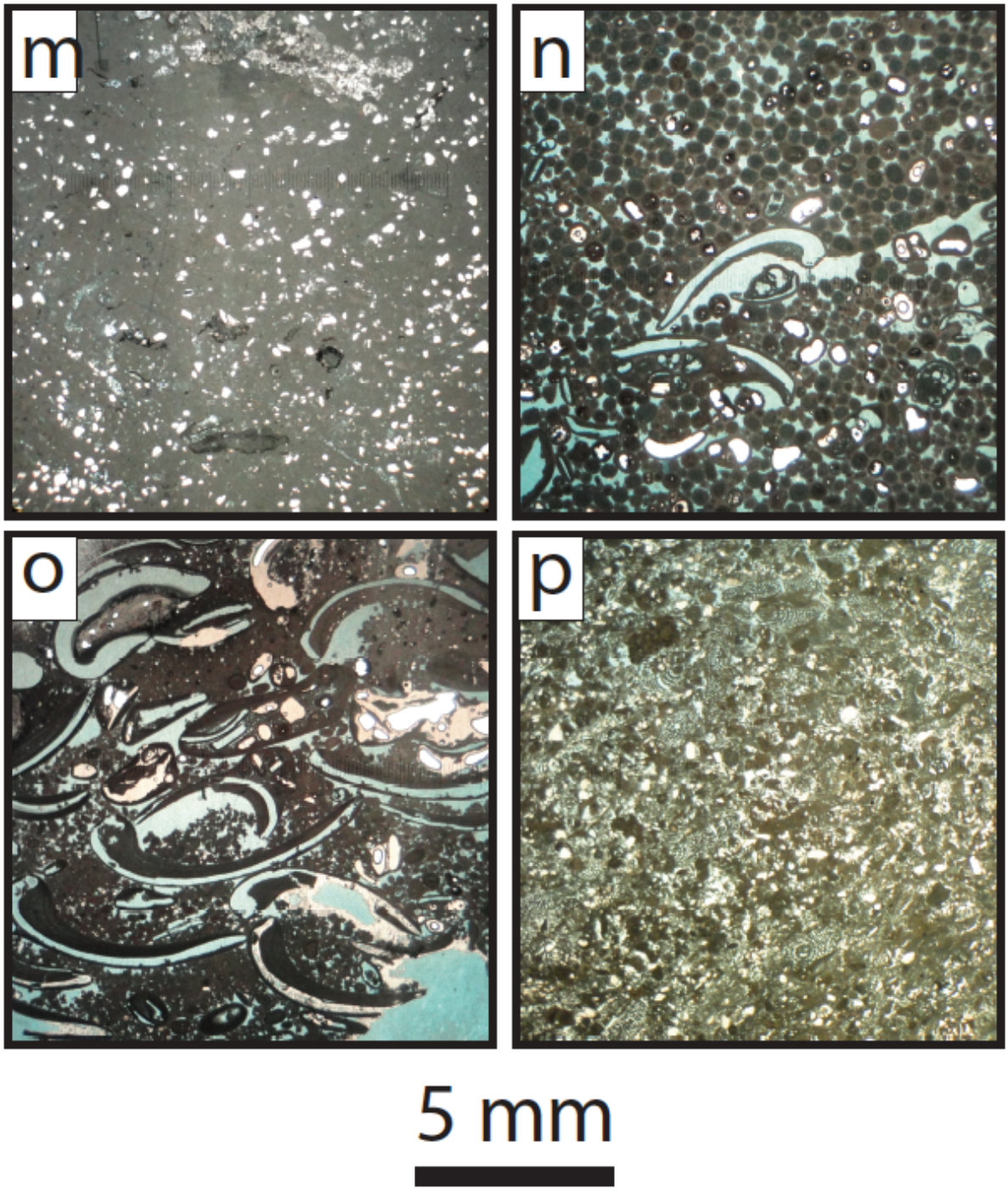

Figure 2.9 ***continued.*** Thin sections of carbonate facies: m) Mudstone-wackestone composed of fine peloid with variable fine to medium size quartz (pond/shallow restricted lagoon). n) Grainstone composed of medium sand size ooids, some granule size leached bivalves (Agitated hypersaline shoal or tidal bars). o) Packstone to rudstone composed of granule size leached bivalves with medium size peloids, calcite cemented (border of hypersaline shallow-moderately deep embayments). p) Grainstone to packstone medium to coarse sand size peloids, granule size benthic foraminifera Archaias, lime mud matrix (Seagrass meadows).

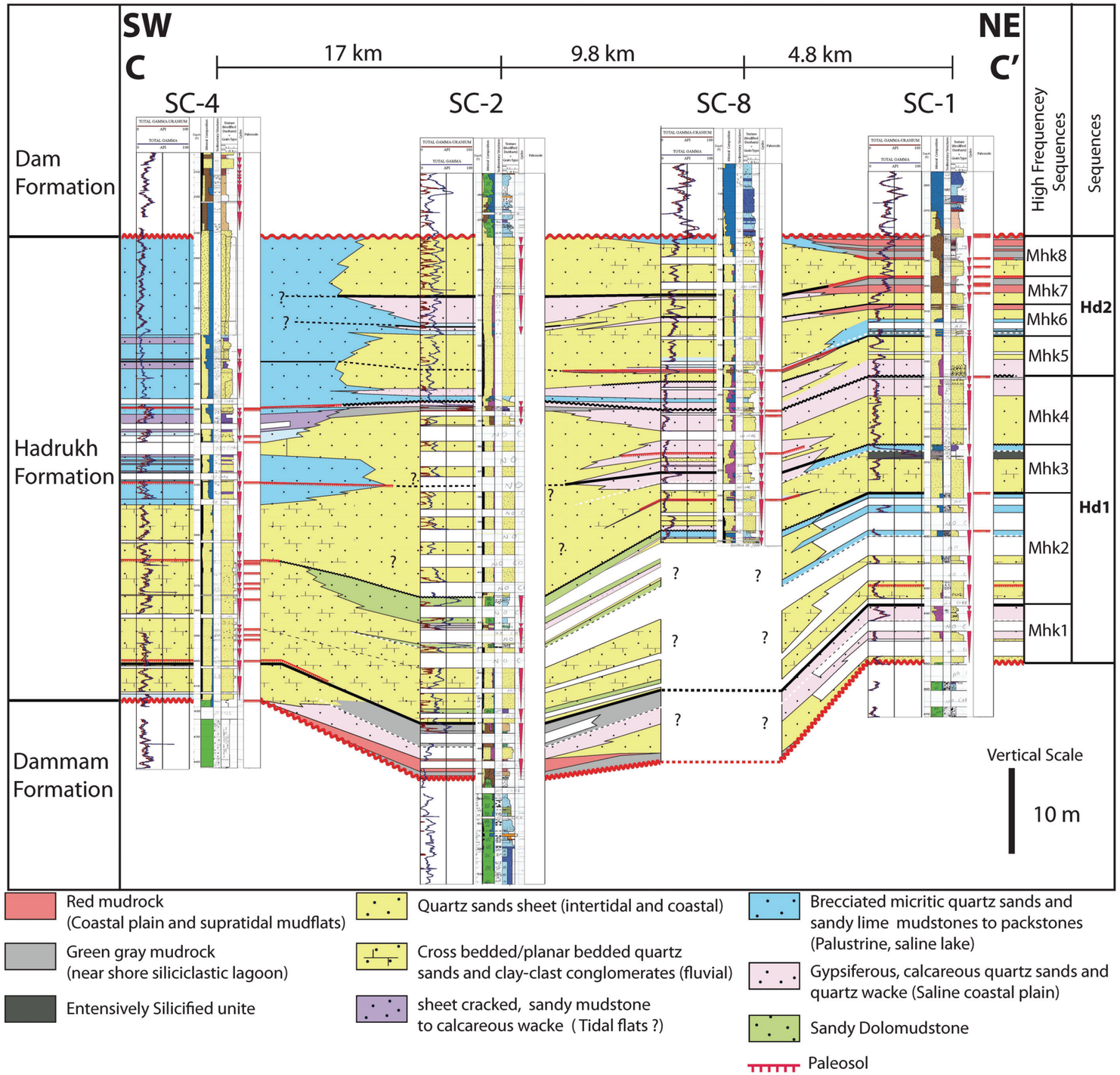

Figure 2.10 Regional facies cross section of the Early Miocene Hadrukh Formation based on core data, showing tentative sequence stratigraphic picks. Sequences and bounding surfaces within these siliciclastic-dominated units are difficult to pick and trace across the study area due to lateral facies changes and lack of regional marker beds. Updip carbonate prone palustrine facies (light blue) are highly brecciated. Lithology, sedimentary structures and lithofacies legends are in APPENDIX B.

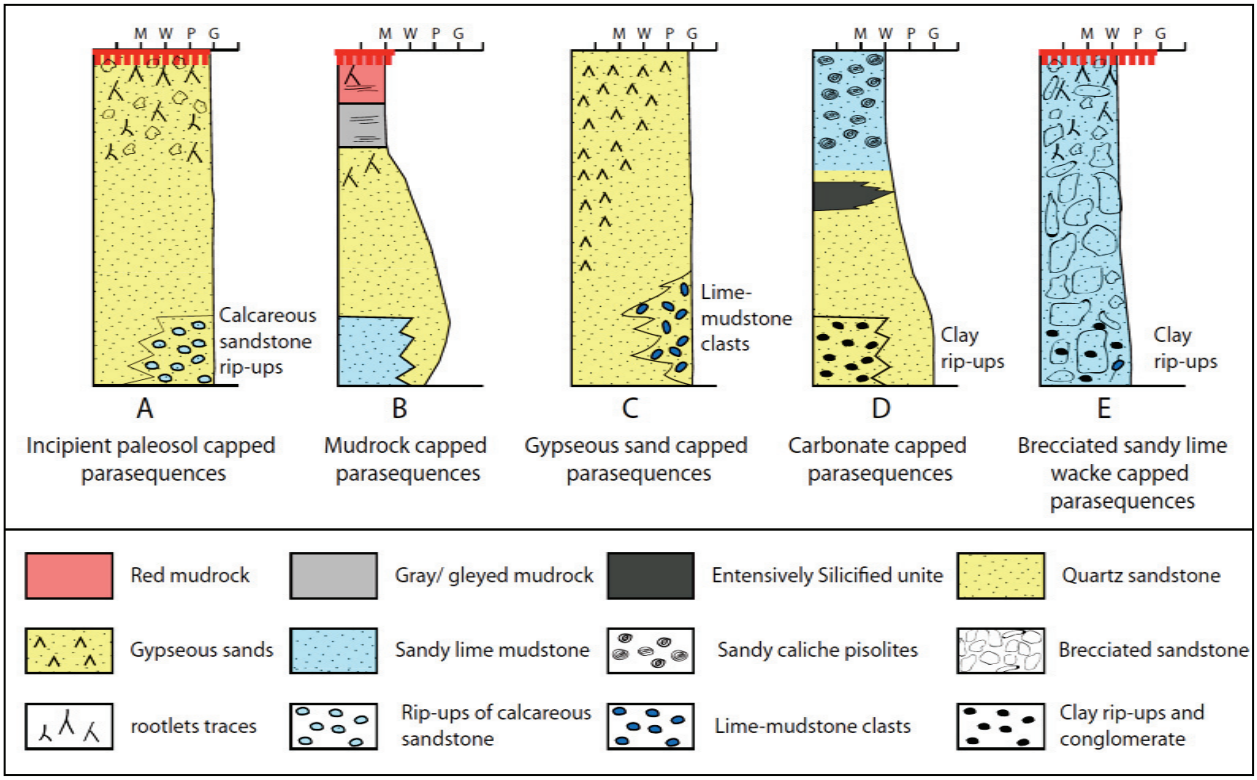

Figure 2.11 Generalized parasequence types within the Hadrukh Formation: A) Incipient paleosol capped parasequences. B) Mudrock capped parasequences. C) Gypseous sand capped parasequences. D) Carbonate capped parasequences. E) Brecciated sandy lime-wacke capped parasequences.

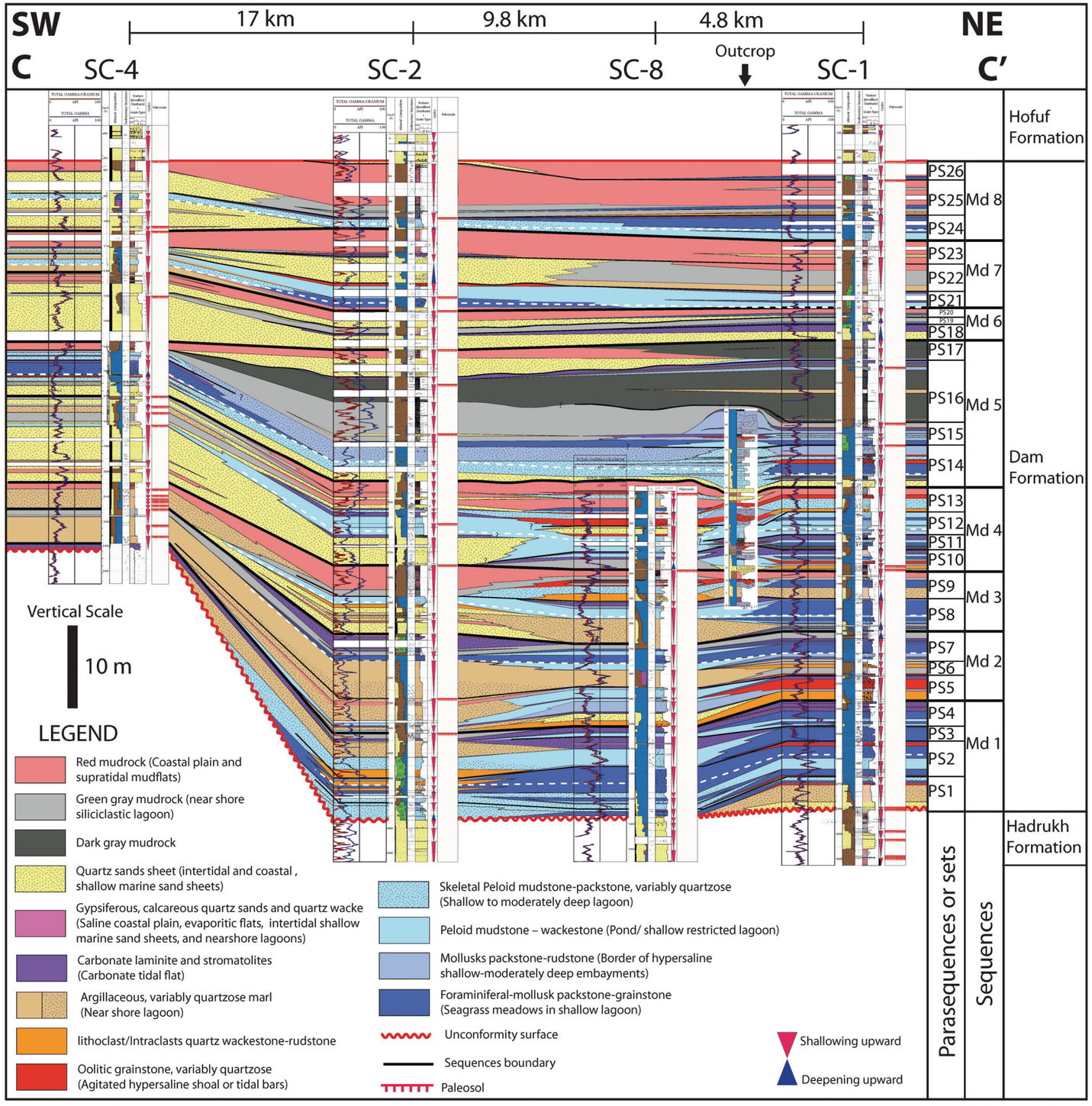

Figure 2.12 Regional facies cross section of the of the Early to Middle Miocene Dam Formation, based on core data. The broad tripartite subdivision of the formation into a basal marl (pale tan) a middle limestone (blue colors) and an upper siliciclastic unit (yellow, red and gray) is evident. Sequences and bounding surfaces most easily recognized in the carbonate prone units (right) and are traceable across the study area into updip siliclastics prone sections (left). Lithology, sedimentary structures and lithofacies legends are in APPENDIX D.

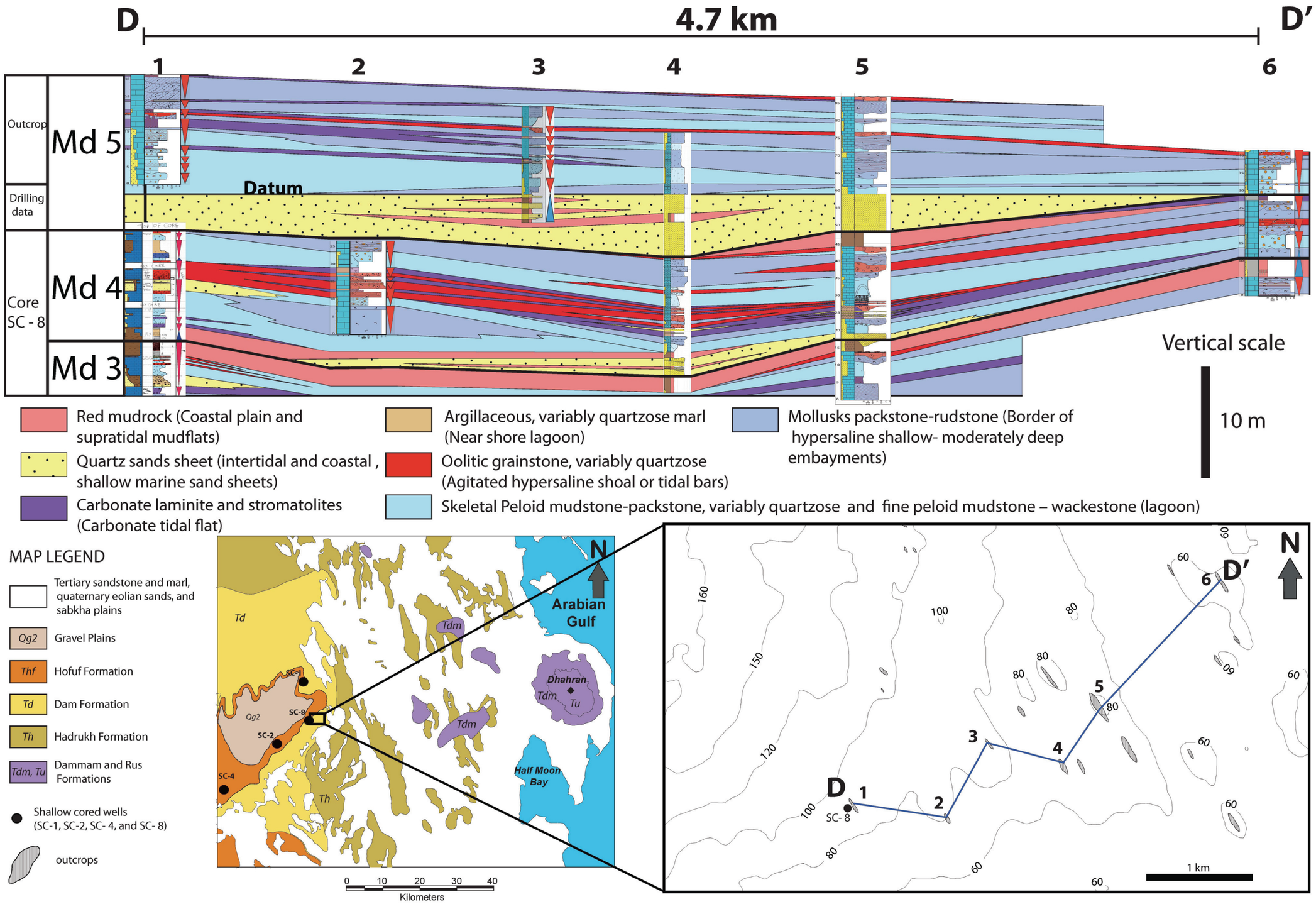

Figure 2.13 Facies cross section of Early Miocene Dam Formation from outcrops, in Lidam area. Sequences of Md 3, Md 4, and Md 5 were correlated and traced using core data of SC-8. Topographic elevation is in meters.

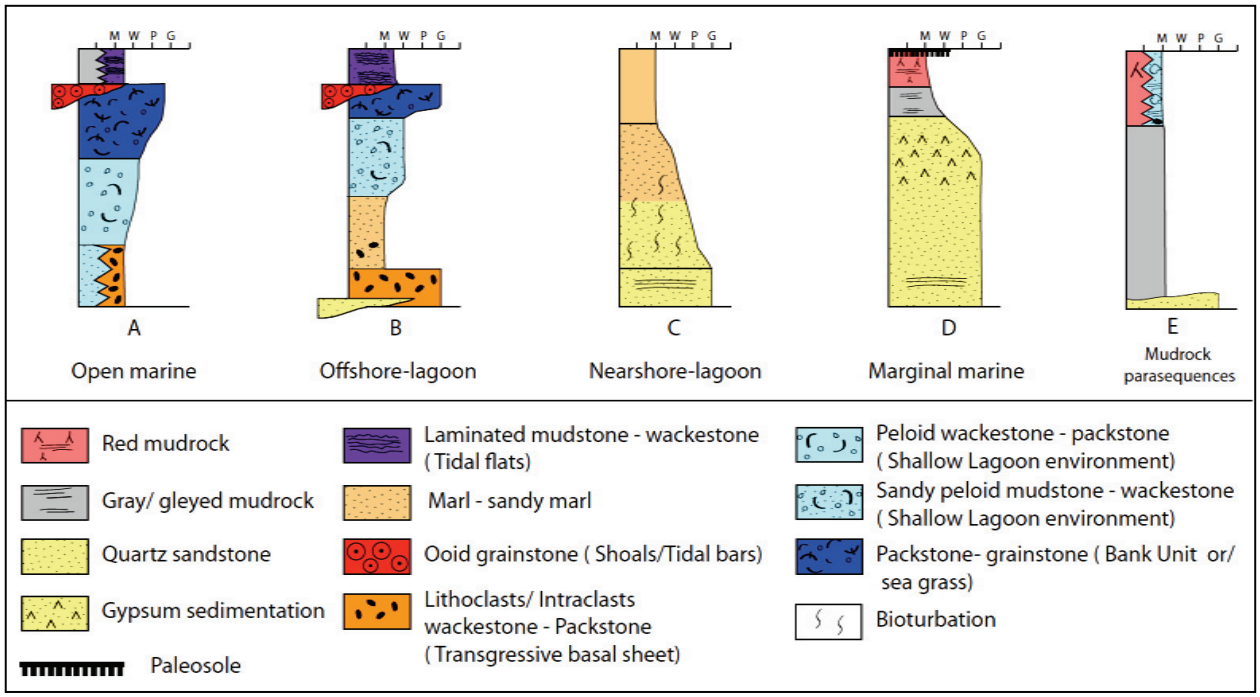

Figure 2.14 Generalized parasequence types within the Dam Formation: A) Open marine. B) Offshore-lagoon. C) Nearshore-lagoon. D) Marginal marine. E) Mudrock parasequences.

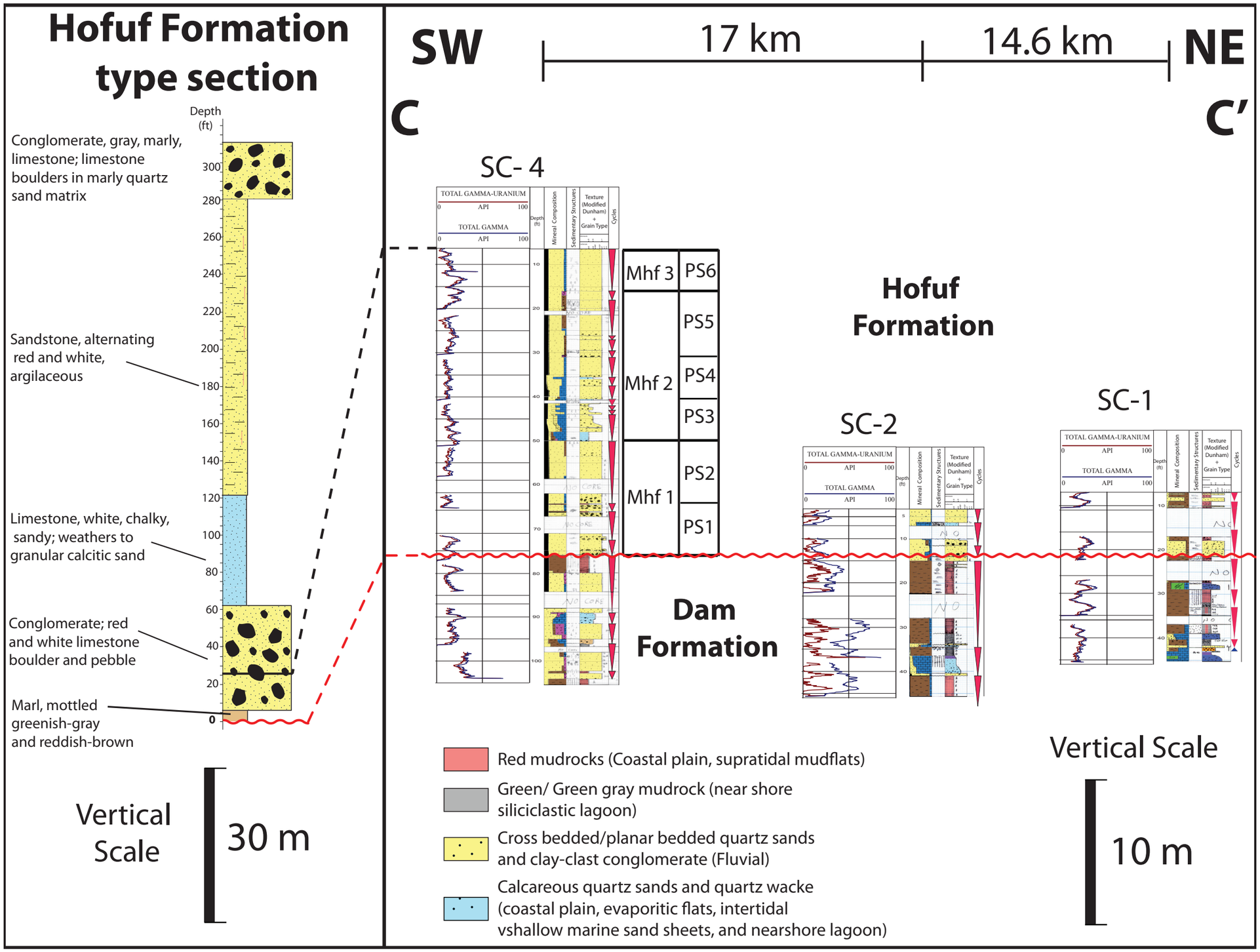

Figure 2.15 Lithologic columns showing the cored lower 20 m of the Hofuf Formation. Sequence picks are very tentative, given the limited data set. Inset shows the generalized 90 m thick Hofuf type section of Steineke and Koch (1935).

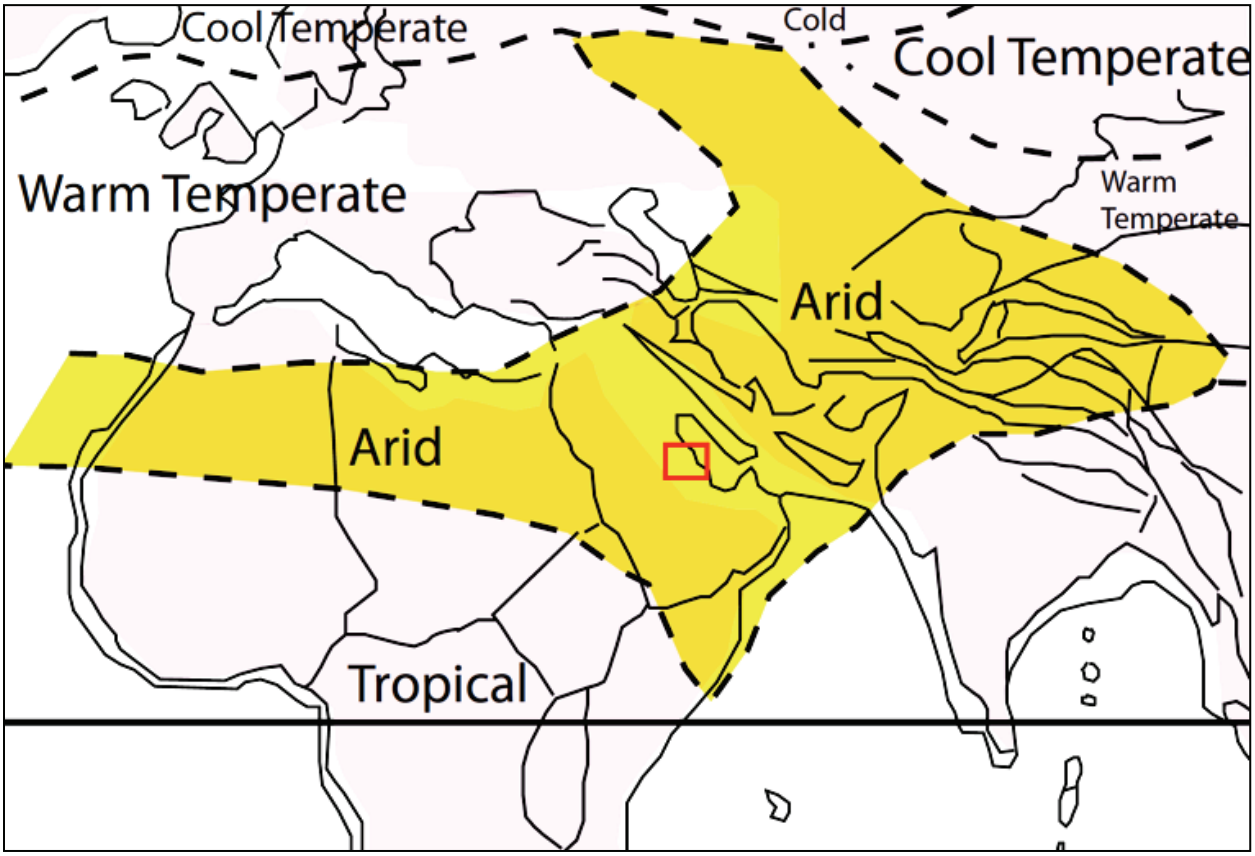

Figure 2.16 Paleoclimate of the Middle East and environs during the Miocene; arid zone shaded yellow. Study area shown by red box within Arabian Plate, which lay between 20 and 30 degrees N. Area with arid climate has evaporite deposits. Modified after (Scotese, 2001).

TABLES AND TABLE CAPTIONS

Table 1. Siliciclastic Facies

	Paleosols	Cross bedded/planar bedded quartz sands and clay-clast conglomerates (fluvial)	Red mudrock (Coastal plain and supratidal mudflats)	Green gray mudrock (near shore siliciclastic lagoon)	Brecciated micritic quartz sands and sandy lime mudstones to packstones (palustrine or ephemeral lake)	Gypsiferous, calcareous quartz sands and quartz wacke (Saline coastal plain, evaporitic flats, intertidal shallow marine sand sheets, and nearshore lagoons)	Quartz sands sheet (coastal, intertidal and shallow marine)
Occurrence	Hadrukh and Dam Formation.	Lower Hofouf, Dam, and Hadrukh Formation.	Upper Hadrukh; lower, middle, and upper Dam formation.	Middle and upper Dam formation.	Upper Hadrukh Formation in northwest below unconformity	Middle Hadrukh and upper Dam formation in up dip areas.	Hadrukh and lower Hofouf formations.
Color	Red, green mottled	Reddish and greenish tan.	Red, gleyed tops locally	Gray green	light tan to gray	Pale tan to light gray.	Reddish tan to light gray.
Thickness	20 cm to 3 m.	60 cm – 1.5 m.	20 cm – 1.5 m.	20 cm – 1.5 m.	Up to 8 m.	30 cm - 1 m.	1 - 10 m.
Structure	Blocky fabrics, with crumb texture; root traces filled with quartz sand; calcite nodules and ferruginous nodules locally	Cross-bedded and planar bedding commonly at the base and top. Bioturbation by roots.	Structureless, rooted and locally laminated at the base.	Massive to faintly laminated; rooted.	commonly brecciated and Infiltrated with more quartzose facies; fenestral cracks and small micrite-lined spar-filled branching tubules (rootlets?). Rare quartz grains cracked.	Structureless, locally with rootlets and root-hair traces filled with gypsum.	Structureless, locally with rootlets and rhizoconcretions; some root traces filled with quartz sand.
Texture, grain size, composition	Typically silty mudrocks composed of clay and silt-size quartz, and less commonly superimposed on quartz sands.	Quartz sandstone composed of fine-to-medium sand size quartz with lags of granules cobble-size clasts of red clay mudrock; quartz pebbles.	Silty mudrock composed of clay and silt size quartz.	Sandy mudrock composed of clay, silt and lesser fine to medium sand-size quartz.	Variable mixtures of bimodal medium to coarse, rounded quartz sand very fine to fine angular quartz sand, commonly mixed with lime mudstone; locally pisolitic and peloidal; locally microbial clots; Shelly fossils absent.	Quartz sandstone and quartz wacke composed of fine-to-medium sand size quartz with clay matrix.	Quartz sandstone composed of fine to medium quartz grains, rare granular clasts of calcite cemented sandstone.
Cement/Dolomatization		Very friable occasionally calcareous	Calcareous.	Calcareous, calcite nodules in some intervals	Cemented with micrite; calcite spar locally in cracks and tubules.	Calcite and gypsum cemented.	Mainly friable but some are calcite cemented. Gypsum and calcite nodules present in some intervals. Caliche nodules locally present in Hadrukh Formation.

Table 2. Carbonate Facies

	Brecciated carbonate sheet (Incipient paleosols), and Karstified units.	Lime/clay clast quartz wackestone-rudstone	Carbonate laminite and stromatolites (Carbonate tidal flat and shallow subtidal)	Argillaceous, variably quartzose marl (Near shore lagoon)	Fine peloid mudstone – wackestone (Pond/ shallow restricted lagoon)	Oolitic grainstone, variably quartzose (Agitated hypersaline shoal or tidal bars)	Mollusks packstone-rudstone (Border of hypersaline shallow-moderately deep embayments)	Foraminiferal-mollusk packstone-grainstone (Seagrass meadows)	Skeletal Peloid mudstone-packstone, variably quartzose (Shallow to moderately deep lagoon to low energy shelf)
Occurrence	Middle and upper Hadrukh and Dam formation.	Lower Dam Formation.	Middle Hadrukh, upper and lower Dam formation.	Middle Dam formation.	Middle Hadrukh and Dam formation.	Middle and upper Dam formation.	Lower middle and upper Dam Formation.	Lower, Middle, and upper Dam formation.	Lower, middle, and upper Dam formation.
Color	Gray - pale grey and tan.	Cream – greenish tan.	Tan.	Tan	Light tan – tan and creamy mottled.	Dark tan.	Tan – dark tan.	Pale tan.	Gray – pale tan.
Thickness ranges of units	Paleosol is 20 cm – 1.5 m. Karstified unit can be 6 – 12 m.	50 cm – 1.5 m.	20 cm – 0.5 m.	1 – 3 m.	0.5 - 2 m.	20 cm - 1 m.	20 cm – 1.5 m.	0.5 - 2 m.	30 cm – 1 m.
Sedimentary Structures	Carbonates have fitted fabric breccia; sheet cracks, burrows/root traces.	Structureless.	Laminae of alternating sand and lime mud; some bioturbation; overprinted with tepees and fitted fabric breccia locally.	Structureless, locally desiccation cracks.	Structureless – burrowed, some rootlets.	Multiple thin beds with normal grading and bidirectional cross bedding.	Generally structureless, but some intervals have burrow fills of coarse quartz sand. Occasionally hardgrounds at top.	Structureless.	Structureless locally burrowed (burrow mottled); some are laminated at top.
Texture, fabrics and grain types	Paleosol is sandy mudrock to lime wackestone/ mudstone host composed of carbonate and lesser terrigenous mud and fine to medium sand size quartz. Karst-modified facies are Irregular to angular carbonate clasts in matrix of variably sandy lime mudstone/ wackestone; more siliciclastic rich in updip.	Wackestone – rudstone of poorly sorted unit, composed of fine to Pebble size clasts of different origin (white clay mudrock, abraded lime mudstone, skeletal grainstone, quartzose dolomudstone, green mudrock in quartz wacky matrix.	Microbial laminite composed of clay, silt, and fine-to-medium sand-size peloids and quartz with some granule-size clay clasts.	Mudstone composed of terrigenous clay silt to very fine-to-fine sand size quartz, and locally some clay clasts.	Variably sandy mudstone and wackestone composed of silt-to-medium sand-size peloids, quartz grains, some granule-size lime mudstone clasts, variable clay content, fine green clay clasts,	Grainstone composed of fine-to coarse-sand-size ooids, Variable amount of quartz and less whole/ fragmented mollusk	Grainstone-packstone composed of fine to medium sand and granule-sized peloids, whole/ fragments skeletal (including mollusk and crab), and Foraminifera. Rare clasts of ooid grainstone	Grainstone-packstone composed of fine to coarse sand size whole and fragmented bivalves, gastropods, nodular and encrusting bryozoans, foraminifera, and crab fragments; some lime mud matrix in packstone	Packstone, wackestone, and mudstone. Packstone composed of silt-to-medium size peloids, medium – very coarse skeletal fragments, and foraminifera. Occasionally clasts of black-edge clay, bored hardgrounds, and green clay; Locally granule size lime mudstone clasts. Variable amounts of quartz.
Cement/ Dolomatization	Argillaceous calcite cemented/ gypsiferous, clay seams.	Argillaceous and calcareous; Infiltrated with green clay at top.	Limestone, fractures filled with gypsum.	Anhydrite nodules, clay infiltrated.	Iron staining, gypsum crystals calcite cement. Leached shells filled with calcite and clay.	Calcite cement.	Calcite cement.	Infiltrated lime mud, rare clay, and patchy cement.	Locally with infiltrated green clay, iron stained. Calcite cement. Dolomite crystals, calcite nodules, and rare gypsum crystals. Patchy calcite cement, leached clams filled with quartz grains.

Table 3. Hadrukh Formation sequences and system tracts.

Sequence and age	Lithostrat and sequence thickness (meters)	Basal boundary	LST	Transgressive system tract (TST)	Maximum flooding surface (MFS)	Highstand system tract (HST) (top may include LST)	Parasequence
Mhk1	Lower Hadrukh; 9.5 m updip (NE) to 7 m downdip (SW), onlaps on Dammam and Hadrukh unconformity.	Sharp erosional unconformity contact on dolomitic mudstone of Dammam Formation beneath conglomeratic sandstone (fluvial channel) updip and clay mudrock in the basin.	Not observed	TST conglomeratic quartz sandstone (channel) updip and red clay mudrock (downdip) grads to gypseous quartz sandstone.	MFS within thick gypseous quartz sandstone updip, at the base of green mudrock downdip	HST gypseous quartz sandstone shallow to less gypsum content on updip; downdip it is green mudrock shallow to gypseous wacky	2 parasequences
Mhk2	Lower Hadrukh; 6 m updip (NE) to 9 m downdip (SW)	Paleosol contact On top of fitted fabric gypsiferous quartz sandstone updip, and gypsiferous clay mudrock downdip, all beneath quartz sandstone.	Not observed	TST is irregular thick lamination of quartz sandstone on updip; downdip is grading from quartz sandstone to dolomudstone, of sheet cracks filled with green clay.	MFS at the base of caliche unit updip and within dolomudstone downdip.		4 parasequences
Mhk3	Lower Hadrukh; 5 m updip (NE) to 3 m downdip (SW)	At the top of a calichefied and fitted fabric sandstone (paleosol) on updip and downdip; in the basin it is on top of a sharp contact of quartzose dolomudstone, all beneath quartz sandstone.	Not observed				5 parasequences updip and 2 downdip.
Mhk4	Middle Hadrukh; 14 m updip (NE) to 23.5 m downdip (SW).	Sharp erosional contact on quartzose mudstone (tidal flat) updip (NE), overlain by quartz sandstone.	Not observed				3 parasequences
Mhk5	Upper Hadrukh; 5 m on the NE and 6 m on the SW, becoming more flat.	Sharp erosional contact on top of gypseous quartz sandstone (updip) and on top of fitted fabric brecciated sandstone (paleosol) downdip; all overlain by conglomeratic sandstone (fluvial channel).	Not observed	TST is gypseous quartz sandstone grads to quartzose lime mudstone.	MFS at the base of lime mudstone.	HST shallowing of gypseous quartz sandstone to less gypsum and capped by red mudrock.	About 4 parasequences in central depression and 1 parasequence in downdip.
Mhk6	Upper Hadrukh; 7.5 m on the NE; canot be correlated SW due to Karstification.	Sharp transgressive contact on top of gypseous sandstone and green mudrock, overlain by calcite cemented quartz sandstone.	Not observed	TST is quartzose lime mudstone on downdip, and gypseous quartz sandstone updip.	MFS within quartzose lime mudstone.	HST gypseous quartz sandstone updip, and shallowing from quartz sandstone to red mudrock paleosole downdip.	3 parasequences in downdip.
Mhk7	Upper Hadrukh; 7.5 m updip (SW) to 5 m downdip (NE); cannot be correlated far updip due to Karstification.	Sharp contact at top of terrigenous red mudrock overlain by quartz sandstone.	Not observed	None	None	HST quartz sandstone updip, and shallowing from quartz sandstone to red mudrock paleosole downdip.	3 parasequences in downdip.
Mhk8	Upper Hadrukh; 3 m downdip (NE), truncated by Dam and Hadrukh unconformity.	Sharp erosional contact on sandstone with clay content beneath calcite cemented quartz sandstone updip; on top of a terrigenous red mudrock overlain by creamy mudrock downdip; Truncated by Dam/Hadrukh erosional surface on updip.	Not observed	TST clayey quartz sandstone increased in lime content as cement upwards.	None	Non	3 parasequences in downdip.

Table 4. Dam Formation sequences and system tracts.

Sequence and age	Lithostrat and sequence thickness (meters)	Basal boundary	LST	Transgressive system tract (TST)	Maximum flooding surface (MFS)	Highstand system tract (HST) (top may include LST)	Parasequence Sets
Md1	Lower Dam Formation; 1.2 m updip to 10 m downdip.	Sharp contact of Dam limestone and marl on top of siliciclastic Hadrukh Formation; clay clasts locally.	Not observed	TST of dolomite peloid wackestone (shallow lagoon) and skeletal packstone-grainstone (sea grass influenced). Onlaps on unconformity on Hadrukh Formation.	MFS within skeletal- fragment grainstone (sea grass facies), and locally beneath lithoclast and peloid wackestone (shallow lagoon). Onlaps unconformity on Hadrukh Formation.	Updip HST is peloid wackestone grading upward into marl and downdip a skeletal fragment grainstone fining up into argillaceous carbonate laminite (tidal flat).	4 parasequence sets.
Md2	Lower Dam Formation; 5 m updip to 9 m downdip.	Downdip: sharp contact of transgressive lithoclast / intraclast unit on laminated sheet cracked, tidal flat facies. Updip has marl on top of tidal flat facies.	Not observed	TST; basal lithoclast rudstone grading up into oolitic grainstone, skeletal peloid packstone downdip; updip, TST dominated by sandy marl/	MFS at the base of skeletal fragment grainstone.	HST is foraminifera skeletal fragment packstone – grainstone shallowing upwards into laminite (tidal flat) and mudrock.	2 parasequence sets updip and 3 downdip.
Md3	Lower Dam Formation; 4 m updip to 7 m downdip.	Sharp contact on red and green mudrock or laminites (tidal flat) beneath marl, fluvial sandstone, or lagoonal limestone.	Not observed	TST updip, fluvial sandstone interbedded with red mudrock, passing downdip into marl and then skeletal grainstone.	MFS at base of regional limestone (skeletal-fragment packstone and wackestone).	Updip, HST is marl with paleosols, grading downdip into peloid skeletal fragment packstone capped by red mudrock paleosols. Downdip HST is skeletal fragment grainstone shallowing upwards into marl and red mudrock.	1 parasequence set updip and 2 downdip.
Md4	Middle Dam Formation; almost a uniform thickness about 10 m updip and downdip.	Sharp erosional contact on red mudrock (paleosol) beneath fluvial sandstone updip, and estuarine sandstone downdip.	Not observed	Updip, TST of sandstone (estuarine to fluvial) capped by carbonate laminite (tidal flat); downdip, TST is series of laminite or marl-capped parasequences.	MFS placed at base of regional marine limestone.	HST is peloid wackestone-packstone (lagoon) shallowing to laminite mudstone (tidal flat) to red mudrock (paleosols) updip. Downdip is oolitic grainstone inter fingering with peloid skeletal packstone (lagoon) capped by green mudrock.	4 parasequence sets.
Md5	Middle Dam Formation; 6.5 m updip to 16.5 m downdip.	Sharp erosional contact on red mudrock beneath fluvial sandstone.	Not observed	TST of thin fluvial sandstone grading upwards into peloid skeletal fragment packstone (lagoon) then skeletal fragment and bryozoan packstone-grainstone (sea grass influenced bank).	MFS at the base of regional skeletal-fragment limestone.	HST updip is skeletal fragment packstone-grainstone (bank) shallowing upwards to red mudrock, sandstone, and downdip into thick dark gray mudrock and minor carbonate laminite.	2 parasequence sets updip to 4 parasequences downdip.
Md6	Upper Dam Formation; 8.5 m updip to 5.5 m downdip	Sharp erosional contact on red mudrock updip and on top of gray mudrock downdip; overlain by fluvial sandstone.	Not observed	Updip, TST of sandstone grading up in to reddish sandstone and shale (paleosol); downdip grading into tidal flat laminites and mudrocks.	MFS at the base of extensive marl passing into limy mudrock and calcareous sandy wacky updip.	HST is green mudrock and marl and minor limestone along with quartz sand sheets to red mudrock (paleosol).	3 parasequence sets.
Md7	Upper Dam Formation; 5 m updip to 8 m downdip.	Sharp contact on red mudrock; overlain by	Not observed	TST of updip is marl and local skeletal fragment grainstone; pinches out downdip.	MFS at the base of regional skeletal limestone.	HST is peloid and skeletal carbonate, minor oolitic grainstone and subtidal quartz sand sheets capped by red mudrock.	3 parasequence sets.
Md8	Upper Dam Formation; 8.5 m updip to 9.5 m downdip.	Sharp erosional contact on red mudrock overlain by fluvial sandstone updip, and lagoonal carbonates downdip.	Not observed	TST fluvial up into marine sandstone (gypsiferous at top) pinches out downdip.	MFS at base of regional limestone.	HST updip is thin limestone, then quartz sandstone and red mudrock. Downdip HST is skeletal limestone shallowing upwards into gray then red mudrock.	2 parasequence sets updip and 3 parasequences downdip.

REFERENCES

Abreu, V.S., J. B. Anderson 1998. Glacial eustasy during the Cenozoic: sequence stratigraphic implications. American Association of Petroleum Geologists Bulletin, 82, p.1385– 1400.

Abdulasamad, E.O. and R. Barbieri 1999. Foraminiferal distribution and palaeoecological interpretation of the Eocene-Miocene carbonates at Al Jabal Al Akhdar (northeast Libya). Journal of Micropalaeontology, v. 18, no. 1, p. 45–65.

Abu-Ali, M. and R. Littke 2005. Palaeozoic petroleum systems of Saudi-Arabia – a basin modelling approach: Geo Arabia, 10, p. 131-168.

Abuserwil, A.K. 1996. Foraminiferal study of the Miocene from well D2-NC41, northwestern offshore, Libya. Petroleum Research Journal, v. 8, p. 25–48.

Adams, C. G., A. W. Gentry and P. J. Whybrow 1983. Dating the terminal Tethyan event, p. 273–298 in J. E. Meulenkamp (ed.), Reconstruction of Marine Paleoenvironments. Utrecht Micropaleontological Journal 30.

Al-Enezi, S.S. 2006. Comparison of Recent and Miocene foraminifera from Eastern Saudi Arabia. Master of Science Thesis, King Fahd University of Petroleum and Minerals.

Al-Husseini, M.I. 2000. Origin of the Arabian Plate structures: Amar Collision and Najd Rift, GeoArabia, v. 5, no. 4, p. 527–542.

Alkhaldi, F. 2009. Controls on Hierarchy of Miocene Buildups within a High resolution Cycle Stratigraphic Framework of Dam Formation, Lidam Area. Master of Science Thesis, King Fahd University of Petroleum and Minerals.

Al-Saad, H. and M.I. Ibrahim 2002. Stratigraphy, micropalaeontology, and pa-laeoecology of the Miocene Dam Formation, Qatar. GeoArabia, v. 7, no. 1, p. 9-28.

Alsharhan, A.S. and C.G.St.C. Kendall 2002. Holocene carbonate/ evaporites of Abu Dhabi, and their Jurassic ancient analogs. In: Barth, H.J., Boer, B.B. (Eds.), Sabkha Ecosystems. Kluwer Academic Publishers, p. 187–202.

Al-Sulaimi, J.S. and A.F. Pitty 1995. Origin and depositional model of Wadi Al-Batin and its associated alluvial fan, Saudi Arabia and Kuwait. Sediment. Geol. 97: p. 203-229.

Al-Tawil, A., T. C. Wynn, and J. F. Read 2003. Sequence response of a distal to proximal foreland ramp to glacio-eustasy and tectonics; Mississippian, Appalachian Basin, West Virginia-Virginia, U.S.A: Special Publication – Society for Sedimentary Geology, v. 78, p. 11-34.

Andrews, P. and J. A. H. Van Couvering 1975. Palaeoenvironments in the African Miocene. Contrib. Primatol. 5, p. 62-103.

Bahroudi, A. and C. J. Talbot 2003. The Configuration Of The Basement Beneath The Zagros Basin. Journal of Petroleum Geology, 26, p. 257–282.

Banner, J. L. 1995. Application of the trace element and isotope geochemistry of strontium to studies of carbonate diagenesis. Sedimentology, 42, p. 805–824.

Barron, J., B. Larsen and J.G. Baldauf 1991. Evidence for late Eocene to early Oligocene Antarctic glaciation and observations on late Neogene glacial history of Antarctica: results from Leg 119. In: Barron, J., Larsen, B., Baldauf, J.G. (Eds.), Proc. ODP Sci. Results 119, p. 869-891.

Bassiouni, M.A., O.H. Cherif and S.A. Ghanam 1975. Microfacies, sedimentation and stratigraphy of the Neogene-Quaternary sediments of the Mersa Matruh area, Western Desert, Egypt. 9th Arab Petroleum Congress, Paper 3(B-3).

Bellini, E. 1969. Biostratigraphy of the 'Al-Jaghbub' (Giarabub) Formation in Eastern Cyrenaica (Libya). Proceedings of the 3rd African Micropaleontology Colloquium, Cairo (1968), p. 165–183.

Berger, A., M. F. Loutre and J. Lascar 1992. Stability of the astronomical frequencies over the earth's history for paleoclimate studies. Science 255, p. 560–566.

Beydoun Z.R. 1993. Evolution of the northeastern Arabian Plate margin and shelf: hydrocarbon habitat and conceptual future potential. Revue de l'Institut Francais du Petrole, v. 48, p. 311–345.

Billups, K., J. E. T. Channell and J. Zachos 2002. Late Oligocene to early Miocene geochronology and paleoceanography from the subantarctic South Atlantic, Paleoceanography, 17(1): p. 4-10.

Bordenave, M.L. and R. Burwood 1990. Source rock distribution and maturation in the belt: provenance of the Asmari and Sarvak reservoirs oil accumulations. Organic Geochemistry, 16, p.369-387.

Boreen, T.D., and N.P. James 1993. Holocene sediment dynamics on a cool-water carbonate shelf: Otway, southeastern Australia: Journal of Sedimentary Petrology, v. 63, p. 574–588.

Boulila, S., B. Galbrun, K. G. Miller, S. F. Pekar, J. V. Browning, J. Laskar and J. D. Wright 2011. On the origin of Cenozoic and Mesozoic "third-order" eustatic sequences, Earth-Science Reviews, v. 109, Issues 3–4, p. 94-112.

Bristow, C. S. 1999. Aeolian and sabkha sediments in the Miocene Shuwaihat Formation, Emirate of Abu Dhabi, United Arab Emirates. Chap. 6 in Fossil Vertebrates of Arabia, pp. 50-60 (ed. P. J. Whybrow and A. Hill). Yale University Press, New Haven.

Chaube, A.N. and J. Al-Samahiji 1995. Jurassic and Cretaceous of Bahrain—Geology and petroleum habitat, in Al-Husseini, M.I., ed., Geo-94, Middle East Petroleum Geosciences Conference: Gulf Petrolink, Manama, Bahrain, v. 1, p. 295–305.

Collinson, M. E. 1982. Reassessment of fossil Potamogetoneae fruits with description of new material from Saudi Arabia. Tertiary Research 4, p. 83-104.

Cox, L. R. 1936. Fossil MoUusca from southern Persia (Iran) and Bahrain Island: Geol. Survey India, Paleont. Indica, n.s., v. 22, no. 2, p. 69.

Crossley, R., C. Watkins, M. Raven, D. Cripps, A. Carnell and D. Williams 1992. The Sedimentary Evolution of the Red Sea and Gulf of Aden. Journal of Petroleum Geology, v. 15, no. 2, p. 157–172.

Darwish, A.H. and C. D. Conley 1989. Pleistocene-Holocene sedimentation and diagenesis along the King Fahd Causeway between Saudi Arabia and Bahrain: Journal of King Abdulaziz University, Earth Sciences, v. 3, p. 63–79.

DAVIES, G. R. 1970. Algal·laminated sediments, Gladstone Embayment, Shark Bay, Western Australia: Am. Assoc. Petrol. Geol. Memoir 13, p. 169-205.

DeCelles, P. G. and K. A. Giles 1996. Foreland basin systems: Basin Research, v. 8, no. 2, p. 105–123.

Denton, G.H. and T. J. Hughes 2002. Reconstructing the Antarctic ice sheet at the Last Glacial Maximum. Quaternary Science Reviews 21, p. 193–202.

Denton, G. H., M. L. Prentice, and L. H. Burckle 1991. Cainozoic history of the Antarctic ice sheet, in R. J. Tingey, ed., The geology of Antarctica: Oxford, Clarendon Press, p. 365–433.

Dickson, J.A.D. 1966. Carbonate identification and genesis as revealed by staining. Journal of Sedimentary Petrology, v. 36, p. 491-505.

Dill, H.G. and H. Friedhelm 2007. Strontium (87Sr/86Sr) and calcium isotope ra-tios ($^{44}Ca/^{40}Ca$-$^{44}Ca/^{42}Ca$) of the Miocene Dam Formation in Qatar: tools for stratigraphic correlation and environment analysis. GeoArabia. V. 12, No. 3, p. 61-76.

Dill, H.G., R. Botz, Z. Berner, D. Stüben, S. Nasir and H. Al-Saad, 2005. Sedi-mentary facies, mineralogy, and geochemistry of the sulphate-bearing Miocene Dam Formation in Qatar. Sedimentary Geology, v. 174, p. 63-96.

Dunagan, S.P. 2000a. Constraining Late Jurassic paleoclimate within the Morrison paleoecosystem: insights from the terrestrial carbonate record of the Morrison Formation (Colorado, USA). GeoResearch Forum, Proceedings of the Fifth International Symposium on the Jurassic System. Trans Tech Publications, Switzerland, p. 523–532.

Dunagan, S.P. 1998. Lacustrine and palustrine carbonates from the Morrison Formation (Upper Jurassic), east-central Colorado, USA: implications for depositional patterns, paleoecology, paleohydrology, and paleoclimatology. PhD Thesis, University of Tennessee, Knoxville.

Dunham, R.J. 1962. Classification of carbonate rocks according to depositional texture, in Ham, W.E., ed., Classification of Carbonate Rocks: American Association of Petroleum Geologists, Memoir 1, p. 108–121.

Edgell, H.S. 1992. Basement Tectonics of Saudi Arabia as Related to Oil Field Structures, in Basement Tectonics, Rickard, M.J., et al., Eds., Dordrecht: Kluver Acad. Publ., vol. 9, p. 169–193.

Edgell, H.S. 1996. Salt tectonism in the Persian Gulf Basin, in Salt Tectonics, edited by J.L. Alsop, D.J. Blundell, and I. Davison, Geological Society Special Publications, 100, p. 129-151.

Ehrmann, W.U. 1991. Implications of sediment composition on the southern Kerguelen Plateau for paleoclimate and depositional environment. In: Barron, J., Larsen, B., Baldauf, J.G. (Eds.), Proc. ODP Sci. Results 119, p. 185-210.

Embry, A.F. and J. E. Klovan 1971. A Late Devonian reef tract on north-eastern Banks Island, N.W.T.: Bulletin of Canadian Petroleum Geology, v. 19, p. 730–781.

Enos, P. 1991. Sedimentary parameters for computer modeling. Kansas Geological Survey, no. 233, p. 63-99.

Esteban M. and C. F. Klappa 1983. Subaerial exposure environment, in Scholle, P.A., Bebout, D.G., and Moore, C.H., eds., Carbonate Depositional Environments: American Association Petroleum Geologists, Memoir 33, p. 1–54.

Flower, B.P. and J. P. Kennett 1993. Middle Miocene ocean/climate transition: high-resolution oxygen and carbon isotopic records from DSDP Site 588A, Southwest Pacific. Paleoceanography, 8, p. 811-843.

Flower B.P. and J. P. Kennett 1995. Middle Miocene deep water paleoceanography in the southwest Pacific: Relations with East Antarctic ice sheet development. Paleoceanography, 10, p. 1095-1112.

Fryberger, S.G., A.M. Al-Sari and T.J. Clisham 1983. Eolian Dune, Interdune, Sand Sheet And Siliciclastic Sabkha Sediments of an Offshore Prograding Sand Sea, Dhahran Area, Saudi Arabia. American Association of Petroleum Geologists Bulletin v. 67, no.2, p. 280-312.

Gentry, 1987b. Ruminants from the Miocene of Saudi Arabia. Bulletin of the British Museum (Natural History), Geology. 41, p. 433-439.

Gischler E. and A.J. Lomando 2005. Offshore sedimentary facies of a modern carbonate ramp, Kuwait, northwestern Arabian-Persian Gulf. Facies 50, p. 443–462

Glennie, K. W. 1970. Desert Sedimentary Environments. In Developments in Sedimentology, v. 12, Elsevier Scientific Publishing, Amsterdam, p. 222.

Glennie K. W. and A. K. Singhvi 2002. Event stratigraphy, paleoenvironment and chronology of SE Arabian deserts. Quaternary Science Reviews 21, p. 853-869.

Goff J.C., R. W. Jones and A. D. Horbury 1995. Cenozoic basin evolution of the northern part of the Arabian Plate and its control on hydrocarbon habitat. In: Al-Husseini M.I. (Ed.): GEO '94: The Middle East petroleum geosciences (selected papers from the Middle East Geosciences Conference, 1994). Gulf Petro Link, Manama, Bahrein, p. 402–412.

Gradstein, F.M., J. G. Ogg and A. G. Smith 2004. A Geologic Time Scale 2004, Cambridge University Press. , p. 589.

Grobe, H., D. K. Fütterer and Spieß 1990. Oligocene to Quaternary sedimentation processes on the Antarctic continental margin, ODP Leg 113, Site 693. In Barker, P.F., Kennett, J.P., et al., Proc. ODP, Sci. Results, 113: College Station, TX (Ocean Drilling Program), p. 121–131.

Hagan, G. M., and B. W. Logan 1974. Development of carbonate banks and hypersaline basins, Shark Bay, Western Australia: Am. Assoc. Petrol. Geologists Memoir No. 22, p. 61-139.

Hambrey, M.J., W. U. Ehrmann and B. Larsen 1991. Cenozoic glacial record of the Prydz Bay continental shelf, East Antarctica. In: Barron, J., Larsen, B., Baldauf, J.G. (Eds.), Proc. ODP Sci. Results 119, p. 77-132.

Hamilton, W. R., P. J. Whybrow and H. A. McClure 1978. Fauna of fossil mammals from the Miocene of Saudi Arabia. Nature 274, p. 248-249.

Hammad, F.A., B.M. Mosa, M.A. Bassiouni and M.A. Boukhary 1976. Contribution to the stratigraphy and petrography of the area between El Alamein and the Qattara Depression (Western Mediterranean coastal desert, Egypt). 9th Arab Petroleum Congress, Paper 132 (B-3).

Haq, B. U. 1980. Biogeographic history of Miocene calcareous nannoplankton and paleoceanography of the Atlantic Ocean. Micropalaeontology 26, p. 414-443.

Haq, B. U. and A. M. Al-qahtani 2005. Phanerozoic cycles of sea-level change on the Arabian

Platform. GeoArabia 10, p. 127–160.

Hardenbol, J., J. Thierry, M. B. Farley, T. Jacquin, P. C. Graciansky and P. R. Vail 1998. Mesozoic and Cenozoic sequence chronostratigraphic framework of European Basins. In Graciansky, C. P., Hardenbol, J., Jacquin, T. & Vail, P.R. (eds.): Mesozoic and Cenozoic Sequence Stratigraphy of European Basin, SEPM Special Publication 60, p. 13–603. SEPM Society for Sedimentary Geology, Tulsa.

Hays, J.D., J. Imbrie and N. J. Schackleton 1976. Variations in the Earth's orbit: Pacemaker of the ice ages. Science 194, p. 1121–1132.

Henson, F. R. S. 1951. Observations on the geology and petroleum occurrences of the Middle East: Proceedings, 3rd World Petroleum Congress, The Hague, sec. 1, p.118-140.

Hewaidy, A. 1991. Contribution to the stratigraphy of Miocene sediments in Qatar. Middle East Research Center, Ain Shams University, Egypt, Earth Science Series, v. 5, p. 160-170.

Hughes C. M. W. and A. J. Keij 1973. Organisms as producers of carbonate sediment and indicators of environment in the southern Persian Gulf. In: Purser (ed) The Persian Gulf: Holocene carbonate sedimentation in a shallow continental sea. Springer-Verlag, New York, p. 33–56.

Hussain, M., F. Al-Khalefah and N. I. Khandaker 2006. The Jabal Al Qarah Caves of Hofuf Area, Northeastern Saudi Arabia: A Geological Investigation. Journal of Cave and Karst Studies.

Huybrechts, P. 2002. Sea-level changes at the LGM from ice-dynamic reconstructions of the Greenland and Antarctic ice sheets during the glacial cycles. Quaternary Science Reviews 21, p. 203– 231.

Howarth, R.J. and J.M. McArthur 1997. Statistics for strontium isotope stratigraphy with a look-up table version. Journal of Geology, v. 105, p. 441-456.

Ibrahim, M.W., M. S. Khan and H. Khatib 1981. Structural evolution of Harmaliyah oil field, Eastern Saudi Arabia: American Association of Petroleum Geologists Bulletin, v. 65, p. 2403–2416.

Imbrie, J. and K. P. Imbrie 1979. Ice Ages: Solving the Mystery (MA: Harvard University

Press).

Jacobi, R. D. 1981. Peripheral bulge- a causal mechanism for the Lower Ordovician unconformity along the western margin of the northern Appalachians. Earth Plan. Sci. Let., 56, p. 245-251.

Jahnert, R. J. and L.B. Collins, 2011. Significance of subtidal microbial deposits in Shark Bay, Australia. Marine Geology, v. 286, Issues 1–4, p. 106-111.

Jones, R. W. and A. Racey 1994. Cenozoic stratigraphy of the Arabian peninsula and Gulf. In Micropaleontology and Hydrocarbon Exploration in the Middle East, p. 273-307 (ed. M. Simmons). Chapman and Hall, London.

Kendall C. G. S. C. and P. Skipwith 1969. Geomorphology of a recent shallow-water carbonate province: Khor Al Bazam, Trucial Coast, southwest Persian Gulf. Geol Soc Am Bull 80, p. 865– 892.

Kennett, J. P. 1995. A review of polar climate evolution during the Neogene, based on the marine sediment record. In: Vrba, E.S., Denton, G.H., Partridge, T.C., Burckle, L.H. (Eds.), Paleoclimate and Evolution, with Emphasis on Human Origins. Yale University Press, New Haven, p. 49-64.

Kennett, J. P. and P. F. Barker 1990. Latest Cretaceous to Cenozoic climate and oceanographic developments in the Weddell Sea, Antarctica: an ocean-drilling perspective. In: Barker, P.F., Kennett, J.P. (Eds.), Proc. ODP Sci. Results 113, p. 937-960.

Khalifa, H. and M. Mahmoud 1993. New occurrence of algal stromatolites and benthonic foraminifera from the Miocene of Al-Nikhsh area, southwest Qatar Peninsula (Arabian Gulf): implication on their palaeoenvironmental meaning. Arabian Gulf Journal of Science Research, v. 11, no. 3, p. 325–338.

Kingston, J. D. and A. Hill 1999. Late Miocene palaeoenvironments in Arabia. In, Fossil Vertebrates of Arabia, p. 389-407 (ed. P. J. Whybrow and A. Hill). Yale University Press, New Haven.

Kirkham, A. 1998. A Quaternary proximal foreland ramp and its continental fringe, Arabian Gulf, UAE. In: Wright VP, Burchette TP (eds) Carbonate ramps. Geol Soc Spec Publ 149, p.15–41.

Koop, W.J. and R. Stoneley 1982. Subsidence history of the Middle East Zagros Basin, Permian to Recent. Philosophical Transactions of the Royal Society, London, Series A, v. 305, p. 149–168.

Kortlandt, A. 1972. New perspectives on ape and human evolution. Stichting Voor Psychobiologie, Amsterdam.

Kraus, M.J. 1999. Paleosols in clastic sedimentary rocks: their geologic applications: Earth-Science Reviews, v. 47, p. 41–70.

Kroon, D., T. N. F. Steens and S. R. Troelstra 1991. Onset of monsoonal related upwelling in the western Arabian Sea. In: Prell, W.L., Niitsuma, N., et al. (Eds.), Proceedings of the ODP, Sci. Results 117, p. 257–264.

Kutzbach J. E., W. L. Prell and W. F. Ruddiman 1993. Sensitivity of Eurasian climate to surface uplift of the Tibetan plateau. J Geology 101, p. 177-190.

Laskar, J., P. Robutel, F. Joutel, M. Gastineau, A. C. M. Correia and B. Levrard 2004. A longterm numerical solution for the insolation quantities of the Earth. Astronomy and Astrophysics 428, p. 261–285.

Lawver, L.A. and L. M. Gahagan 2003. Evolution of Cenozoic seaways in the circum-Antarctic region, Palaeogeography, Palaeoclimatology, Palaeoecology, vol. 198, p. 11-37.

Lee, T. Y. and L. A. Lawver 1995. Cenozoic plate reconstruction of Southeast Asia. In: Hilde, T.W.C., Flower, M.F.J. (Eds.), Southeast Asia Structure and Tectonics. Tectonophysics 251, p. 85-138.

Logan, B.W., D. E. Cebulski 1970. Sedimentary environments of Shark bay, Western Australia. Memoir — American Association of Petroleum Geologists 13, p. 1–37.

Logan, B. W., P. Hoffman and C. D. Gebelein 1974. Algal mats, cryptalgal fabrics, and structures, Hamelin Pool, Western Australia, in Logan, B. W., ed., Evolution and Diagenesis of Quaternary Carbonate Sequences, Shark Bay, Western Australia: Am. Assoc. Petrol. Geol. Memoir No. 22, p. 140-194.

Lomando A. J. 1999. Structural influences on facies trends of carbonate inner ramp systems, examples from the Kuwait-Saudi Arabian coast of the Arabian Gulf and northern

Yucatan, Mexico. GeoArabia 4, p. 339–360.

Loreau, J.P. and B.H. Purser 1973. Distribution and ultrastructure of Holocene ooids in the Persian Gulf In: Purser, B.H.(ed.), The Persian Gulf, Springer- Verlag, Berlin, p. 279-328.

Trauth M. H., J. C. Larrasoaña and M. Mudelsee 2009. Trends, rhythms and events in Plio-Pleistocene African climate, Quaternary Science Reviews, Volume 28, Issues 5–6, p. 399-411

Matthews, R.K., C. Frohlich 2002. Maximum flooding surfaces and sequence boundaries: comparisons between observations and orbital forcing in the Cretaceous and Jurassic (65–190 Ma). GeoArabia 7, p. 503–538.

McClure, H. A. 1978. The Rub 'al Khali. In Quaternary period in Saudi Arabia, p. 252-263 (ed. S. S. Al-Sayyari and J. E. Zotl). Springer-Verlag, New York.

Miller, K. G., E. Barrera, R. K. Olsson, P. J. Sugarman, S. M. Savin 1999. Does ice drive early Maastrichtian eustasy? Global δ18O and New Jersey sequences. Geology 27, p. 783–786.

Miller, K. G., R. G. Fairbanks and G. S. Mountain 1987. Tertiary oxygen isotope synthesis, sea-level history, and continental margin erosion. Paleoceanography 2, p. 1– 19

Miller, K. G., G. S. Mountain, J. D. Wright and J. V. Browning 2011. A 180-million year record of sea level and ice volume variations from continental margin and deep-sea isotopic records: Oceanography, v. 24, p. 40-53.

Miller, K. G., J. D. Wright, J.D. and R. G. Fairbanks 1991. Unlocking the ice house: Oligocene–Miocene oxygen isotopes, eustasy, and margin erosion. Journal of Geophysical Research 96, p. 6829– 6848.

Mitchell, D. J. W., R. B. Allen, W. Salama, and A. Abouzakm 1992. Tectonostratigraphic framework and hydrocarbon potential of the Red Sea: Joumal of Petroleum Geology, v. 15, p. 187-210.

Mitchum, R. M., J. R. , and J. C. Van Wagoner 1991. High frequency sequences and their stacking patterns: Sequence stratigraphic evidence of high-frequency eustatic cycles: Sedimentary Geology, v. 70, p. 131-160

Moore, D.G. and P.C. Scruton 1957. Minor internal structures of some recent unconsolidated sediments: American Association of Petroleum Geologists Bulletin, v. 41, p. 2723-2751.

Otero, O. and M. Gayet 2001. Paleoichthyofaunas from the Lower Oligocene and Miocene of the Arabian Plate. Palaeogeography, Palaeoclimatology, Palaeoecology, v. 165, no. 1, p. 141–169.

Ouda, K. 1998. Biostratigraphy, paleoecology and paleogeography of the Middle and Late Tertiary deposits of the northern Western Desert, Egypt. Neues Jahrbuch für Geologie und Paläontologie Abhandlungen, v. 207, no. 3, p. 311–394.

Patton, T. L. and S. J. O'Connor 1988. Cretaceous flexural history of northern Oman mountain foredeep, United Arab Emirates. Bull. Am. Ass. Petrol. Geol., 72, p. 797-809.

Peebles, R.G. 1999. Stable isotope analysis and dating of the Miocene of the Emirate of Abu Dhabi, United Arab Emirates. In, P.J. Whybrow and A. Hills (Eds.), Fossil Vertebrates of Arabia. Yale University Press, p. 88–107.

Pekar, S.F., N. Christie-Blick, M. A. Kominz and K. G. Miller 2002. Calibrating eustasy to oxygen isotopes for the early icehouse world of the Oligocene. Geology 30, p. 903– 906.

Pekar S. F. and R. M. Deconto 2006. High-resolution ice-volume estimates for the early Miocene: evidence for a dynamic ice sheet in Antarctica. Palaeogeography, Palaeoclimatology, Palaeoecology 231, p. 101–109.

Pettijohn, F. J., P. E. Potter and R. Siever 1987. Sand and Sandstone, p. 617. Springer-Verlag, Berlin.

Pope, M. and J. F. Read 1997. High-Resolution Surface and Subsurface Sequence Stratigraphy of Late Middle to Late Ordovician (Late Mohawkian-Cincinnatian) Foreland Basin Rocks, Kentucky and Virginia. American Association Petroleum Geologists Bulletin, v. 81, no. 11, p. 1866 – 1893.

Powers, R. W. 1968. Lexique stratigraphique international: Saudi Arabia: vol III, Asie, fasc. 10b1: Centre National de la Recherche Scientifique, Paris, p. 177.

Powers, R. W., L. F. Ramirez, C. D. Redmond and E. L. Elberg 1966. Geology of the Arabian Peninsula: sedimentary geology of Saudi Arabia: United States Geological Survey

Professional Paper 560-D, p. 147.

Prentice, M. L. and R. K. Matthews 1988. Cenozoic Ice Volume History: Development of a Composite Oxygen Isotope Record. Geology, v. 16, p. 963-966.

Pye, K. and H. Tsoar 1990. Aeolian Sand and Sand Dunes: London, Unwyn Hyman, p. 396.

Read, J. F. 1998. Phanerozoic carbonate ramps from greenhouse, transitional and icehouse worlds: clues from field and modeling studies. In: Wright, V.P. & Burchette, T.P. (eds) Carbonate Ramps. Geological Society, London, Special Publications, 149, p. 107-135.

Retallack, G. J. 1993. Classification of paleosols: discussion and reply. Discussion Geol. Soc. Am. Bull. 105, p. 1635–1636.

Riding, R., J.M. Martin and J.C. Braga 1991a. Coral stromatolite reef framework, Upper Miocene, Almerla, S.E. Spain. Sedimentology.

Roberts, N. and H. E. Wright 1993. Vegetational, lake-level, and climatic history of the Near East and Southwest Asia. In Wright, H.E., Kutzbach, J.E., Webb, T. III, Ruddimann, W.F., Street-Perrott, F.A. and Bartlein, P.J., editors, Global climates since the last glacial maximum, Minneapolis: University of Minnesota Press, p. 194–220.

Sadek, A. M. 1999. Sedimentological and paleoenvironmental studies of the subsurface Miocene-Pleistocene sequence at Al-Dabaa, North Western Desert, Egypt. Unpublished PhD thesis, Alexandria University, p. 247.

Sarnthein M., and E. Walger 1973. Classification of modern marl sediments in the Persian Gulf by factor analysis. In: Purser BH (ed) The Persian Gulf Holocene Carbonate sedimentation and diagenesis in a shallow epicontinental sea. Springer-Verlag, New York, p. 471.

Saner, S., K. Al-Hinai and D. Perincek 2005. Surface expressions of the Ghawar structure, Saudi Arabia: Marine and Petroleum Geology, v. 22, p. 657–670.

Scotese, C. R. 2001. Atlas of Earth History, Volume 1 Paleogeography, PALEOMAP Project, Arlington, Texas, p. 52.

Scotese, C.R. 2002. http://www.scotese.com, (PALEOMAP website).

Seilacher, A. and T. Aigner 1991. Storm deposition at the bed, facies, and basin scale, The

geological perspective. In: Einsele G., Ricken W., and Seilacher A., eds. Cycles and Events in Stratigraphy, Springer-Verlag, Berlin, p. 249-268.

Sen, S. and H. Thomas 1979. Découverte de rongeurs dans le Miocène moyen de la Formation Hofuf (Province du Hasa, Arabie Saoudite). Comptes Rendus Sommaire de la Société géologique de France 1, p. 34-37

Shackleton, N. J. and J.P. Kennett 1975. Paleotemperature history of the Cenozoic and initiation of Antarctic glaciation: Oxygen and carbon isotopic analyses in DSDP Sites 277, 279, and 281. Initial Reports of the Deep Sea Drilling Project 29, p. 743–755.

Shanmugam, G. 2011. Process-sedimentological challenges in distinguishing paleo-tsunami deposits. Natural Hazards, Springer.

Sharland, P.R., D.M. Archer, D.M. Casey, R.B. Davies, A.P. Hall, A.D. Horbury and M.D. Simmons 2001. Arabian Plate Sequence Stratigraphy. GeoArabia, Special Publication no. 2, p. 371.

Sharland, P.R., D.M. Casey, R.B. Davies, M.D. Simmons and O.E. Sutcliffe 2004. Arabian Plate Sequence Stratigraphy – revisions to SP2. GeoArabia, v. 9, no. 1, p. 199-214.

Shinn, E.A. 1973. Sedimentary Accretion Along the Leeward, Southeast Coast of Qatar Peninsula, Persian Gulf. In B.H. Purser (Ed.), The Persian Gulf, Springer-Verlag, Berlin, p. 200-209.

Smith, L.B., A. A. Al-Tawil and J. F. Read 1995. Regional, interbasinal fourth-order sequence stratigraphy, Late Mississippian, Illinois to Appalachian Basins (abstract): American Association of Petroleum Geologists, Official Program, v. 4, p. 90A.

Snedden, J. W. and C. Liu 2010. A Compilation of Phanerozoic Sea-Level Change, Coastal Onlaps and Recommended Sequence Designations: Search and Discovery Article #40594.

Steineke, M. and R. A. Bramkamp 1952. Mesozoic rocks of Eastern Saudi Arabia (abstract) American Association of Petroleum Geologists Bulletin, vol. 36, p. 909.

Steineke, M., R. A. Bramkamp and N. J. Sander 1958. Stratigraphic relations of Arabian Jurassic oil: American Association of Petroleum Geologists Symposium, Tulsa, USA, p 1294-

1329.

Steineke, M. and Hoover 1936. Unpublished report in Powers, R.W., 1968, Lexique stratigraphique international: Saudi Arabia: vol III, Asie, fasc. 10b1: Centre National de la Recherche Scientifique, Paris, p. 177.

Sugden, W. 1962. Structural analysis and geometrical prediction of change of form with depth of some Arabian plains-type folds: AAPG Bulletin, v. 46, p. 2213-2228.

Thomas, H. 1979. Le rôle de barrière ècologique de la ceinture saharo-arabique au Miocène: arguments paléontologiques. Bulletin du Muséum national d'Histoire naturelle, Paris 1, p. 127-135.

Thomas, H. 1983. Les bovidae (Artiodactyla: Mammalia) du miocene moyen de la formation Hofuf (Province du Hasa, Arabie Saoudite). Palaeovertebrata 13, p. 157-206.

Thomas, H., S. Sen, M. Khan, B. Battail and G. Ligabue 1982. The lower Miocene fauna of Al-Sarrar (Eastern Province, Saudi Arabia). ATIAI, The Journal of Saudi Arabia Archaeology 5, p. 109-136.

Thomas, H., P. Taquet, G. Ligabue and C. Del'Agnola 1978. Découverte d'un gisement de vertébrés dans les depôts continentaux du Miocène moyen du Hasa (Arabie Saoudite). Comptes Rendus Sommaire de la Société géologique de France, p. 69-72.

Tucker, M. E. 2003. Sedimentary Rocks in the Field, 3rd ed. Wiley, Chichester, U.K.

Vincent, E. and W. H. Berger 1985. Carbon dioxide and polar cooling in the Miocene: The Monterey hypothesis in Sundquist, E.T., et al., eds., Natural variations Archean to present: American Geophysical Union, Geophysical Monographs, v. 32, p. 455–468.

Wagner, C.W. and C. Van der Togt 1973. Holocene sediment types and their distribution in the southern Persian Gulf. In: Purser, B.H. (Ed.), The Persian Gulf. Springer, New York, p. 123–156.

Walker, R. G. and D. J. Cant 1984. Sandy fluvial systems, in Walker, R. G., ed., Facies models (2nd edition): Kitchener, Ontario, Geoscience Canada, Reprint Series 1, The Geological Association of Canada, p. 71-90.

Warren, J. K. 2006. Evaporites: Sediments, Resources and Hydrocarbons. New York: Springer.

Weaver, C.E. and K. C. Beck 1977. A model for chemical sedimentation in a peri-marine environment. Aliocene of the S.£. United Stales, Amsterdam, p. 201-225.

Wender, L. El, J. W. Bryant, M. F. Dickens, A. S. Neville and A.M. Al-Moqbel 1998. Paleozoic (Pre-Khuff) hydrocarbon geology of the Ghawar Area, Eastern Saudi Arabia. GeoArabia, v.3, no. 2, p. 273–302.

Whitney, J. W., D. J. Faulkender and M. Rubin 1983. The environmental history and present conditions of the northern sand seas of Saudi Arabia. Open File Report 83-749. U. S. Geological Survey, Wshington, D. C.

Whybrow, P. J. 1984. Geological and faunal evidence from Arabia for mammal "migrations" between Asia and Africa during the Miocene. Courier Forschungsinstitüt Senckenberg 69, p.189-198.

Whybrow, P. J. and H. A. McClure 1981. Fossil mangrove roots and palaeoenvironments of the Miocene of the eastern Arabian peninsula. Palaeogeography, Palaeoclimatology, Palaeoecology32, p. 213-225.

Whybrow, P. J., M. E. Collinson, R. Daams, A. W. Gentry and H. A. McClure 1982. Geology, fauna (Bovidae, Rodentia) and flora from the Early Miocene of eastern Saudi Arabia. Tertiary Research 4, p. 105-120.

Whybrow, P. J., H.A. McClure and G.F. Elliot 1987. Miocene stratigraphy, geology and flora (algae) of Eastern Saudi Arabia and the Ad Dabtiyah vertebrate locality. Bulletin of the British Museum (Natural History), v. 41, p. 371–382.

Whybrow, P. J., P.F. Friend, P.W. Ditchfield and C.S. Bristow 1999. Local stratigraphy of the Neogene outcrops of the coastal area: western region, Emirate of Abu Dhabi, United Arab Emirates. In, P. Whybrow and A. Hill (Eds.), Fossil, Vertebrates of Arabia. Yale University Press, p. 28-37.

Williams, H., F. J. Turner and C. M. Gilbert 1982. Petrography, 2nd ed.: W. H. Freeman, San Francisco, p. 626.

Wood, W. W., W. E. Sanford 1990. Groundwater control of evaporite deposition. Econ. Geol. 85, p. 1226 – 1235.

Wright, J.D., K. G. Miller and R. G. Fairbanks 1992. Early and middle Miocene stable isotopes: implications for deepwater circulation, climate and tectonics. Paleoceanography 7, p. 357– 389.

Wright, V. P. 1990. Lacustrine Carbonates, In: M. E. Tucker, V. P. Wright and J. A. D. Dickson Eds., Carbonate Sedimentology, Blackwell, p. 164-190.

Wright, V. P. and S. B. Marriott 1993. The sequence stratigraphy of fluvial depositional systems: the role of floodplain storage. Sediment. Geol. 86, p. 203–210.

Wynd, J. G. 1965. Biofacies of the Iranian Oil Consortium Agreement Area, unpublished report cited in Jones and Racey (1994).

Zachos, J.C., M. Pagani, L. Sloan, E. Thomas, K. Billups 2001. Trends, rhythms, and aberrations in global climate 65 Ma to present. Science 292, p. 686-693.

CHAPTER 3

C and O Isotope Chemostratigraphy of Early and Middle Miocene Hadrukh, Dam and Hofuf Formations, eastern Saudi Arabia.

Abstract

Carbon and Oxygen isotope profiles were obtained from the carbonate fraction of siliciclastic and minor carbonate sediments in an updip Miocene core in the Lidam area, Eastern Province, Saudi Arabia .The updip succession consists of the Aquitanian Hadrukh sands (non-marine, 52 m thick) up into Aquitanian to Langhian, Dam mixed siliciclastics and carbonates (marginal marine, up to 47 m thick), and capping Langhian-Serravallian Hofuf sands (non-marine; only lower 23 m sampled). High frequency negative excursions of $d^{13}C$ within the succession appear to relate to near-surface diagenesis by soil gas depleted in ^{13}C beneath sequence boundaries. Several positive C isotope excursions evident in the Lidam Miocene section can be tied to similar excursions in Qatar and UAE, where Sr isotope dates constrain the ages of the units. The overall C isotope profile at Lidam shows depleted values early in the Miocene to heavy values in the Middle Miocene, becoming lighter again in the late Miocene,. The profile appears to follow the long-term global $d^{13}C$ curve. However the excursions were highly amplified perhaps as a result of migration of light-C ground waters into the system in the early and later Miocene, while the middle Miocene was marine influenced. Incursion of meteoric groundwaters into the study area was driven by the long-term global sea level changes.

The $d^{18}O$ values in the Lidam Miocene are surprisingly light, extending down to -12.5 ‰ $_{VPDB}$. They similarly reflect incursion of meteoric waters with very negative $d^{18}O$ values into the

region during siliciclastic phases with an intervening phases of more marine-influenced deposition with heavier $d^{18}O$ values. The very light $d^{18}O$ values of the meteoric waters may be explained by rainfall associated with enhanced Miocene Indian monsoons, and with far travelled air mass trajectories migrating across north Africa and from the polar region.

INTRODUCTION

C and O stable isotopes from the calcareous siliciclastic units of the Early and Middle Miocene Hadrukh, Dam and Hofuf formations, eastern Saudi Arabia (Figures 3.1 and 3.2) were obtained from a core drilled in the Lidam area. The stable isotopes were sampled to evaluate their use for inter-regional correlation, correlation with the deep-sea $d^{18}O$ based global curve (Abreu and Anderson, 1998), and to evaluate diagenetic overprinting of the succession by meteoric groundwaters.

Carbon isotopes show a distinctive signal in the Miocene sediments from the deep-sea cores, with light $\partial^{13}C$ values initially, which become heavier into the Middle Miocene, before becoming lighter into the Late Miocene (Woodruff and Savin, 1989; Poore et al., 2006). These trends grossly correlate with the long-term Miocene sea level curve (Woodruff and Savin, 1989) suggesting a causal relationship. The C isotope data from the study area appear to show the long-term trends evident in the deep-sea data, which provides a reasonable correlation tool, and the mechanisms for this are evaluated (Butzin et al., 2011). However, correlation to isotope profiles in other Middle East countries is more complex and may reflect diagenetic and local climatic factors.

Diagenesis by meteoric aquifer systems can modify C and O isotopic compositions typically shifting them to lighter values. To evaluate this, the C and O isotope signal was tied to

the sequence stratigraphic framework, and any significant shifts noted. The shifts are interpreted in terms of diagenesis by advancing and retreating meteoric aquifer systems within the long-term regressive-transgressive-regressive framework of the succession, and its internal bounding unconformities. The very light O isotope values (commonly -9 to -12 ‰ $_{VPDB}$) are surprising, and are interpreted within the framework of rainfall and groundwater sources evident today modified for the Miocene climate.

Regional Setting And Stratigraphic Framework

The Miocene sediments of the Lidam area formed on the distal part of the Arabian foreland, bordering the Zagros fold and thrust belt (Figure 3.1). By the end of the Eocene, the Tethys completely closed due to the collision of India with Asia (Rögl, 1999). Around the Eocene – Oligocene boundary, the isolated Paratethys Sea had opened north of the Mediterranean Sea and the Indo-pacific seaway remained open east of the Arabian Plate (Baldi, 1980). The Arabian Gulf today is considered a relict of the Indo-pacific seaway. This Indo-pacific seaway remained open through Early Miocene, Aquitanian to the end of Burdigalian. By end of Burdigalian a collision of the Arabian plate with the Anatolian plate to the north resulted in closing of the Indo-pacific seaway from the Mediterranean Sea (Rögl, 1999). During Middle Miocene, Langhian time, the Indo-pacific seaway reopened and reconnected to the Mediterranean Sea but finally closed in the early Serravallian (Rögl, 1999). This seaway narrowed by Late Miocene, Tortonian time due to collision of Arabia with the Iranian plates (Rögl, 1999).

The paleogeographic position of Arabia in the Miocene was between 20 and 30 degrees north latitude (Scotese, 2001). The Miocene climate in the region was broadly similar to today but warmer (Scotese, 2002). The Early Miocene may have been more humid than today

(Andrews and van Couvering, 1975), and it became drier with intermittent arid conditions during the late Early Miocene (Whybrow et al., 1982; Collinson, 1982; Whybrow, 1984; Kingston and Hill, 1999; Dill et al., 2005). The Middle to Late Miocene was characterized by arid to hyperarid conditions (Pye and Tsoar, 1990; Bristow, 1999; Kingston and Hill, 1999).

The Miocene succession overlies the Eocene carbonates with a major unconformity, marking non-deposition of the Oligocene. It is overlain unconformably by Quaternary sediments (Steineke et al., 1968). The Miocene succession consists of the Hadrukh Formation (composed of 2 sequences), the Dam Formation (composed of 8 sequences), and the Hofuf Formation (of which only the lower part is exposed), but which may contain a total of 2 sequences (Chapter 2).

PREVIOUS ISOTOPIC STUDIES OF THE MIOCENE

Isotopic Studies, Dam Formation, Qatar

A study of carbonate rocks of the Dam formation of Qatar by Dill (2005) revealed that carbon and oxygen isotopes have a spread of -2.1‰ +4.6‰ $_{VPDB}$ ($\partial^{13}C$) and -9.9 to 1.4‰ $_{VPDB}$ ($\partial^{18}O$), respectively (Figure 3.2). The Qatar Dam Formation section was assigned an age of approximately 22–18 Ma (Aquitanian– Burdigalian) using Sr isotopes (Dill et al., 2005) (Figure 3.2). The $\partial^{13}C$ values of marine carbonates of the Dam Formation were near 0 ‰ $_{VPDB}$, and were interpreted as a result of the primary atmospheric carbon source (Dill et al., 2005). The light oxygen isotope values were interpreted to result from impact of freshwater on carbonate precipitation (Dill et al., 2005). The intermediate oxygen isotope values of -3.0 and -3.7‰ $_{VPDB}$ reflect brackish conditions (Dill et al., 2005). Interpretation of mixing of marine brines with continental waters (e.g., run-off, ground water) was supported by the depletion of measured ^{34}S isotopes coeval with the decreased $\partial^{18}O$ values as low as -10‰ $_{VPDB}$ (Dill et al., 2005).

Isotopic Studies, Gachsaran Formation, United Arab Emirates

The Gachsaran Formation in UAE, equivalent to the Dam Formation in Saudi Arabia, was assigned an Early-Middle Miocene (Burdigalian to Early Langhian) in Abu Dhabi based on Sr isotope dating (Figure 3.2; Peebles, 1999). Samples from dolomitic mudstone, massive gypsum and massive nodular anhydrite were analyzed for $\partial^{13}C$ / $\partial^{18}O$, all revealed strongly positive $\partial^{18}O$ and $\partial^{13}C$ values (Figure 3.2). The strongly positive $\partial^{18}O$ values of the dolomites were attributed to evaporitic depositional conditions (Peebles, 1999) and low temperatures of formation (non-burial temperatures) (Allan and Wiggins, 1993). The positive $\partial^{13}C$ values were interpreted as the result of microbial or bacterial methane production that generated isotopically heavy CO_2 in pore water, creating pore waters with positive $\partial^{13}C$ values (Peebles, 1999), although these are much lighter than carbonates attributed to methanogenesis generally. The $\partial^{13}C$ and $\partial^{18}O$ values observed in the Gachsaran Formation are typical of sediments produced in arid coastal environment (Morse and Mackenzie, 1990; Allan and Wiggins, 1993; Peebles, 1999).

METHODS

Powder samples of calcareous sandstone, sandy calcareous shale, sandy limestone and limestone were taken from SC-4 core for $\partial^{13}C$ and $\partial^{18}O$ isotope analysis. This core is in an updip position and is dominated by calcareous siliciclastic sediments. The isotope analyses were done at Saudi Aramco Research and Development Laboratories, Dhahran, Saudi Arabia supervised by Peter D. Jenden. The $\partial^{13}C$ and $\partial^{18}O$ values were reported as per mil (‰) VPDB. The low carbonate contents in some of the siliciclastic samples necessitated a number of reruns on samples. Based on pooled standard deviations of replicate analyses, the uncertainty in %CaCO3 was estimated to be +/- 6.7% by weight; standard deviation for $\partial^{13}C$ analyses was +/- 0.07 ‰

and for $\partial^{18}O$ values, it was +/- 0.10 ‰ respectively.

The C and O isotope data were plotted as profiles against the stratigraphic column of core SC-4. Carbon and oxygen isotope profiles from nearby countries were also plotted, along with the Miocene deep-sea data for comparison. The ages of the SC-4 succession are broadly constrained by biostratigraphy, and by the global sea level cycle chart (Abreu and Anderson, 1998), in the absence of $^{87/86}Sr$ dates (discussed in Chapter 2). However, the sequence framework allowed its lower part to be tied to the Sr dated Qatar section.

RESULTS

The carbon and oxygen isotope profiles are shown on the chronostratigraphic chart (Figure 3.2) and are plotted alongside the detailed lithologic log of the core, which also shows the major and minor sequences (Figure 3.3). The C and O isotope profiles show substantial variations in each of the Early to Middle Miocene Hadrukh, Dam and Hofuf formations. The positive carbon excursions identified in this study were informally labeled C1 to C10 (Figure 3.2). The carbon and oxygen isotope values are shown on the cross plot (Figure 3.4) to evaluate the effects of diagenesis/meteoric water influence.

Hadrukh Formation Stable Isotopes

Stable isotopes of the Hadrukh Formation samples are more negative than the Dam and Hofuf Formations (Figures 3.3 and 3.4). Overall the C and O isotope profiles of the Hadrukh Formation are relatively uniform with only a small variation (Figure 3.3). The $\partial^{18}O$ values range from-12.5 to -11.4‰ $_{VPDB}$ with about 1.1‰ range in the data, while $\partial^{13}C$ values range from -8.8‰ to -7.1‰ $_{VPDB}$ with about 1.7‰ range in the data. The C isotope profile shows three $\partial^{13}C$ excursions (C1 to 3), one in the basal Hadrukh, one in the middle of the Hadrukh Formation near

the top of Hd 1 and one near the top of the formation (Figures 3.2 and 3.3). However, at a finer scale, the carbon isotope profile shows a series of small increases and decreases that appear to correlate with parasequences within the formation, in which $\partial^{13}C$ values decrease upward toward the parasequence boundary (Figure 3.3). The $\partial^{13}C$ and $\partial^{18}O$ cross plot shows a tight clustering of the data from the Hadrukh Formation (Figure 3.4), with values that are the most negative of all the Miocene successions in the region.

Dam Formation Stable Isotopes

The lower part of Dam sequence Md 6 and the upper part of Md 8 lacked sufficient carbonate for isotope analysis. Only a thin part of Md 1 is present in the SC-4 core. In terms of C and O isotopes, the Dam Formation samples range from slightly more positive to markedly enriched relative to Hadrukh Formation samples (Figure 3.4). The C and O isotope profile shows considerable variation (Figure 3.3). The $\partial^{18}O$ profiles in the Dam Formation can be divided into two stratigraphic groupings (Figure 3.3). Sequences Md1 to Md5 has $\partial^{18}O$ values ranging from -11.6 ‰ to -9.6 ‰ $_{VPDB}$ (with about a 2‰range), extending up to -8.6‰ $_{VPDB}$ at the base of Md 4. Sequences Md6 to Md8 has more positive $\partial^{18}O$ values of -6 ‰ to -2.8 ‰ $_{VPDB}$ and a range of about 3.2‰ with a negative excursion at the end of sequence Md7 that reached to -10‰ $_{VPDB}$.

The $\partial^{13}C$ values within the lower Dam Formation are between -8.5 to -5‰ $_{VPDB}$ and increase to -4.5 to -2.5‰ $_{VPDB}$ in the upper Dam Formation. The $\partial^{13}C$ values within the eight Dam sequences typically increase upward within the sequence and then decrease toward the top of the sequence (Figure 3.3). This is evident in sequences Md 2, 3, 4, 5, and 7. Only the upper part of Md 6 was sampled, and showed an increase up toward the top boundary. Only the middle part of Md 8 had sufficient carbonate for analysis thus any internal trends are not known. Thus

there are seven positive carbon isotope excursions within the Dam Formation, labeled C4 to C10 (Figures 3.2 and 3.3).

The C and O isotope profiles in the Dam Formation (Figure 3.3) are negatively correlated in sequences Md 1 to lower Md 3, and positively correlated in lower Md 4 and upper Md 6. They tend to show a weak positive correlation in upper Md 5 and lower 7.

Hofuf Formation

The lowermost Hofuf Formation samples lacked carbonate thus no isotope data is available for this interval. The upper two thirds of the lower Hofuf Formation sampled has more positive $\partial^{13}C$ and $\partial^{18}O$ values compared to the Hadrukh Formation and they are slightly heavier than those of the lower Dam Formation (Figure 3.3), but are lighter than the upper Dam values (Figure 3.4). The ∂13C values range from -4.1 ‰ to -7 ‰ $_{VPDB}$ (range of 2.9 ‰ excursion in data, while $\partial^{18}O$ values are from -9.0 ‰ to -10.7 ‰ $_{VPDB}$, with a range of about 1.7 ‰. The $\partial^{13}C$ and $\partial^{18}O$ values are negatively correlated.

DISCUSSION

Origin of the Carbonate Fraction

The origin of the carbonate fraction in the units studied is critical to interpreting the isotopic signal evident in Figures 3.3, 3.4 and 3.5. In the Hadrukh and the Hofuf formations, which are both dominantly quartz sand-prone units in the study area, and in much of the up-dip Dam Formation, the calcite fraction (commonly admixed with minor fine-grained gypsum), forms a fine-grained matrix or fine grained calcite cement between quartz grains. This carbonate component thus is likely to have been deposited from ground waters that permeated the sands.

In some units the carbonate fraction is the dominant component, resulting in the quartz grains floating in the carbonate matrix. These units likely are limy sand deposits of marginal marine lake In either case, the carbonates probably precipitated from groundwater systems, either between pore spaces of sands, or in shallow siliciclastic lakes fed by groundwaters, where they were admixed with the terrigenous component. In contrast, the carbonate-prone units in the Dam Formation are the updip tongues of the marine carbonate units that dominate the Dam succession downdip. Thus these carbonate-prone units are likely to be originally marine carbonates that have undergone some diagenetic alteration within regional aquifer systems.

Diagenetic Effects

The Miocene succession of the study area has undergone very limited burial beneath Plio-Pleistocene sediments, which are less than 50 m thick (Powers et al., 1966). This would tend to rule out diagenetic resetting of the carbonate signal by burial diagenesis. However, it is possible that the stable isotope signal of the sediments was diagenetically reset in near-surface settings. In sedimentary units in which the disconformity surface was vegetated, light C from plants within the carbon dioxide-charged soil zone results in relatively light $\partial^{13}C$ signatures at tops of parasequences or sequences (Allan and Matthews, 1982). Given the climatic setting of the study area in the Miocene, the terrestrial flora would include C3 plants ($\partial^{13}C$ values ranging from -24 to -34 ‰ $_{VPDB}$) and C4 plants (includes desert and salt marsh plants and tropical grasses with $\partial^{13}C$ values from -6 to -19 ‰ $_{VPDB}$; Deines, 1980).

The major shift in $\partial^{13}C$ values (from -2 to -6 ‰ $_{VPDB}$) and $\partial^{18}O$ values (from -1 to -10 ‰ $_{VPDB}$) at the top of the Eocene Dammam Formation appears to be related to major diagenetic overprinting in the uppermost, karsted and brecciated Dammam sediments. This overprinting reset the uppermost highly karstified Dammam dolomites, which were deposited in an evaporitic

setting, to values more like the overlying Hadrukh sediments, which was deposited in a more humid setting (Andrews and van Couvering, 1975).

Negative excursions in $\partial^{13}C$, albeit small (0.25 to over 1 ‰ $_{VPDB}$), are evident beneath paleosols in the Hadrukh Formation, (Figure 3.3). Negative excursions in $\partial^{13}C$ toward sequence boundaries are well expressed in the Dam Formation sequences Md 2, 3, 4, 5 and 7. In contrast, the $\partial^{13}C$ values appear to increase toward the top of Md 6, and there is insufficient data available for Md 8.

The $\partial^{18}O$ values show much more variation, with only a few decreasing toward sequence or parasequence boundaries. Decrease in $\partial^{18}O$ would reflect the effects of meteoric water diagenesis, shifting the $\partial^{18}O$ signal to lighter values (Allan and Matthews, 1982). The lack of sulfate evaporites capping cycles in the Dam Formation in the study area rules out decrease in C and O toward tops of cycles as being related to sulfate reduction (Chafetz et al., 1999).

Correlation using Carbon Isotopes

In terms of large-scale excursions in C isotopes, the Miocene succession of the Lidam area appears to mimic the change in $\partial^{13}C$ values evident in the deep sea Miocene (Figure 3.2; Woodruff and Savin, 1989). However the Lidam excursions are highly exaggerated relative to the deep-sea signal. Both show relatively low $\partial^{13}C$ values in the Early Miocene Aquitanian-early Burdigalian, changing to more positive values in the late Burdigalian-early Langhian, and then decreasing into the Middle Miocene Langhian-Serravallian. Nevertheless, the Lidam carbon isotope curve supports the initial correlations based on the sea level cycle chart of Abreu and Anderson (1998), which shows the Dam Formation extending up into the Langhian (Chapter 2).

The correspondence between the deep sea $\partial^{13}C$ signal and the global sea level curve suggests a causal relationship with depleted $\partial^{13}C$ values during lowered sea levels and enriched values during higher sea levels (Woodruff and Savin, 1989), although actual oceanographic causes are likely to be more complex (Poore et al., 2006). It is likely that the Lidam Miocene $\partial^{13}C$ curve was amplified by the relative movement of light C continental groundwaters into the system during Hadrukh and Hofuf deposition, and relatively heavy C marine waters dominating the system during Dam deposition (especially during the upper Dam Formation). The $\partial^{13}C$ values of the Hadrukh and Hofuf carbonate fraction is similar to that of many lacustrine carbonates which usually have relatively negative $\partial^{13}C$ values (-7.2 to -8.8‰ $_{VPDB}$) due to incorporation of CO_2 derived from the decay of plant material in hinterland soil (probably from C4 plants; Deines, 1980).

In terms of inter-regional correlation, the positive excursions on the C-isotope profiles appear to be useful in correlation with the Qatar Dam Formation (Dill et al., 2005) and UAE Dam equivalent (Peebles, 1999; Figure 3.2). Within the Dam Formation of this study, the positive excursions in the $\partial^{13}C$ profile labeled C4 through C7 can be correlated with the Dam section in Qatar, indicating that the Qatar section dated by Sr isotopes spans Lidam sequences Md 1 through 4. Lidam C-isotope excursions C8 and 9 also can be correlated with the Sr isotope dated UAE section of the Gachsaran Formation (Dam equivalent). Thus the C-isotope correlations allow the Sr isotope dated sections of Qatar and UAE to be tied to the Lidam succession, supporting the relative ages based on biostratigraphy and the sea level cycle chart (Chapter 2).

Significance of the Oxygen Isotope Profiles

Covariance of C and O isotopes has been used to support a primary signal unaltered by

diagenesis in which positive C isotope excursions relate to increased surface productivity due to increased thermohaline circulation as ice caps grow, resulting in positive oxygen isotope excursions (Zachos et al., 2001). In contrast, C and O isotope covariance also been used to support diagenetic alteration of carbonates (Allan and Matthews, 1982). In stable isotope *profiles* of the Lidam succession, there is limited covariance between C and O isotopes. However, the commonly observed trend of $\partial^{13}C$ decreasing up toward sequence boundaries is suggestive of early diagenesis associated with light C isotopes within soil zones. The lack of a similar trend toward lighter oxygen isotope values toward the upper sequence boundaries as a result of meteoric water diagenesis (except possibly Md 5 and 7) may imply that $\partial^{18}O$ values of meteoric waters commonly were increased by evaporation during the emergence event. Alternatively it could be argued that the heavier $\partial^{18}O$ values near the boundaries reflects increase in $\partial^{18}O$ values of the global ocean with cooling, as in the Pleistocene (Hays et al., 1976; Zachos et al., 2001), which was reflected in the oxygen isotope composition of the rainfall. For the marine units in the Dam Formation, more positive $\partial^{18}O$ values near boundaries could also reflect a shallowing trend which in relatively arid settings can result in near-shore waters having increased $\partial^{18}O$ values compared to offshore waters (Gischler and Lomando, 2005). However the expected concomitant increase in $\partial^{13}C$ may have had been overprinted by diagenesis to give the light C values near the boundaries.

The extremely light $\partial^{18}O$ values observed within the Miocene succession at Lidam (-8.5 to -12.5 ‰ $_{VPDB}$) are among the lightest reported for the Miocene in the region. The light $\partial^{18}O$ values in the Dam carbonates of Qatar were interpreted as being related to impact of light meteoric groundwaters on carbonate precipitation, while intermediate values were interpreted to reflect more brackish conditions (Dill et al., 2005). However the $\partial^{18}O$ values of the study area

are even lighter than those in Qatar, which thus likely relates to its paleogeographic position with relation to air masses and isotopic composition of rainfall.

The $\partial^{13}C$ and $\partial^{18}O$ cross plot (Figure 3.5) for all the isotopic data combined for the Miocene succession in this study (Hadrukh, Dam, and Hofuf Formations) shows a moderate correlation between $\partial^{13}C$ and $\partial^{18}O$ (R^2= 0.64). Such a trend is suggestive of meteoric influence on carbonate deposition, with the light C-O values being meteoric water dominated and the heavier C –O values being more typical of the marine signal. However, according to Hendy (1971) this correlation also could indicate that calcite precipitated by non-equilibrium isotopic fractionation with the parent water, and thus should not be used for paleoenvironmental reconstructions. In contrast, Dorale and Liu (2009) argue that simultaneous enrichment of $\partial^{13}C$ and $\partial^{18}O$ in stalagmites is the indication of change in both climate and vegetation type or productivity. Fleitmann et al. (2003) suggested that even if $\partial^{13}C$ and $\partial^{18}O$ were correlated, the $\partial^{18}O$ can be used as a proxy for the amount of rainfall especially for tropical and subtropical areas, and the oxygen isotopic composition of the rainfall is inversely related to the amount of rainfall.

To have an idea of the oxygen isotope composition of paleo-water or paleo-groundwater we used the water-calcite fractionation equation: ($10^3 \ln a = 2.78 (10^6 T^2) - 2.89$; Friedman and O'Neil, 1977). Using the -9 to -12.5 ‰ $_{VPDB}$ range of $\partial^{18}O$ values of the calcites of the Hadrukh, lower Dam and Hofuf formations, and assuming mean temperature of 35 degrees C, would require waters ranging from about -5 to about -8.5 ‰ $_{SMOW}$, and at 45 degrees C (assuming slight geothermal heating), would require waters of -4 to -7.5 ‰ $_{SMOW.}$ All these values suggest relatively light rainfall values.

Isotopic Composition of Rainfall in relation to Air Circulation Patterns

Today the climatic pattern of Arabian Peninsula is influenced by three major fronts of moisture (air masses) (Figure 3.6) (MacLaren, 1979; Al Qurashi, 1981; Sen, 1983; Alyamani & Sen, 1993; Fleitmann et al., 2004; Trauth et al., 2009). During autumn, the retreating monsoon front (tropical air masses) reaches the area from the southern Arabian Peninsula. This front originates from the Indian Ocean and Arabian Sea and contains warm and moist air. This monsoon front often picks up further moisture, as it is moves through the Red Sea trough. Autumn rains become more frequent and are characterized by medium to high intensity over the western and northwestern regions of the country (Alyamani, 2001).

During winter, there are two fronts involved: warm and moist continental tropical air masses coming from the Atlantic Ocean through the middle and north African continent, and polar air masses impacting the eastern Mediterranean Sea (Alyamani, 2001). The recharge sources of the ground-water and springs in the *western* region are thought to be related to the seasonal monsoon air masses (Alyamani, 2001; Fleitmann et al., 2004) whereas winter storms originating from the Atlantic Ocean might be less important for the ground-water balance (Alyamani, 2001). The continental tropical air masses of Atlantic origin also might have contributed to the formation of rainfall of over the western region (Alyamani, 2001).

The isotopic compositions of the rainwater in western Arabia show that autumn storms are isotopically enriched in $\partial^{18}O$ (-0.53 to -1.91‰ $_{VSMOW}$) compared with winter storms (-0.56 to -2.90‰ $\partial^{18}O_{VSMOW}$) (Gat & Carmi, 1970; Leguy et al., 1983; Alyamani, 2001). In northern Oman, $\partial^{18}O$ values of precipitation originating from Arabian Sea moisture is between -2 to -9 ‰ $\partial^{18}O_{VSMOW}$ (Weyhenmeyer et al., 2000; 2002). Averaged $\partial^{18}O$ values of analyzed Late Pleistocene stalagmites from eastern and northern Saudi Arabian caves are between -8 to -13 ‰

$\partial^{18}O_{VPDB}$, and were interpreted to be precipitated from monsoonal rainfall during warm interglacial periods (Fleitmann et al., 2004).

In the Arabian Peninsula, autumn storm rainfall and the monsoon rains are slightly enriched in $\partial^{18}O$ compared to highly depleted waters of Mediterranean storms. This is probably because they originated from warm bodies of water (such as the Indian Ocean, Arabian Sea and Red Sea). The high autumn temperatures and low humidity of the air enhance the evaporation of the rainwater and result in oxygen isotope enrichment (Alyamani, 2001). In Saudi Arabia and Bahrain, the $\partial^{18}O$ values of modern rainfall tend to range between -2 to +2‰ $_{VSMOW}$ (Fleitmann et al., 2004) Thus the present day oxygen isotope composition of the rainfall of Arabia is far too heavy to account for the oxygen isotopic compositions of most of the Lidam Miocene carbonate fraction.

In the present day Mediterranean, rainfall can have very light $\partial^{18}O$ values ranging between -5 and -18. The most depleted waters are those that are from polar air masses coming from northeastern Europe and which have a short interaction with the Mediterranean Sea (Rindsberger et al 1983; Dirican et al., 2005). However, depleted rainfall also is associated with air masses that travel over the length of North Africa into the Middle East (Aouad-Rizk et al., 2005). Depleted rainfall sourced from the Indian monsoon was suggested to account for Holocene and Pleistocene oxygen isotope values of cave carbonates (Fleitmann et al., 2004).

Isotopic composition of ground water aquifers in eastern Arabia

Groundwater and springs will have oxygen isotopic values close to rainfall, unless they were subjected to significant evaporation before or during infiltration into the aquifers, which will result in heavier $\partial^{18}O$ values. One of the major aquifers in Saudi Arabia in the Eastern

Province is the Umm er Radhuma (UER) aquifer. It is a single thick hydraulic unit of regional extent. The catchment area (recharge) for this aquifer is the belt of Late Cretaceous Aruma and Paleocene-Eocene Umm er Radhuma carbonate outcrop plus the area mantled by eolian sand of Ad-Dahna to the west of the study area (Powers et al., 1966). A general hydraulic gradient towards the Gulf coast was observed from the piezometric data of the UER aquifer (Hoetzl, 1995). The ground water has a residence time of about 10 to 20 k.y and is thus early Holocene or latest Pliestocene age (Hoetzl, 1995).

Two water paths can be observed (Figure 3.7). The first preferential underground flow channel comes from an area south of Wadi Shaba, where wide areas with uncovered UER limestones are exposed, and flow reaches the coast in the region of the study area. The other preferential flow comes down from the As Sulb plateau, crossing the Wadi Miyah and continuing from there towards the Gulf, where the main flow reaches the coast near Al Qatif to the north of the study area. Isotopic studies by Shampine et al. (1979) showed that water from the Umm er Radhuma (UER) Formation is moving upward in Al Hasa area (south of the study area) which has springs fed by the water from the southern As Summan Plateau. These springs feed the largest oases in the Eastern Province of Saudi Arabia. Upward movement of water from the Paleogene aquifers is probably typical of most of the coastal region of the Eastern Province (Burdon, 1973). Maximum burial depths to the top of the Cretaceous are less than 300 m (Abu-Ali, 2005), which might increase the temperatures of the ascending waters by 10^{o} C, and thus would only account for a roughly 1 per mil shift in precipitated calcite compositions.

The typical range of $\partial^{18}O_{SMOW}$ values measured in modern and fossil groundwaters in the region is -5 to -2‰ (Figure 3.8; Al- Sayari & Zoetl, 1978; Hoetzl and Zoetl, 1978; Hoetzl, 1995; Fleitmann et al., 2004). These waters could have influenced carbonate precipitation or

diagenesis of the upper Dam Formation, but they are too heavy to account for the light values of the Hadrukh, lower Dam and Hofuf formations. This suggests that aquifer waters during much of the Early and Middle Miocene reaching the study area much lighter $\partial^{18}O$ values than present day- and late Pleistocene ground waters. This suggests different atmospheric circulation patterns than today, perhaps associated with generally long air mass trajectories over land, amplified monsoon effects and perhaps warmer climate giving more negative $\partial^{18}O_{SMOW}$ rainfall for a given vapor composition.

Tibetan Plateau Effect on Monsoons

The broad uplift of the Tibetan plateau acts as a source of heating in the lower atmosphere during the summer that creates a low-pressure system over central Asia, which in turn draws in warm and humid air from the Indian Ocean towards the plateau (Webster, 1987; Harris, 2006). This drawing in of warm and humid air affects the Arabian Peninsula during the summer, which causes south westerly winds (sourced from Indian Ocean) that strengthen the Indian monsoon over the area. On the other hand, during winter its effect diminishes and the Indian monsoon became weak over the Arabian Peninsula (Fleitmann et al., 2004). The uplift of the Plateau was driven by the collision between the Indian and Asian plates by the end of the Eocene. The oldest suggested onset of the present monsoon system was in the Oligocene (Ramstein et al., 1977). Subsequent variations in strength of the monsoon were reported during the Miocene (Kroon et al., 1991; Derry and France Lanord, 1996; Quade et al., 1997; and Cerling et al., 1997; Dettman et al., 2001; Guo et al., 2002; clift et al., 2002; Jia et al., 2003) and the Pliocene (An et al., 2001). Uplift of the Tibetan Plateau has affected the evolution of the East- and South Asia monsoon (Liu and Yin, 2002). The strengthening of the Indian monsoon during the late Miocene and East Asia monsoon during the Pliocene was linked to tectonic

activity and uplift of the Tibetan Plateau (Harrison et al., 1995; Zheng et al., 2000). Average isotopic content of precipitation in northeastern Tibet is about -13 ‰ $\partial^{18}O_{VSMOW,}$ and average rainfall in Western Tibet has about $\partial^{18}O_{VSMOW}$ values of about -5‰ (Figure 3.8; Wei and Gasse, 1999).

During the Pleistocene Fleitmann et al. (2004) indicated that monsoon-influenced precipitation of pluvial periods in Oman, Yemen, and Egypt occurred during warm interglacial phases. The pluvial periods were characterized by highly negative $\partial^{18}O_{VPDB}$ values from speleothem records (Figure 3.8). During glacial periods these areas were dominated by arid to hyper-arid climate conditions. Fleitmann et al. (2004) linked higher rainfall pluvial periods during the early to middle Holocene of Arabia and Africa, to the strengthening of the Indian monsoon circulation during summer. Very negative values for monsoon precipitation in summer are attributed to the isotopically depleted warm-moist air masses brought inland from the oceans by the summer atmospheric circulation (Wei and Gasse, 1999). This suggests that the highly negative $\partial^{18}O$ values from speleothem records formed during pluvial periods during rapid interglacial rise in sea level, when compared to the marine oxygen isotope curve (Fleitmann et al., 2004).

The variation in the $\partial^{18}O_{VPDB}$ values of the Miocene succession in the study area, could have been influenced by strengthening and weakening of the Indian monsoon. However, some negative $\partial^{18}O$ values could have originated from Mediterranean air masses penetrating the region during glacial stages, based on Pleistocene stalagmites from Eastern Saudi Arabia caves (Fleitmann et al., 2004). The rapid negative shift in the $\partial^{18}O_{VPDB}$ values along the Eocene-Miocene unconformity suggests that the area was subjected to the Indian monsoon at the beginning of the Miocene. This monsoon effect remained strong through Early Miocene, early

Aquitanian with possible intermittent periods of aridity by the end of sequence Hd 1 of the Hadrukh Formation. This monsoon started to weaken by the end of Aquitanian. As the monsoon weakened, aridity increased and culminated by end of Burdigalian. This is inferred from the increase in $\partial^{18}O$ values in the Burdigalian. The Indian monsoon started to strengthen by the beginning of Middle Miocene, Langhian to the early Serravallian time, and $\partial^{18}O$ values then decreased. This timing ties to the Mid-Miocene Climatic Optimum.

At a finer scale, the $\partial^{18}O$ values in the Dam Formation have complex origins. However $\partial^{18}O$ profiles within quartz sand-prone 3rd order sequences in the Dam Formation decrease upward, reaching minimum values within the sequence then increasing toward the sequence boundaries, as in sequences Md 2, 3, 4, beginning of 5, end of 6, and beginning of 7. Although this mimics the oxygen isotope changes during rise of sea level during interglacial periods, and sea level fall toward sequence boundaries as ice sheets enlarge, it is more likely complicated by evaporation effects of meteoric waters during sequence boundary exposure.

CONCLUSIONS

Carbon and oxygen isotope profiles of the Miocene siliciclastic-prone sediments of the Lidam area, Eastern Province, Saudi Arabia, were sampled for the carbonate fraction in an updip cored section. The succession consists of the Aquitanian Hadrukh sands (non-marine) up into Aquitanian to Langhian, Dam mixed siliciclastics and carbonates (marginal marine), and capping Langhian-Serravallian Hofuf sands (non-marine). The shallow burial history precludes any significant burial diagenesis.

The C isotopes provide a means of enhanced correlation with Sr isotope dated sections in nearby countries, and to the global deep-sea curve. High frequency negative excursions of $d^{13}C$

within the succession appear to relate to near-surface diagenesis by soil gas depleted in ^{13}C beneath sequence boundaries. Several positive C-isotope excursions evident in the Lidam Miocene section can be tied to similar excursions in Qatar and UAE, where Sr isotope dates constrain the ages of the units. The overall C-isotope profile at Lidam from depleted values in the Early Miocene to heavy values in the Middle Miocene, and then becoming lighter again, appear to follow the long-term global $d^{13}C$ curve. However these were highly amplified perhaps as a result of migration of light-C ground waters into the system in the early and later Miocene, while the middle Miocene was marine influenced. This incursion of meteoric groundwaters into the study area was driven by the long-term global sea level changes.

Oxygen isotopes in the Lidam Miocene are surprisingly light, extending down to -12.5 ‰ $_{VPDB}$. They similarly reflect incursion of light meteoric waters into the region during siliciclastic phases with an intervening phases of more marine influenced deposition. The very light meteoric water values may be explained by rainfall associated with enhanced Miocene Indian monsoons, and with far travelled air mass trajectories migrating across north Africa and from the polar region.

FIGURES AND FIGURE CAPTIONS

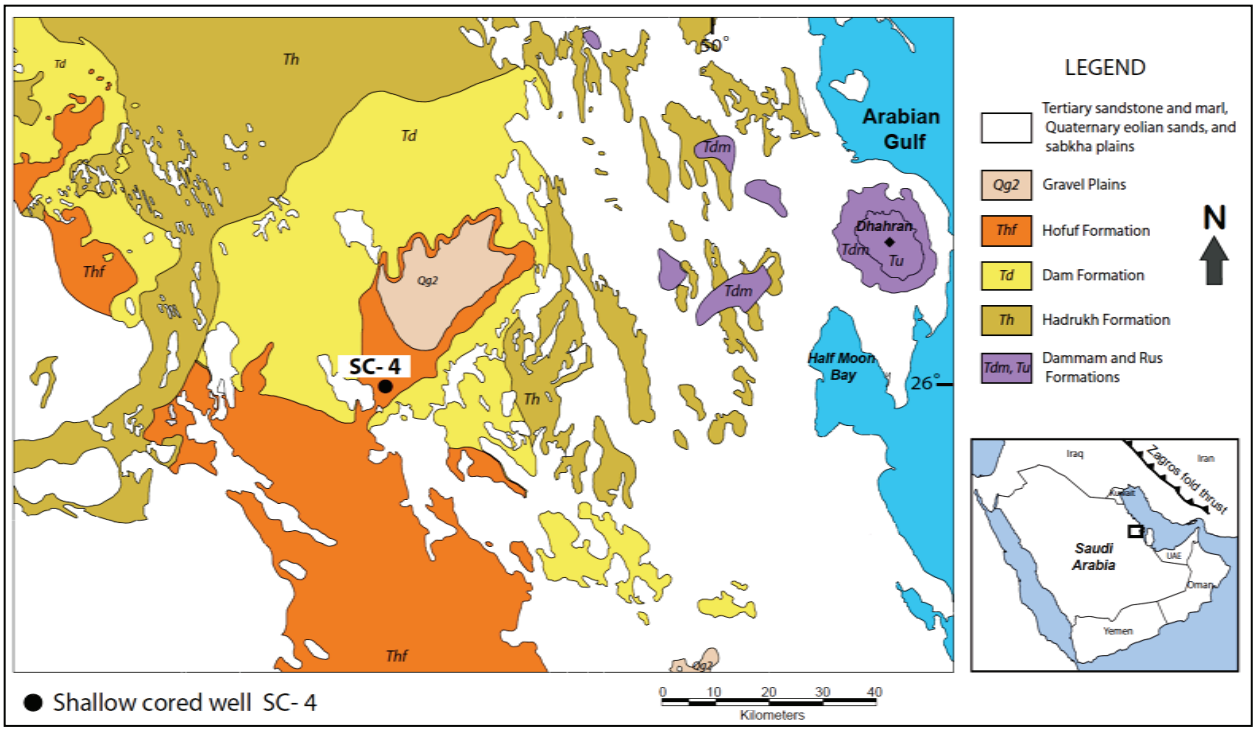

Figure 3.1 Geological map of the Eastern Province, Saudi Arabia with the location of shallow core well SC-4 labeled. The inset map shows location of Eastern Province within Saudi Arabia and the Middle East, and the Zagros fold thrust belt.

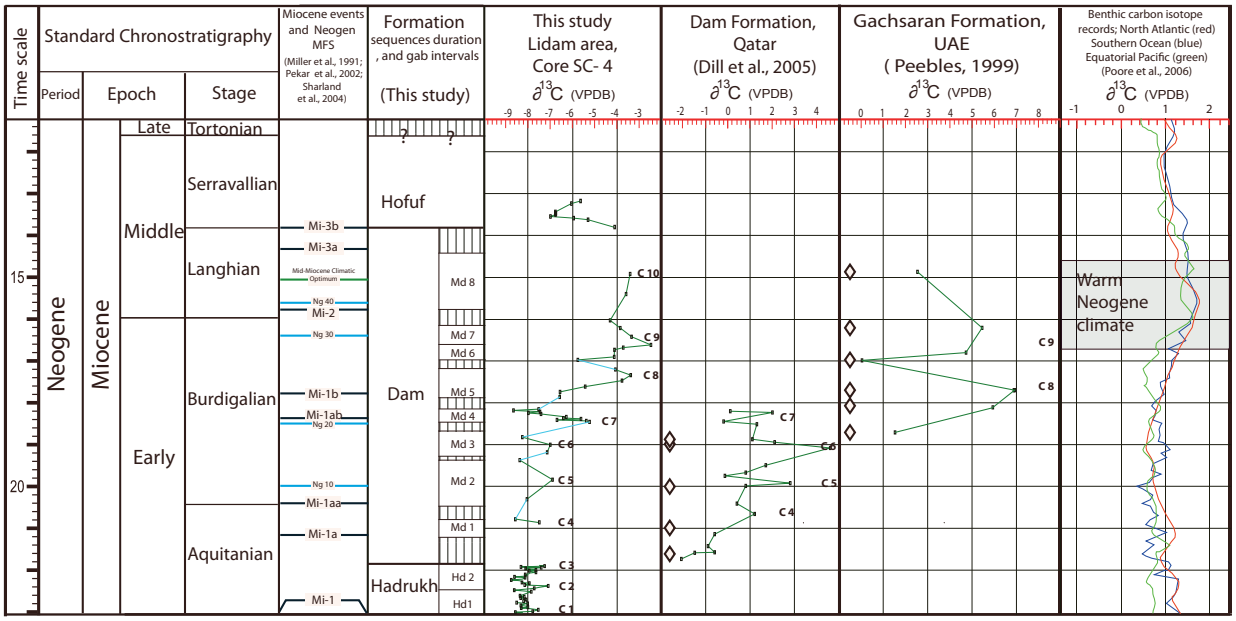

Figure 3.2 Chronostratigraphic chart showing Miocene glacial-events (black lines) (Miller et al., 1991; Pekar et al., 2002) and Neogene flooding events (blue lines labeled Ng (Sharland et al., 2004). and age relations of the Early and Middle Miocene Hadrukh, Dam and Hofuf formations studied. The $\partial^{13}C$ profiles include the Miocene succession (this study), $\partial^{13}C$ of Dam Formation succession in Qatar (Dill et al., 2005), the $\partial^{13}C$ profile of the Gachsaran Formation, UAE (equivalent to Dam Formation) (Peebles, 1999), and the $\partial^{13}C$ curves of deep marine sediments (Poore et al., 2006). The positive carbon excursions identified in this study were informally labeled C1 to C10, to facilitate correlation to Qatar and UAE.

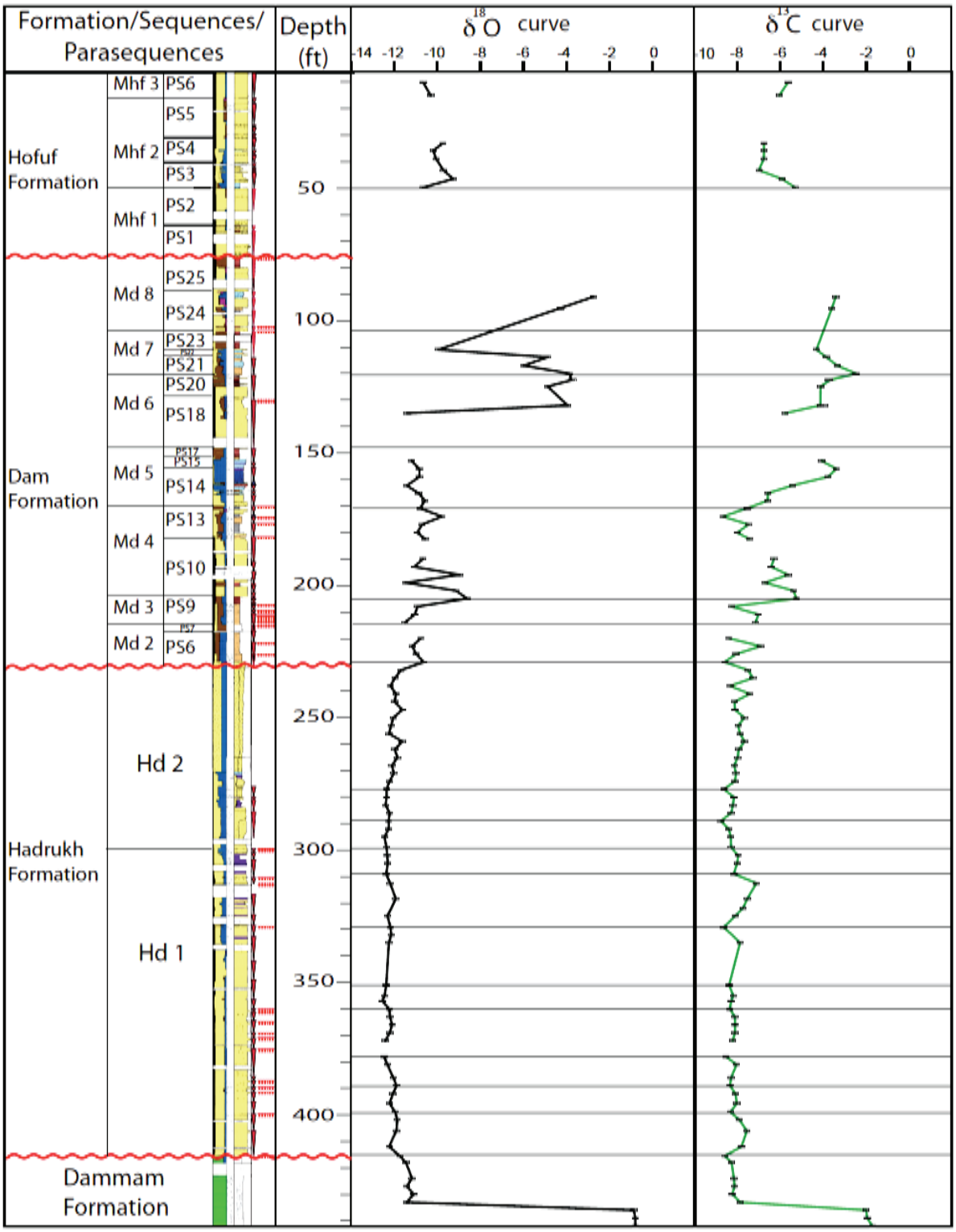

Figure 3.3 Carbon and oxygen isotope profiles plotted alongside the detailed lithologic log of the SC-4 core, which shows the major and minor sequences.

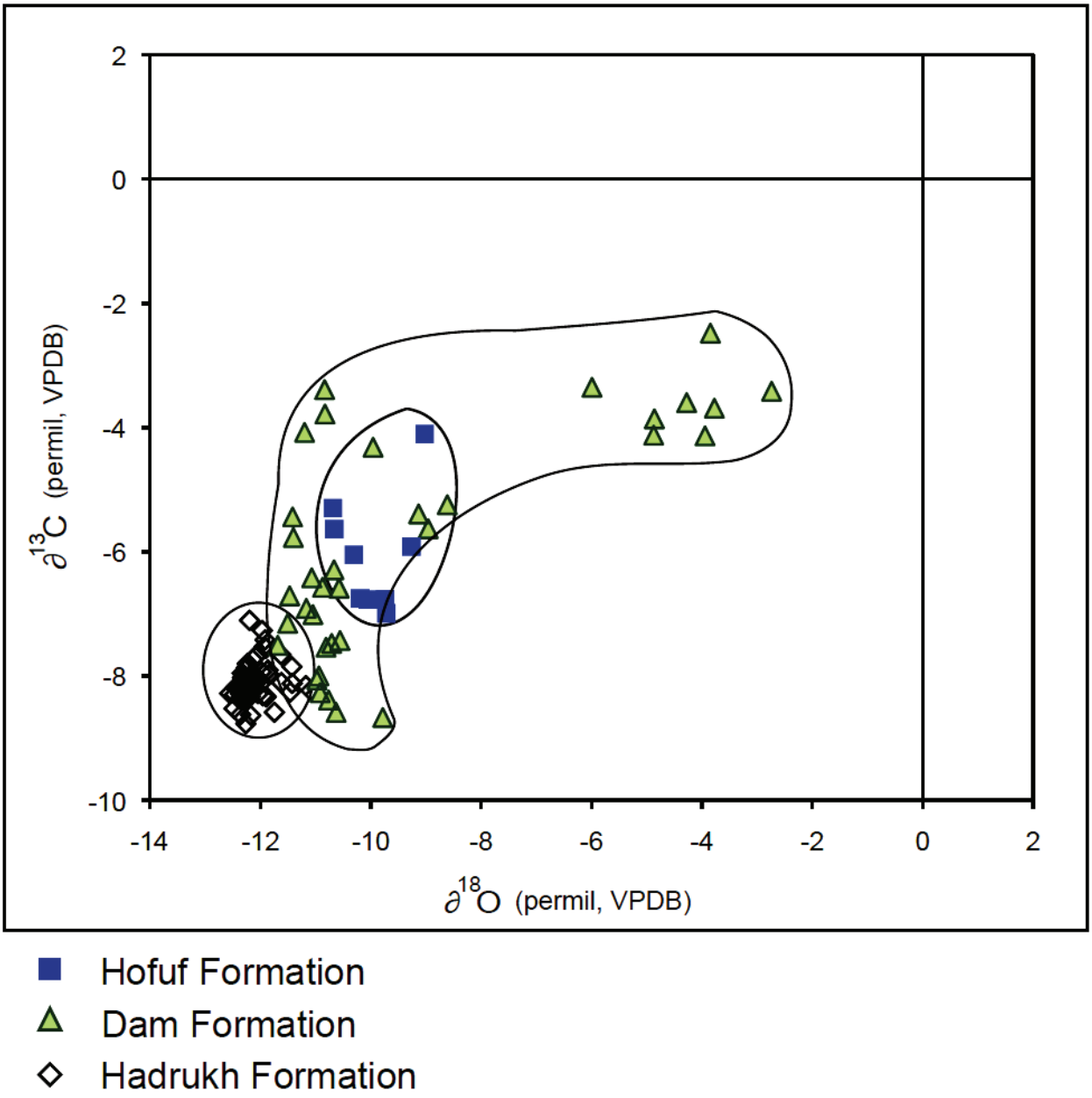

Figure 3.4 Cross plot of $\partial^{13}C$ and $\partial^{18}O$ values showing a tight clustering of the data in the Hadrukh Formation, with values that are the most negative of all the Miocene succession. The Dam Formation samples range from slightly more positive to markedly enriched relative to Hadrukh Formation samples. The Hofuf Formation samples has more positive $\partial^{13}C$ and $\partial^{18}O$ values compared to the Hadrukh and they are slightly heavier than those of the lower Dam Formation, but are lighter than the upper Dam values.

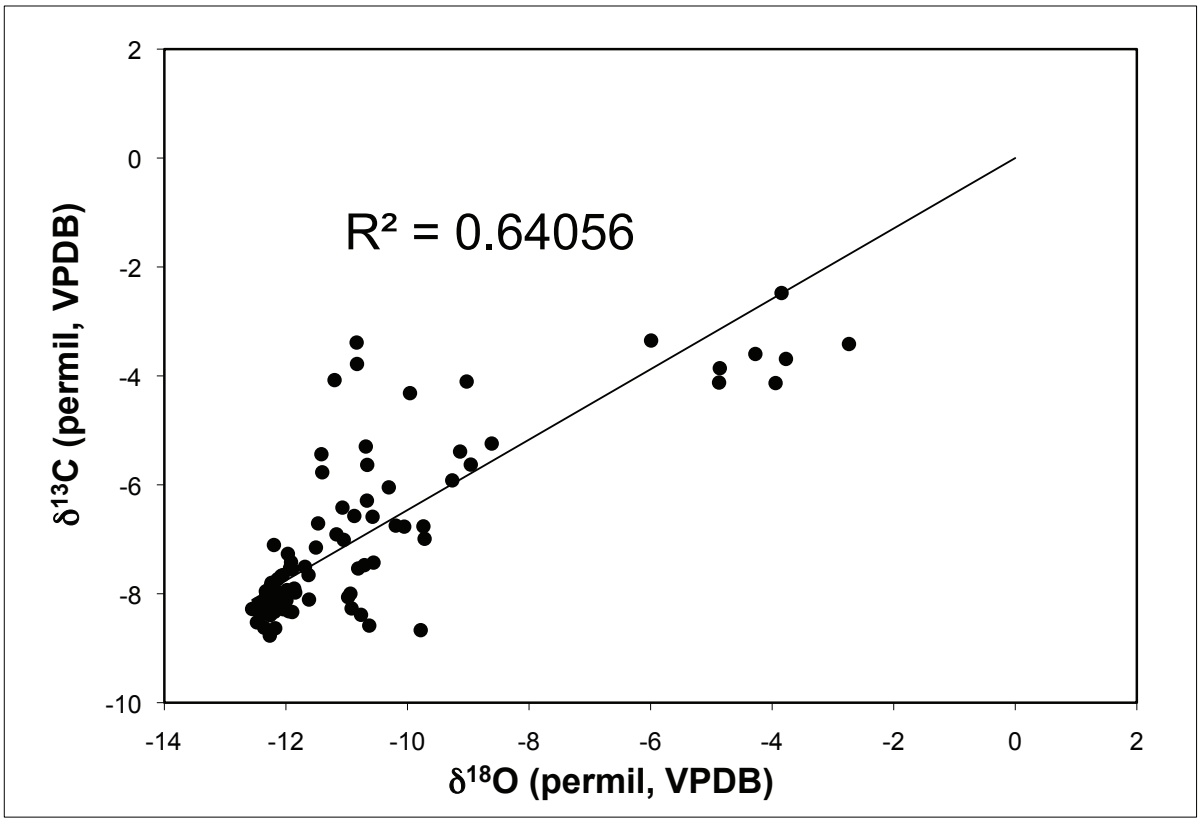

Figure 3.5 Cross plot of all the Miocene $\partial^{13}C$ and $\partial^{18}O$ data from the study area combined (Hadrukh, Dam, and Hofuf Formations). Trend line shows a moderate correlation with R^2= 0.64.

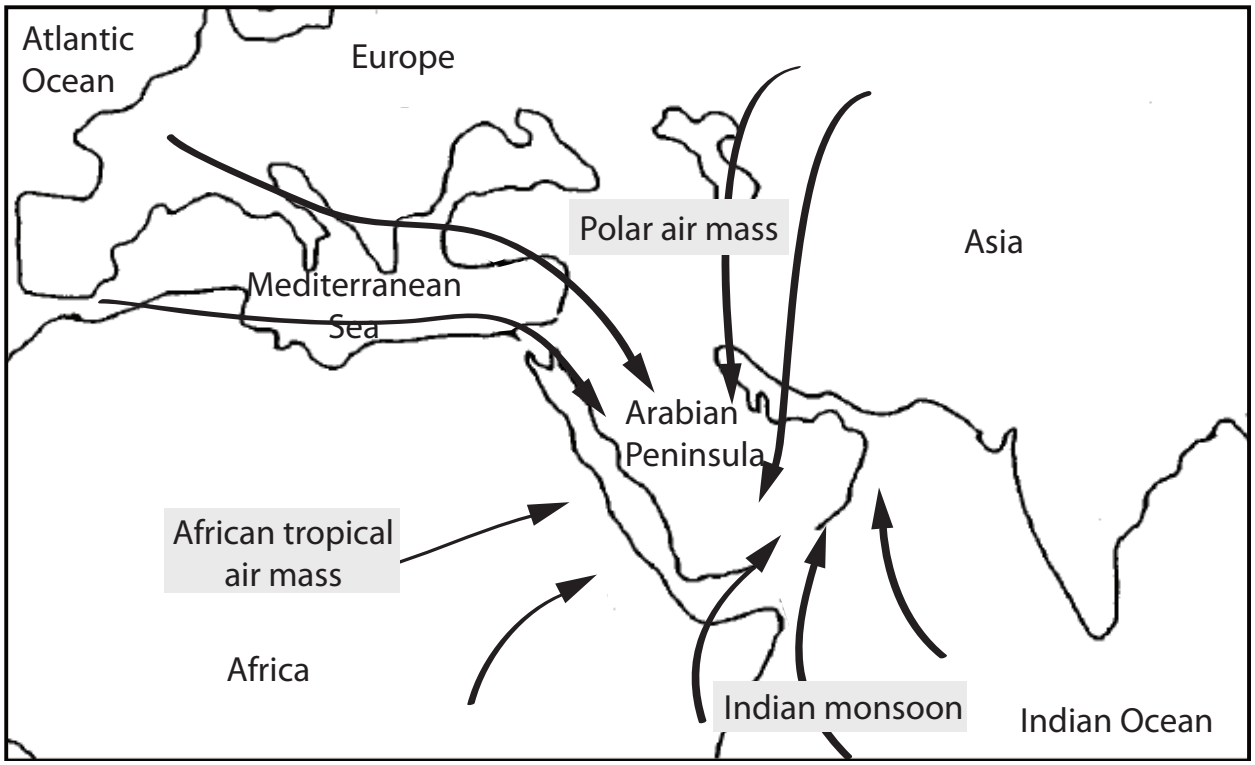

Figure 3.6 Three major fronts of moisture (air masses) influencing the climatic pattern of Arabian Peninsula: Polar air mass, African tropical air mass, and Indian monsoon.

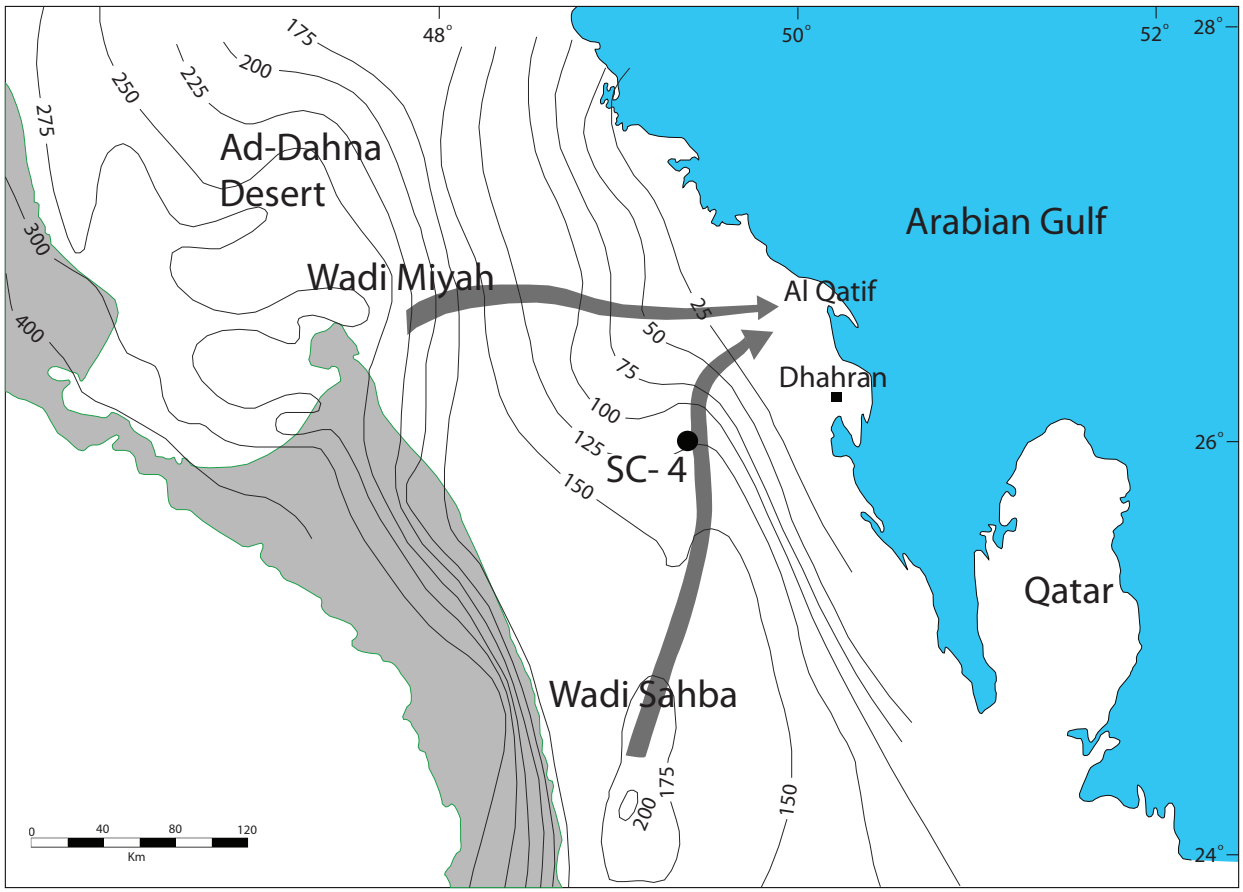

Figure 3.7 Piezometric contour lines for the Umm er Radhuma aquifer (meter a.s.l). Arrows represent two preferential water paths flowing towards the Gulf coast. The first preferential underground flow channel comes from an area south of Wadi Shaba. The other preferential flow comes down from the As Sulb Plateau, crossing the Wadi Miyah and continuing from there towards the Gulf, where the main flow reaches the coast near Al Qatif to the north of the study area. Grey area is UER aquifer outcrop. Modified after Hoetzl (1995).

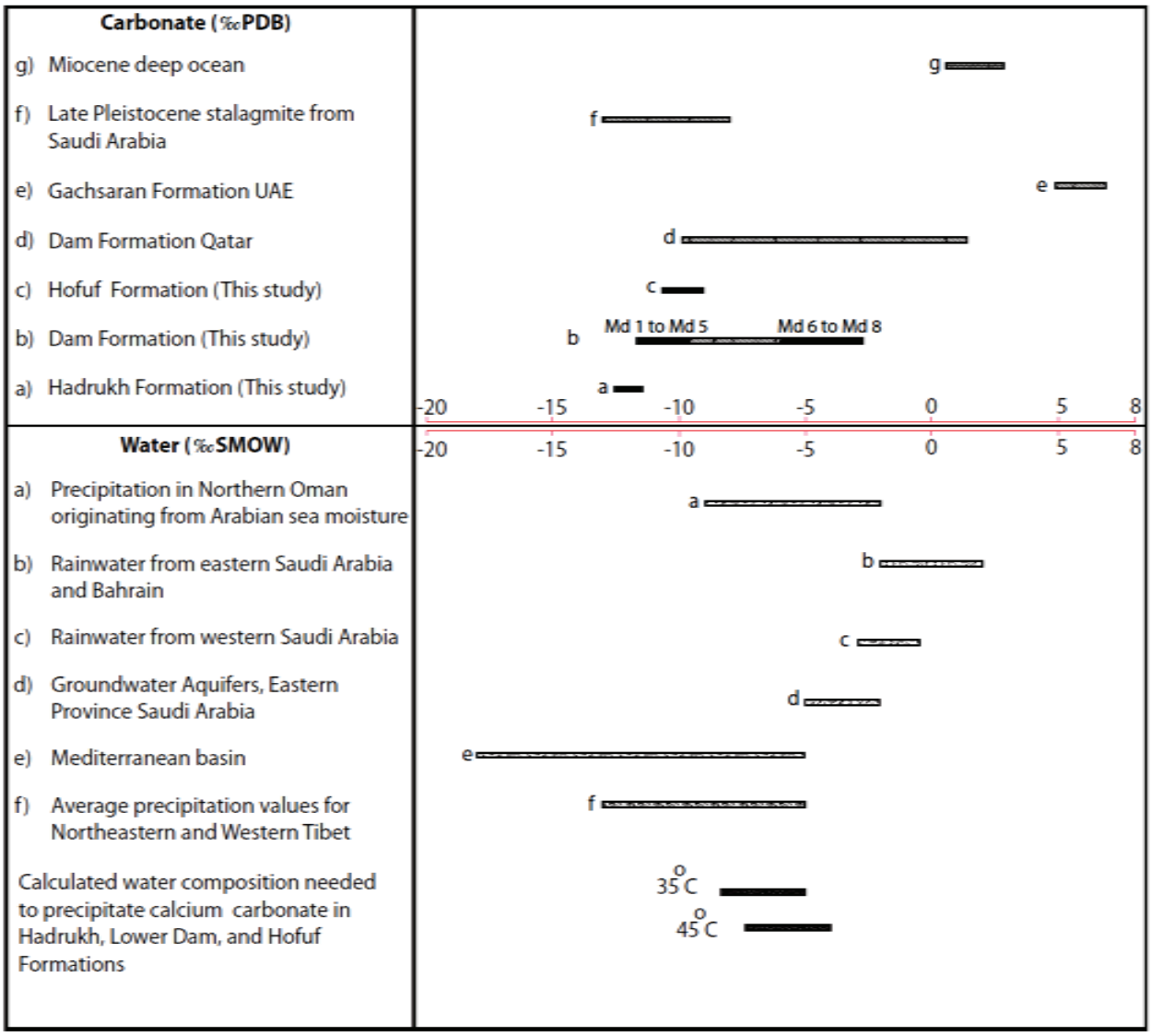

Figure 3.8 Chart summarizing the range of $\partial^{18}O$ recorded from water and Miocene carbonate rocks from the Arabian Peninsula and deep ocean. The $\partial^{18}O$ of water are shown in (SMOW), while values from carbonates are in (VPDB).

REFERENCES

Abreu, V.S. and J. B. Anderson 1998. Glacial eustasy during the Cenozoic: sequence stratigraphic implications. American Association of Petroleum Geologists Bulletin, 82, p.1385-1400.

Abu-Ali, M. and R. Littke 2005. Palaeozoic petroleum systems of Saudi-Arabia – a basin modelling approach: Geo Arabia, 10, p. 131-168.

Al qurashi, M.A. 1981. Synoptic climatology of the rainfall in the southwest region of Saudi Arabia. M.A. Thesis, Western Michigan Uni, USA, 97.

Al-Sayari, S. and J. Zotl 1978. Quaternary Period in Saudi Arabia. Springer-Verlag, Wien, New York, p. 334.

Allan, J.R., and R.K. Matthews 1982. Isotope signatures associated with early meteoric diagenesis. Sedimentology 29, p. 797– 817.

Allan, J.R., and W.D. Wiggins 1993. Dolomite Reservoirs—Geochemical Techniques for Evaluating Origin and Distribution. American Association of Petroleum Geologists, Continuing Education Course Note Series, no. 36, p. 129.

Alyamani, M.S. 2001. Isotopic composition of rainfall and ground-water recharge in the western province of Saudi Arabia. Journal of Arid Environments, v. 49, Issue 4, p. 751-760.

Alyamani, M.S. and Z. Sen 1993. Regional variations of monthly rainfall amounts in the Kingdom of Saudi Arabia. JKAU: Earth Science, 6, p.13-133.

An, Z., J.E. Kutzbach, W.L. Prell, S.C. Porter 2001. Evolution of Asian monsoons and phased uplift of the Himalayan–Tibetan Plateau since Late Miocene times. Nature 411, p. 62–66.

Andrews, P. and J. A. H. Van Couvering 1975. Palaeoenvironments in the African Miocene. Contrib. Primatol. 5, p. 62-103.

Aouad-Rizk A, J.L. Job, W. Najem, Y. Travi, B. Blavoux and L. Gourcy 2005. Oxygen-18 and deuterium contents over Mount Lebanon related to air mass trajectories and local parameters. IAEA-TECDOC-1453, p. 75–82.

Baldi, T. 1980. The early history of the Paratethys. Földt. Közl., Bull. Hung. Geol. Soc., 110, 3–4, p.456–472.

Bristow, C. S. 1999. Aeolian and sabkha sediments in the Miocene Shuwaihat Formation, Emirate of Abu Dhabi, United Arab Emirates. Chap. 6 in Fossil Vertebrates of Arabia, p. 50-60 (ed. P. J. Whybrow and A. Hill). Yale University Press, New Haven.

Burdon, D.J. 1973. Groundwater resources of Saudi Arabia. Science Mono, no. 2, ALESCO.

Butzin, M., G. Lohmann, and T. Bickert 2011. Miocene ocean circulation inferred from marine carbon cycle modeling combined with benthic isotope records. Paleoceanography, 26, PA1203.

Cerling, T.E., J.M. Harris, B.J. MacFadden, M.G. Leakey, J. Quade, V. Eisenmann and J.R. Ehleringer 1997. Global vegetation change through the Miocene/Pliocene boundary. Nature 389, p.153–158.

Chafetz, H.S., Imerito-Tetzlaff and J. Zhang 1999. Stable-isotope and elemental trends in Pleistocene sabkha dolomites: Descending meteoric waters vs. sulfate reduction. Journal of Sedimentary Research, v. 69, p. 268-278.

Clark, I.D., P. Fritz, O.P. Quinn, P.W. Rippon, H. Nash, B. bin Ghalib al Said 1987. Modern and fossil groundwater in an arid environment. A look at the hydrogeology of southern Oman. In: Use of Stable Isotopes in Water Resources Development. IAEA Symposium, vol. 299, Vienna, p. 167–187.

Clift, P., J. Lee, M.K. Clark, J. Blusztajn 2002. Erosional response of South China to arc rifting and monsoon strengthening; a record from the South China Sea. Mar. Geol. 184, p. 207–226.

Collinson, M. E. 1982. Reassessment of fossil Potamogetoneae fruits with description of new material from Saudi Arabia. Tertiary Research 4, p. 83-104.

Deines, P., 1980. The isotopic composition of reduced organic carbon: Handbook of Environmental Isotope Geochemistry, P. Fritz and J.C. Fontes (eds.), y. 1, Elsevier, p. 329-406.

Derry, L.A. and C. France Lanord 1996. Neogene Himalayan weathering history and river $^{87}Sr/^{86}Sr$: impact on the marine Sr record. Earth Planet. Sci. Lett. 142, p. 59–74.

Dettman, D.L., M.J. Kohn, J. Quade, F.J. Ryerson, T.P. Ojha and S. Hamidullah 2001. Seasonal stable isotope evidence for a strong Asian monsoon throughout the past 10.7 m.y. Geology 29, p. 31–34.

Dill, H.G., R. Botz, Z. Berner, D. Stüben, S. Nasir and H. Al-Saad, 2005. Sedi-mentary facies, mineralogy, and geochemistry of the sulphate-bearing Miocene Dam Formation in Qatar. Sedimentary Geology, v. 174, p. 63-96.

Dirican, A., S. Unal, Y. Acar and M. Demircan 2005. The temporal and seasonal variation of H-2 and O-18 in atmospheric water vapour and precipitation from Ankara, Turkey in relation to air mass trajectories at Mediterranean Basin L. Goucy (Ed.), Isotopic composition of precipitation in the Mediterranean Basin in relation to air circulation patterns and climate, IAEA-TECDOC-1453, Vienna.

Dorale J.A. and Z. Liu 2009. Limitations of hendy test criteria in judging the paleoclimatic suitability of speleothems and the need for replication. Journal of Cave and Karst Studies, v. 71, no. 1, p. 73–80.

Fleitmann, D., S.J. Burns, A. Matter 1999. Stable isotope study of the active water-carbonate system in caves in Oman: a test of applicability to Palaeoclimate studies. EOS Transactions AGU 80 (46), Fall Meeting Supplement, Abstract OS22B-12.

Fleitmann, D., S.J. Burns, M. Mudelsee, U. Neff, J. Kramers, A. Mangini and A. Matter 2003. Holocene forcing of the Indian monsoon recorded in a stalagmite from Southern Oman. Science 300, p. 1737–1739.

Fleitmann, D., S.J. Burns, U. Neff, M. Mudelsee, A. Mangini and A. Matter 2004. Paleoclimatic interpretation of high-resolution oxygen isotope profiles derived from annually laminated speleothems from Southern Oman. Quaternary Science Reviews.

Friedman, I. and J.R. O'Neil 1977. Compilation of stable isotope fractional factors of geochemical interest. In: Fleischer, M. (Ed), Data of Geochemistry. U.S. Geol. Surv. Prof. Pap. 440-KK, p. 12.

Gat, J.R. and I. Carmi 1970. Evolution of the isotopic composition of atmospheric waters in the Mediterranean Sea area. Journal of Geophysical Research, 75, p. 3039-3048.

Gischler E. and A.J. Lomando 2005. Offshore sedimentary facies of a modern carbonate ramp, Kuwait, northwestern Arabian-Persian Gulf. Facies 50, p. 443–462

Guo, Z.T., W.F. Ruddiman, Q.Z. Hao, H.B. Wu, Y.S. Qiao, R.X. Zhu, S.Z. Peng, J.J. Wei, B.Y. Yuan and T.S. Liu 2002. Onset of Asian desertification by 22 Myr ago inferred from loess deposits in China. Nature 416, p. 159–163.

Harris N. 2006. The elevation history of the Tibetan Plateau and its implications for the Asian monsoon. Palaeogeography, Palaeoclimatology, Palaeoecology, v. 241, Issue 1.

Harrison, T.M., P. Copeland, W.S.F. Kidd and O.M. Lovera 1995. Activation of the Nyainquentanghla Shear Zone: implications for uplift of the southern Tibet plateau. Tectonics 14, p. 658–676.

Hays, J.D., J. Imbrie and N. J. Schackleton 1976. Variations in the Earth's orbit: Pacemaker of the ice ages. Science 194, p. 1121–1132.

Hendy, C.H., 1971. The isotopic geochemistry of speleothems: the calculations of the effects of different modes of formation on the isotopic composition of speleothems and their applicability as palaeclimate indicators. Geochimica et Cosmochimica Acta 35, p. 801–824.

Hoetzl, H. 1995. Groundwater recharge in an arid karst area (Saudi Arabia). IAHS Publ 232, p.195–207.

Hoetzl, H. and J.G. Zoetl 1978. Climatic changes during the Quaternary period. In: Quaternary Periodin Saudi Arabia (ed. By S. S. Al-Sayari & J. G. Zoetl), v. 2, p. 301-311. Springer-Verlag, Vienna.

Jia, G.D., P.A. Peng, Q.H. Zhao and Z.M. Jian 2003. Changes in terrestrial ecosystem since 30 Ma in East Asia: stable isotope evidence from black carbon in the South China Sea. Geology 31, p. 1093–1096.

Kingston, J. D. and A. Hill 1999. Late Miocene palaeoenvironments in Arabia. In, Fossil Vertebrates of Arabia, p. 389-407 (ed. P. J. Whybrow and A. Hill). Yale University Press, New Haven.

Kroon, D., T. Steens and S.R. Troelstra 1991. Onset of monsoonal related upwelling in the western Arabian Sea as revealed by planktonic foraminifers. Proc. Ocean Drill. Prog., Sci. Results 117, p. 257–263.

Leguy, C., M. Rindsberger, A. Zangwil, A. Issar and J.R. Gat 1983. The relation between the O-18 and deuterium contents of rainwater in the Negev desert and air-mass trajectories. Isotope Geoscience, 1: p. 205-218.

Liu, X. and Z.Y. Yin 2002. Sensitivity of East Asian monsoon climate to the uplift of the Tibetan Plateau. Palaeogeogr. Palaeoclimatol. Palaeoecol. 183, p. 223–225.

MacLaren International Limited 1979. Water and agricultural development studies-Arabian Shield-South. Hydrogeological investigations, Annex 3. Ministry of Agriculture and Water, Riyadh, Saudi Arabia.

Morse, J.W. and F.T. Mackenzie 1990. Geochemistry of sedimentary carbonates. Developments in sedimentology. Elsevier, Amsterdam, p. 707.

Peebles, R.G. 1999. Stable isotope analysis and dating of the Miocene of the Emirate of Abu Dhabi, United Arab Emirates. In, P.J. Whybrow and A. Hills (Eds.), Fossil Vertebrates of Arabia. Yale University Press, p. 88–107.

Poore, H. R., R. Samworth, N. J. White, S. M. Jones and I. N. McCave 2006. Neogene overflow of Northern Component Water at the Greenland- Scotland Ridge, Geochem. Geophys. Geosyst.

Powers, R. W., L. F. Ramirez, C. D. Redmond and E. L. Elberg 1966. Geology of the Arabian Peninsula: sedimentary geology of Saudi Arabia: United States Geological Survey Professional Paper 560-D, p. 147.

Pye, K. and H. Tsoar 1990. Aeolian Sand and Sand Dunes: London, Unwyn Hyman, p. 396.

Quade, J., L. Rae, P.G. DeCelles and T.P. Ojha 1989. Development of Asian monsoon revealed by marked ecological shift during the latest Miocene in northern Pakistan. Nature 342, p. 163–166.

Ramstein, G., F. Fluteau and J. Besse 1997. Effect of orogeny, plate motion and land-sea distribution on Eurasian climate change over the past 30 million years. Nature 386, p.

788–795.

Rindsberger, M., M. Magartiz, I. Carmi and D. Gilad 1983. The relation between air mass trajectories and the water isitope composition of rain in the Mediterranean Sea Area. Geophys. Rev. Lett. 10, p. 43–46.

Rögl, F. 1999. Short Note Mediterranean And Paratethys. Facts And Hypotheses Of An Oligocene To Miocene Paleogeography (Short Overview). North, 50(August), p. 339-349.

Scotese, C. R. 2001. Atlas of Earth History. Paleogeography, Paleomap Project, Arlington, Texas, v.1, p. 52.

Scotese, C.R. 2002. http://www.scotese.com, (PALEOMAP website).

Sen, Z. 1983. Hydrology of Saudi Arabia. Symposium on Water Resources in Saudi Arabia, King Saud University, Riyadh, 1, p. 68-94.

Shampine, W.J., T. Dincer and M. Noory 1979. An evaluation of isotope concentrations in the groundwater of Saudi Arabia. – Isotope Hydrology 1978, II, p. 443-463; Vienna (IAEA).

Steineke, M. and Hoover 1936. Unpublished report in Powers, R.W., 1968, Lexique stratigraphique international: Saudi Arabia: vol III, Asie, fasc. 10b1: Centre National de la Recherche Scientifique, Paris, p. 177.

Trauth M. H., J. C. Larrasoaña and M. Mudelsee 2009. Trends, rhythms and events in Plio-Pleistocene African climate, Quaternary Science Reviews, Volume 28, Issues 5–6, p. 399-411

Webster, P.J. 1987. The elementary monsoon. In: Fein, J.S., Stephens, P.L. (Eds), Monsoons. John Wiley, New York, p. 3-32.

Wei, K., F. Gasse 1999. Oxygen isotopes in lacustrine carbonates of West China revisited: implications for post glacial changes in summer monsoon circulation. Quaternary Science Reviews 18, p. 1315–1334.

Weyhenmeyer, C.E., S.J. Burns, H.N. Waber, W. Aeschbach-Hertig, R. Kipfer, R. Beyerle, H. Loosli and A. Matter 2000. Cool glacial temperatures recorded by noble gases in a groundwater study from northern Oman. Science, 287, p. 842-845.

Weyhenmeyer C. E., S.J. Burns, H.N. Waber, P.G. Macumber and A. Matter 2002. Isotope study of moisture sources, recharge areas, and groundwater flow paths within the eastern Batinah coastal plain, Sultanate of Oman. Water Resour. Res., 38, p. 1184.

Whybrow, P.J. 1984. Geological and faunal evidence from Arabia for mammal "migrations" between Asia and Africa during the Miocene. Courier Forschungsinstitüt Senckenberg 69, p. 189-198.

Whybrow, P.J., M.E. Collinson, R. Daams, A. W. Gentry and H. A. McClure 1982. Geology, fauna (Bovidae, Rodentia) and flora from the Early Miocene of eastern Saudi Arabia. Tertiary Research 4, p. 105-120.

Woodruff, F. and S. M. Savin 1989. Miocene deep water oceanography, Paleoceanography, 4, p. 87–140.

Wushiki, H. 1991. $^{18}O/^{16}O$ and D/H of the meteoric waters in South Arabia. Mass Spectroscopy 39, p. 239–250.

Zachos, J.C., M. Pagani, L. Sloan, E. Thomas, K. Billups 2001. Trends, rhythms, and aberrations in global climate 65 Ma to present. Science 292, p. 686-693.

Zheng, H., C.M. Powell, Z. An, J. Zhou, G. Dong 2000. Pliocene uplift of the northern Tibetan Plateau. Geology 28, p. 715–718.

CHAPTER 4

CONCLUSIONS

The Miocene of the Lidam area, Eastern Province, Saudi Arabia, is an example of the interaction of glacio-esustasy during moderate Antarctic glaciation, on the slowly subsiding distal Arabian foreland, within a small back bulge basin distal from the active Zagros fold-thrust belt.

Climate and sea level controlled siliciclastic input relative to marine carbonate deposition, while tectonics controlled the shape of the embayment within the study area, and the thickness of the units. The succession consists of the Early to Middle Miocene Hadrukh siliciclastics (52 to 66 m thick), Dam mixed siliciclastics and carbonates (47 to 79 m thick), and the Hofuf siliciclastics (90 m thick),

The Hadrukh Formation is dominated by non-marine siliciclastics and minor palustrine carbonates and is a composite sequence with two subsequences and 8 component, poorly defined high frequency sequences. The Dam Formation is a mixed carbonate-siliciclastic composite sequence composed of 8 small-scale 3rd order sequences, each typically composed of about 4 parasequence sets. The Hofuf Formation is a 3rd order non-marine sequence with a lower siliciclastic unit, a middle carbonate unit and upper siliciclastic unit of which only the lower unit was studied.

Facies within the siliciclastic units include paleosols, fluvial cross-bedded sands, mudflats red mudrock, near shore siliciclastic lagoon green gray mudrock, brecciated micritic quartz sands of ephemeral lakes, gypseous calcareous quartz sands and wacke of saline coastal plain and evaporitic flats, and quartz sand sheets of intertidal shallow marine. Carbonate facies

include incipient paleosols of brecciated carbonate sheet, lime/clay clast quartz wackestone transgressive basal sheet, tidal flat microbial laminites and microbial mounds, near shore lagoon argillaceous variably quartzose marl, fine peloid mudstone - wackestone of shallow lagoon, oolitic grainstone shoal or tidal bars, mollusks packstone, and foraminiferal-mollusk packstone-grainstone seagrass meadows.

The low position of sea level promoted deposition of Hadrukh siliciclastics, which pass up into Dam mixed siliciclastics and carbonates as global sea levels rose, peaking with the Middle Miocene climatic optimum, only to be succeeded by Hofuf siliciclastics as global sea level fell. Arid climate stages are evident in the Hadrukh by gypsum-bearing sands, and in the Dam Formation by the carbonate facies (oolite and stromatolites) that are compatible with semi-arid conditions and elevated salinity. The Hofuf Formation probably remained semi-arid but lacks evaporites.

Low subsidence rates of 1 to 4 cm/k.y generated the long-term accommodation, which were considerable slower than those in the proximal foredeep in Iran. Differential warping during the Oligocene and the Miocene generated a structurally controlled embayment within the study area, which controlled bathymetry of facies. Eustatic sea level changes (indicated by oxygen isotope proxies in coeval deep sea sediments) appear to have controlled the timing of the deposition of sequences. These sequences represent the updip terminations of much thicker, more conformable downdip sediment wedges.

Many of sequences appear to be about 1 m.y. duration, suggestive of long term obliquity forcing of sea level, associated with long term obliquity nodes. A few appear to be higher order 400 k.y sequences, perhaps associated with long-term eccentricity. Although sea level changes were 20 to 40 m, only a small amount of the sea level rise affected the study area because of its

updip position. The moderate magnitude sea level changes locally incised sequence boundaries, and caused formation of numerous exposure surfaces with paleosols and brecciation. Individual parasequence sets and parasequences may be orbital eccentricity-precessional and obliquity cycles. The succession contains numerous missing beats reflecting updip position and tens of meters sea level changes that frequently exposed the platform. Paleosols are well developed on siliciclastic redbeds mainly near sequence boundaries in the Hadrukh and the Dam formations. Brecciation of Hadrukh palustrine carbonates occurred during multiple exposure events. Within the Dam carbonates, parasequence and parasequence set boundaries commonly are capped by tidal flat laminites (some of which are incipiently brecciated) that die out updip into siliciclastic units.

C and O isotopes of the Miocene siliciclastic prone sediments of the Lidam area, Eastern Province, Saudi Arabia, were sampled for the carbonate fraction in an updip cored section. The succession consists of the Aquitanian Hadrukh sands (non-marine) up into Aquitanian to Langhian, Dam mixed siliciclastics and carbonates (marginal marine), and capping Langhian-Serravallian Hofuf sands (non-marine). The shallow burial history precludes any significant burial diagenesis.

The C isotopes provide a means of enhanced correlation with Sr isotope dated sections in nearby countries, and to the global deep-sea curve. High frequency negative excursions of $\delta^{13}C$ within the succession appear to relate to near-surface diagenesis by soil gas depleted in ^{13}C beneath sequence boundaries. Several positive C isotope excursions evident in the Lidam Miocene section can be tied to similar excursions in Qatar and UAE, where Sr isotope dates constrain the ages of the units. The overall C isotope profile at Lidam from depleted values early in the Miocene to heavy values in the Middle Miocene, becoming lighter again in the late

Miocene, appear to follow the long term global $\delta^{13}C$ curve. However these were highly amplified perhaps as a result of migration of light-C ground waters into the system in the early and later Miocene, while the middle Miocene was marine influenced. This incursion of meteoric groundwaters into the study area was driven by the long-term global sea level changes.

Oxygen isotopes in the Lidam Miocene are surprisingly light, extending down to -12.5 ‰ $_{VPDB}$. They similarly reflect incursion of light meteoric waters into the region during siliciclastic phases with an intervening phases of more marine influenced deposition. The very light meteoric water values may be explained by rainfall associated with enhanced Miocene Indian monsoons, and with far travelled air mass trajectories migrating across north Africa and from the polar region.

APPENDIX A

Selected detailed stratigraphic columns of cored wells SC- 4 and 1 showing facies stacking within the Hadrukh Formation.

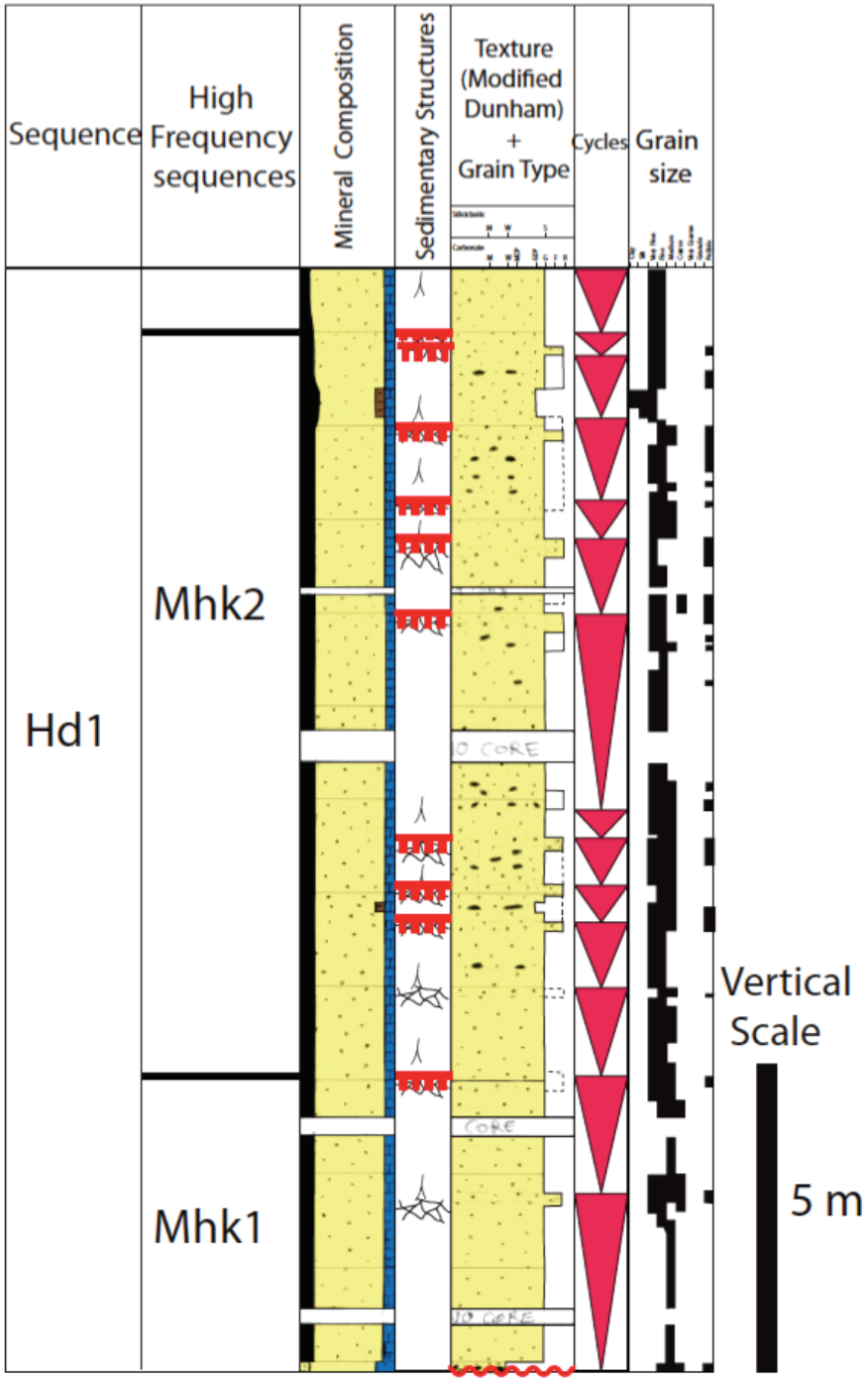

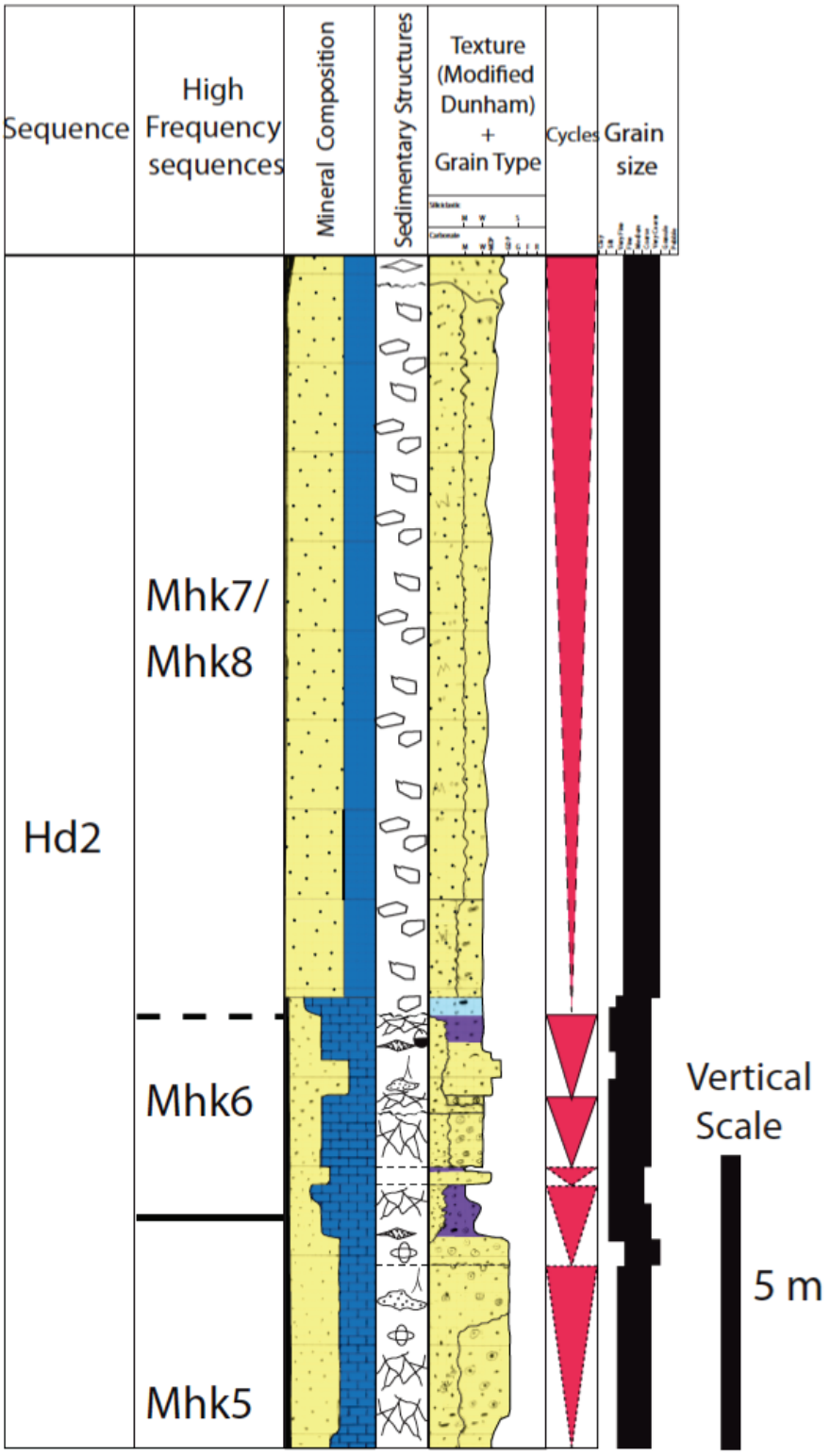
Sequence
High Frequency sequences
Mineral Composition
Sedimentary Structures
Texture (Modified Dunham) + Grain Type
Cycles
Grain size
Hd2
Mhk7/ Mhk8
Mhk6
Mhk5
Vertical Scale
5 m

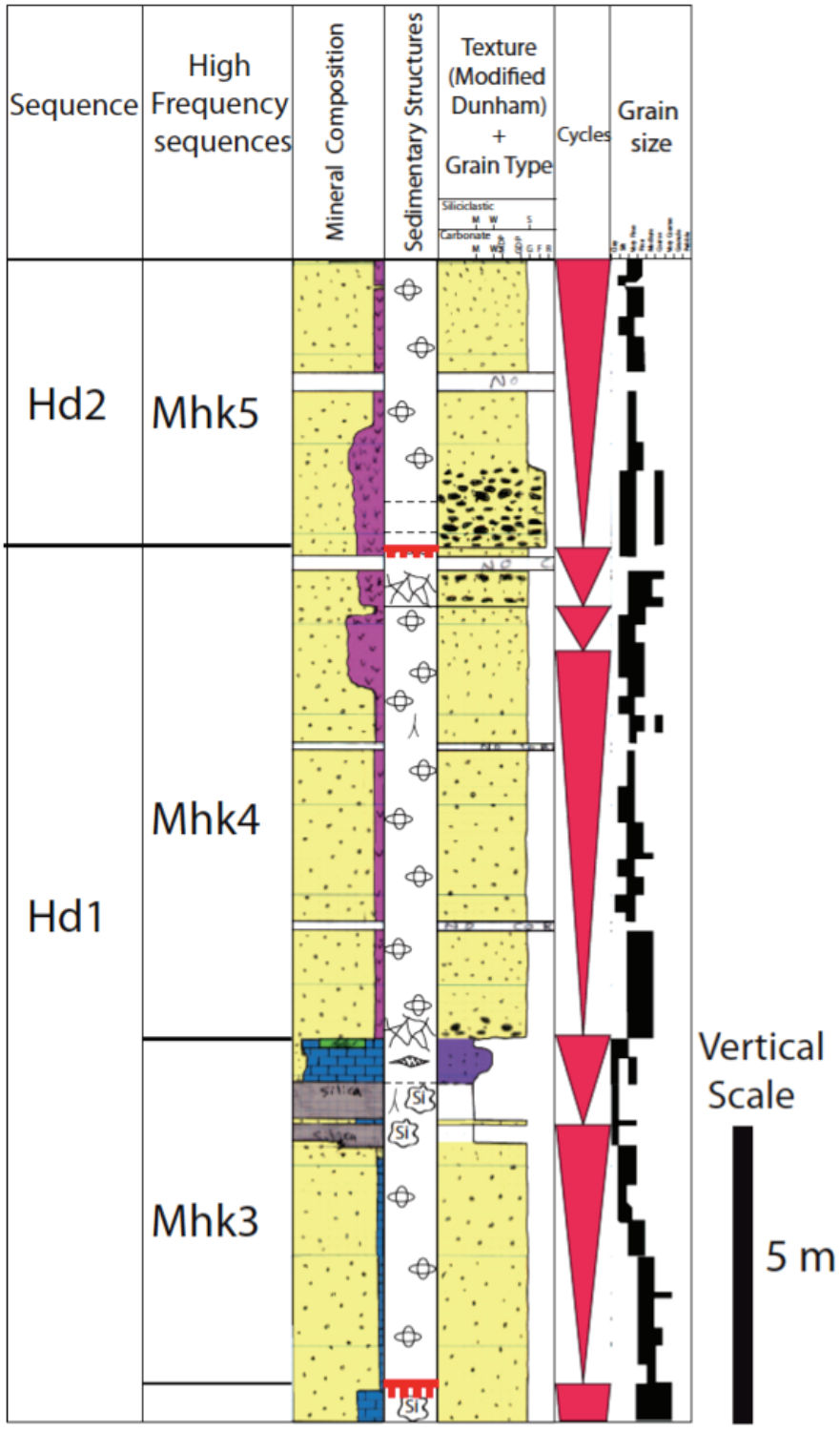
Sequence
High Frequency sequences
Mineral Composition
Sedimentary Structures
Texture (Modified Dunham) + Grain Type
Cycles
Grain size
Hd2
Mhk5
Hd1
Mhk4
Mhk3
Vertical Scale
5 m

APPENDIX B

Symbols for lithology, sedimentary structures and lithofacies for use in cross section and description logs of Hadrukh Formation.

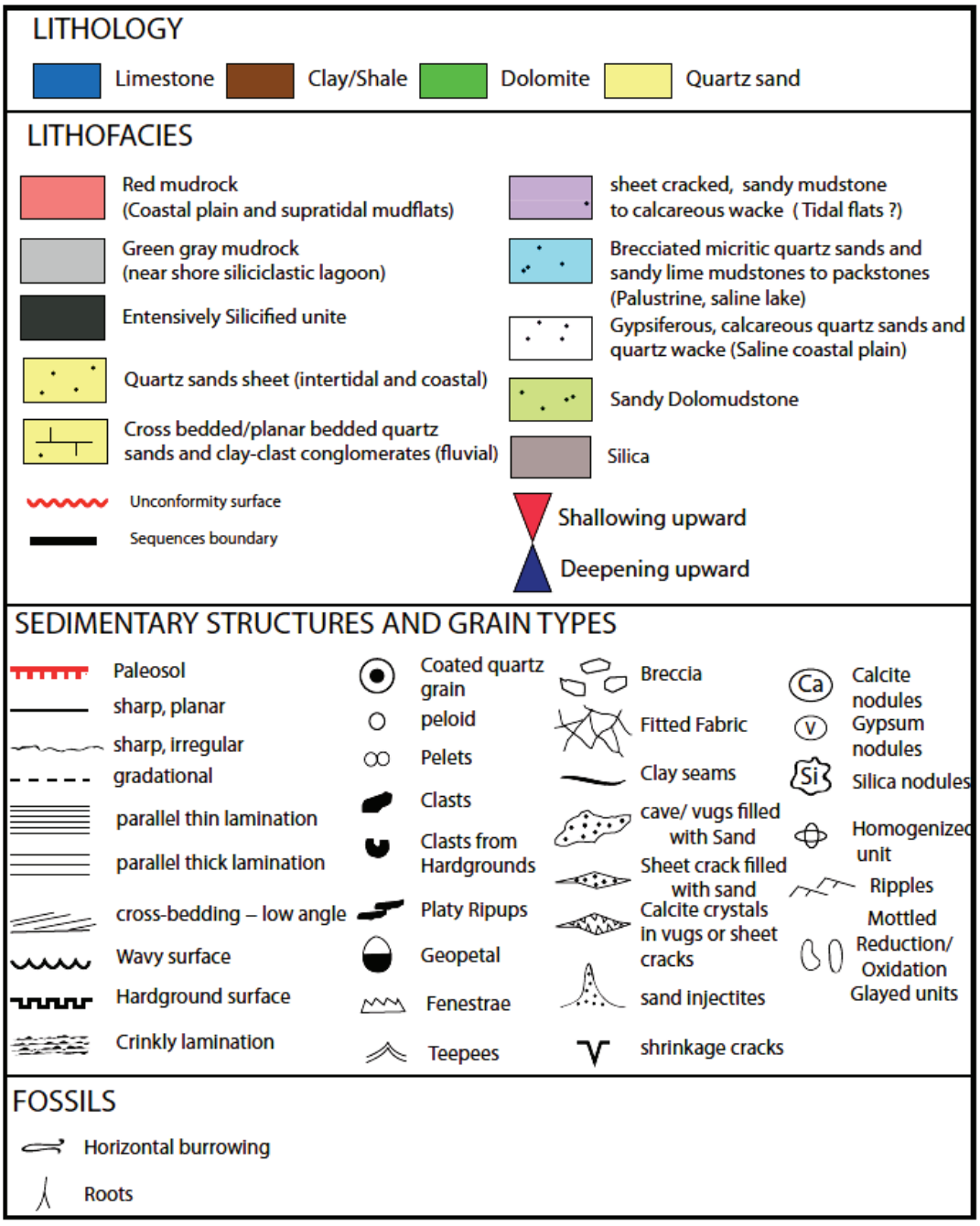

APPENDIX C

Detailed stratigraphic column showing the facies stacking and sequence picks within the Dam Formation in cored well SC-1.

v

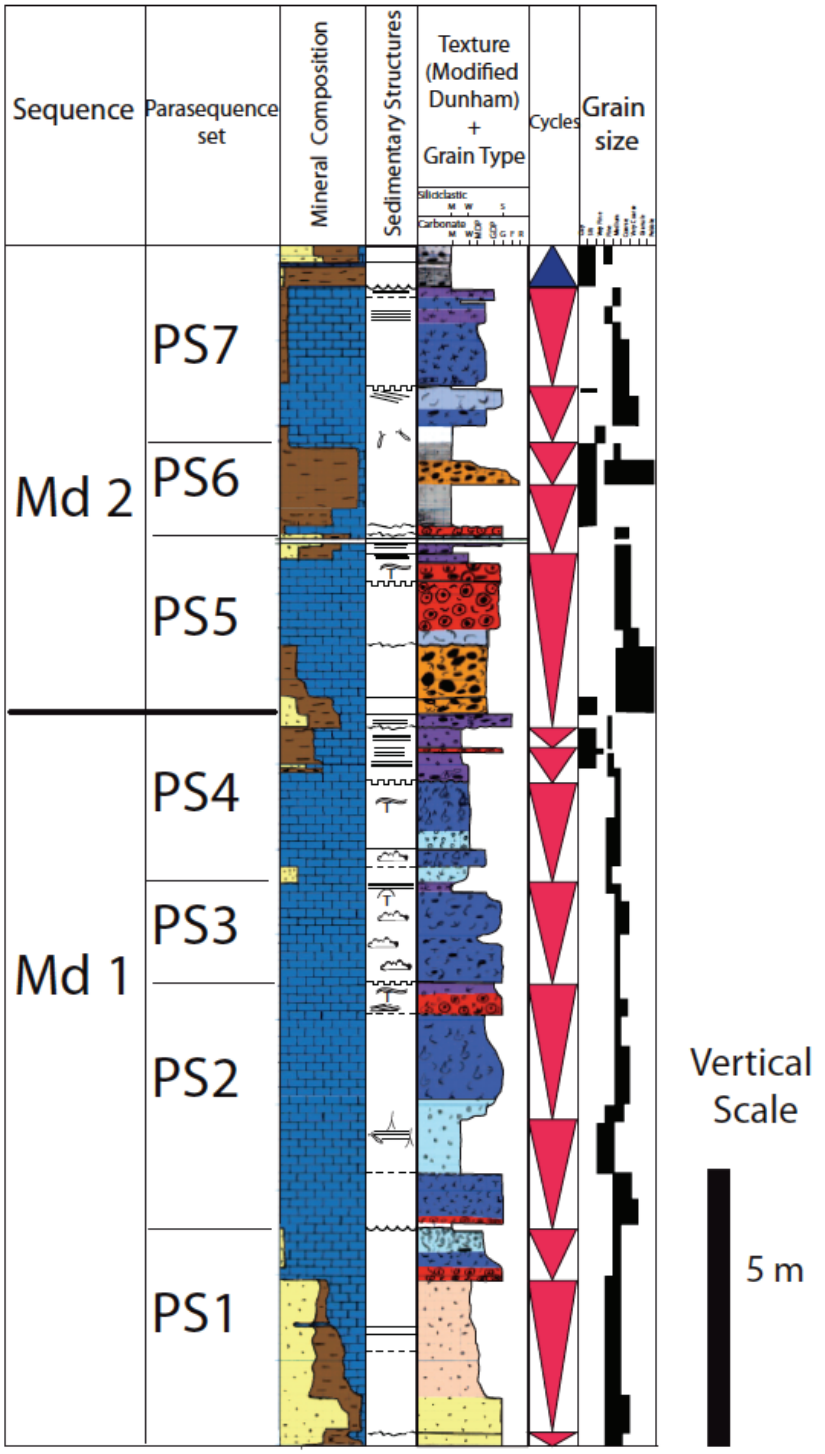

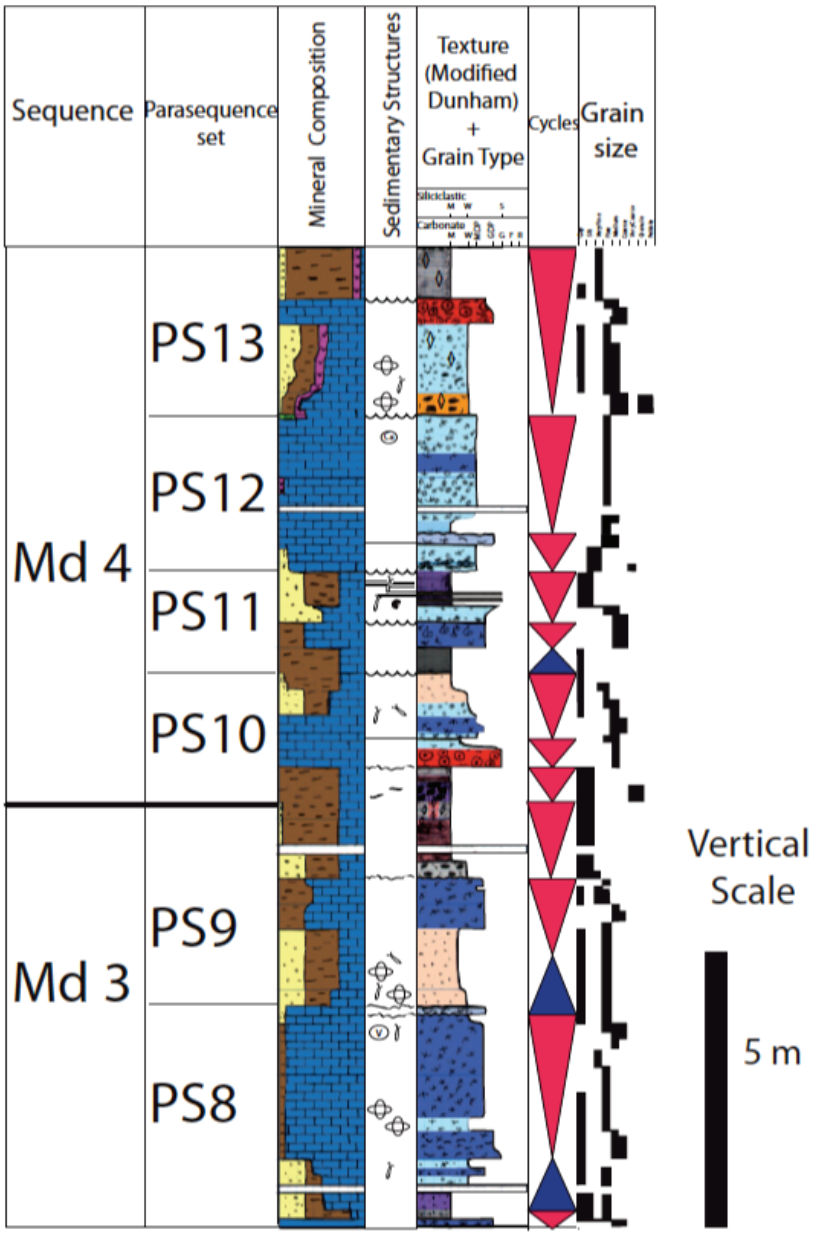
Sequence
Parasequence set
Mineral Composition
Sedimentary Structures
Texture (Modified Dunham) + Grain Type
Cycles
Grain size
Md 4
PS13
PS12
PS11
PS10
Md 3
PS9
PS8
Vertical Scale
5 m

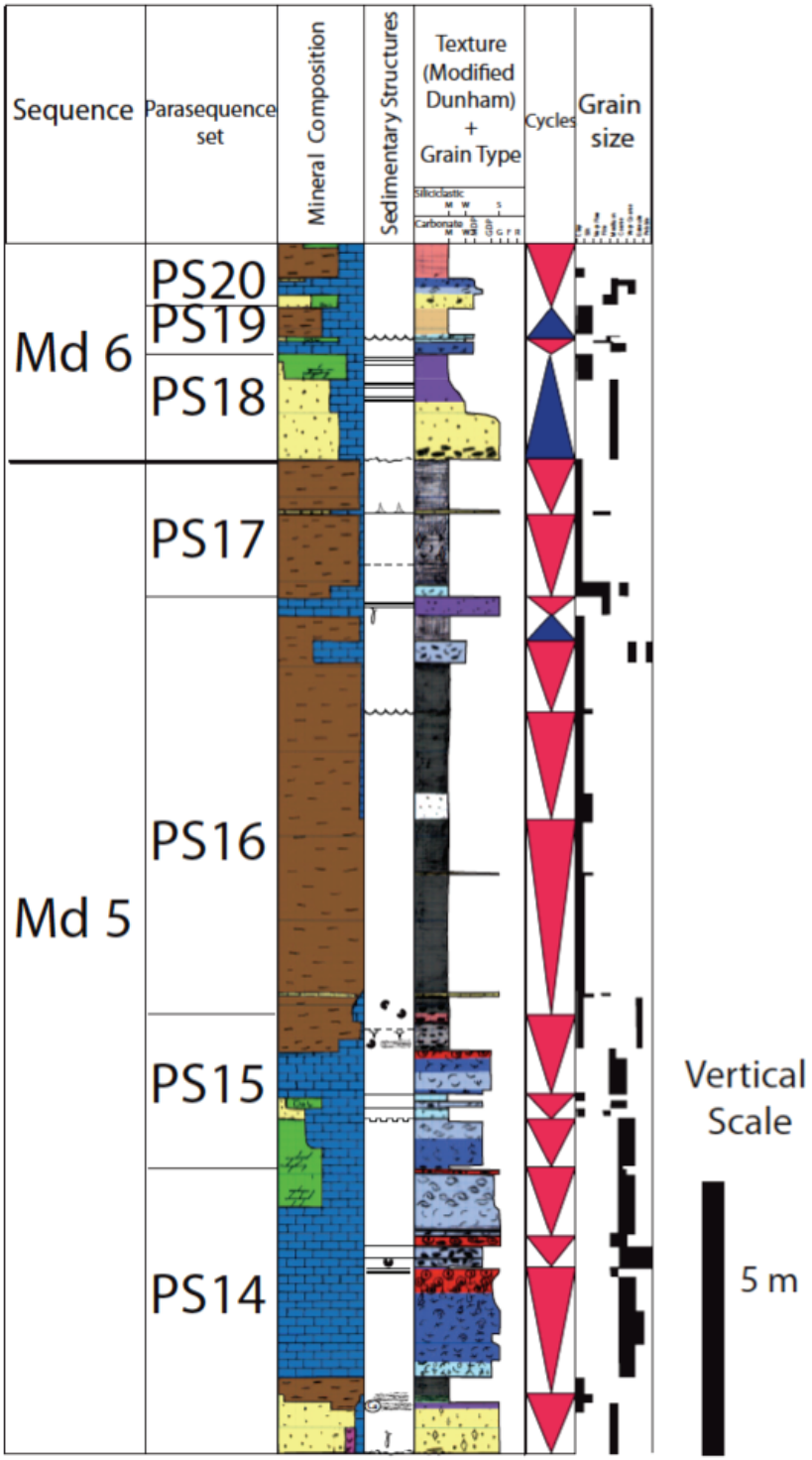
Sequence
Parasequence set
Mineral Composition
Sedimentary Structures
Texture (Modified Dunham) + Grain Type
Cycles
Grain size
Md 6
PS20
PS19
PS18
Md 5
PS17
PS16
PS15
PS14
Vertical Scale
5 m

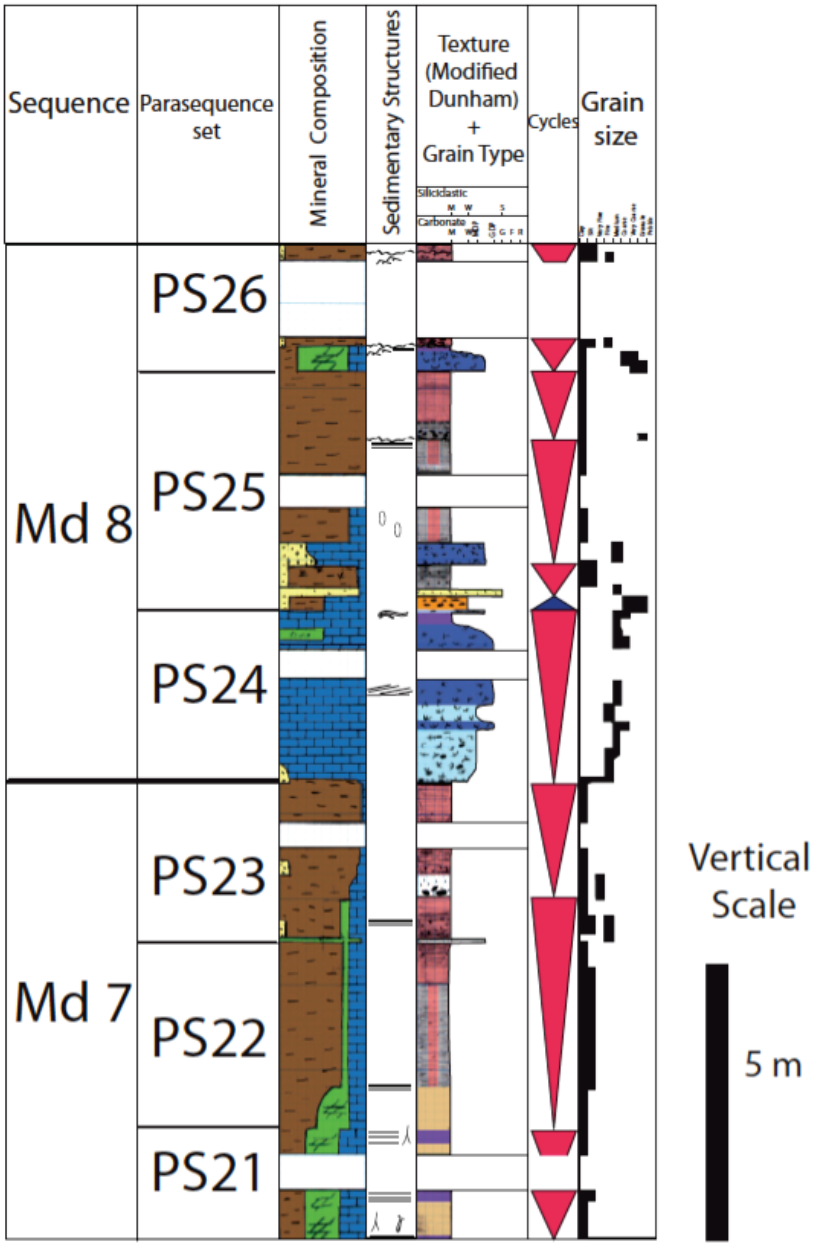
Sequence
Parasequence set
Mineral Composition
Sedimentary Structures
Texture (Modified Dunham) + Grain Type
Cycles
Grain size
Md 8
Md 7
PS26
PS25
PS24
PS23
PS22
PS21
Vertical Scale
5 m

APPENDIX D

Symbols for lithology, sedimentary structures and lithofacies for use in cross section and description logs of Dam Formation.